General Disclaimer

One or more of the Following Statements may affect this Document

- This document has been reproduced from the best copy furnished by the organizational source. It is being released in the interest of making available as much information as possible.

- This document may contain data, which exceeds the sheet parameters. It was furnished in this condition by the organizational source and is the best copy available.

- This document may contain tone-on-tone or color graphs, charts and/or pictures, which have been reproduced in black and white.

- This document is paginated as submitted by the original source.

- Portions of this document are not fully legible due to the historical nature of some of the material. However, it is the best reproduction available from the original submission.

NASA Contractor Report 167976

DESIGN OF HYDRAULIC OUTPUT STIRLING ENGINE

William M. Toscano, Andrew C. Harvey, and Kangpil Lee

Foster-Miller, Inc.
Waltham, Massachusetts

January 1983

Prepared for

NATIONAL AERONAUTICS AND SPACE ADMINISTRATION
Lewis Research Center
Under Contract NAS3-22230

FOREWORD

The design team consisted of Foster-Miller, Inc. of Waltham, Massachusetts, and Sunpower, Inc. (SUNPOWER) of Athens, Ohio. The participants of the program included:

Foster-Miller

William M. Toscano, Program Manager
Andrew C. Harvey
Kangpil Lee
Ira P. Krepchin

SUNPOWER

William T. Beale, Principal Investigator
David Gedeon
Gary J. Wood

CONTENTS

CONTENTS (Continued)

EXECUTIVE SUMMARY

ES.1 INTRODUCTION

ES.1.1 Background and Objectives

A free piston Stirling engine (FPSE) executes a practical Stirling cycle without having a crank mechanism. Instead, the motions of the two reciprocating elements, the piston and the displacer are intimately related to the thermodynamics and fluid dynamics of the engine working gas.

The FPSE has many potential advantages over conventional kinematic Stirling engines. They are:

- Simplicity
- Freedom from leakage
- Potential self starting
- Low noise
- Long life.

A hydraulic power system powered by a FPSE may be a very attractive alternative for stationary or vehicular applications.

Sunpower, Inc., of Athens, Ohio had designed and built a 1 kW FPSE (RE-1000) for research testing by NASA-Lewis. As shown in Figure ES-1, the RE-1000 had a dashpot in order to dissipate the output power.

The objective of the present program is to design and build a suitable hydraulic output mechanism for the RE-1000 FPSE to demonstrate feasibility, efficiency, and potential practicality. This report describes the first phase of the program, design of modifications to this particular engine.

ES.1.2 Design Specifications

The present design of the hydraulic output mechanism has to satisfy the following requirements:

- The design should be easily integrable with the government-owned RE-1000 FPSE.
- Preferably minimal or no modification of the hot section of the RE-1000 should be required.

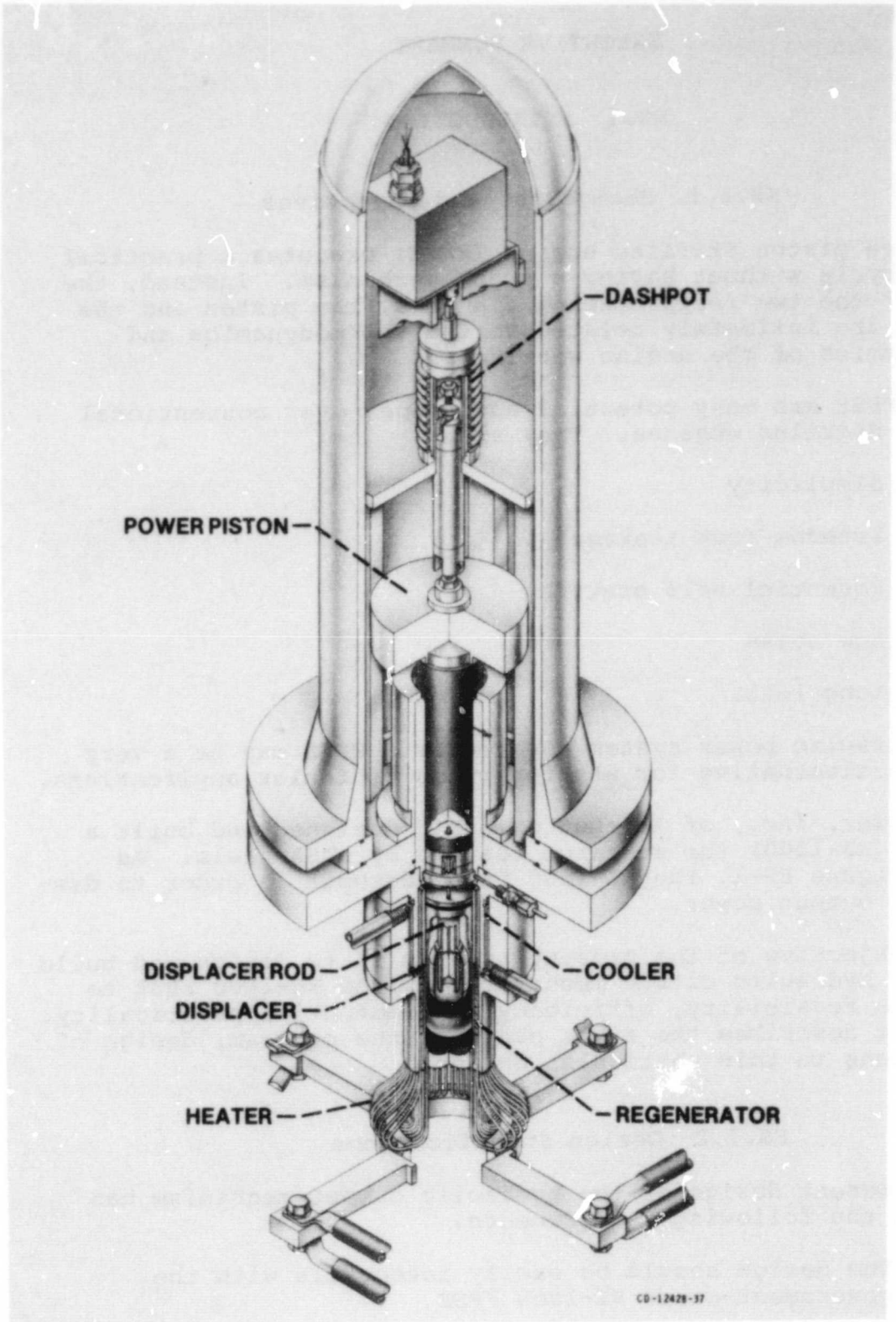

Figure ES-1. - Cutaway view of the RE-1000 Free Piston, Free Displacer Stirling engine built by Sunpower.

- The RE-1000 FPSE should be coupled to the hydraulic fluid through a flexible hermetic interface.
- The following pressure and temperatures are to be used for design point.
  1. Heater tube temperature, 650°C
  2. Coolant temperature, 30°C
  3. Working gas charge pressure, 70 bar.
- The design approach should be scaleable over the power range of 65 to 400 kW.
- The flexible interface should have a fatigue life in excess of 500 hr of operation for test purposes; yet have the potential to design for much longer lifetime.

ES.1.3 Program Description

The program consisted of three tasks. Table ES-1 shows each of the tasks divided into specific subtasks.

TABLE ES-1. - DESCRIPTION OF THE PROGRAM BY TASKS

Task I	Preliminary Analysis and Concept Selection
I.1	Preliminary Systems Analysis
I.2	Analysis and Design of Diaphragm/Bellows
I.3	Development of Three Candidate Design Concepts
I.4	Evaluation and Comparison
I.5	Design Review Meeting
Task II	Detailed Design
II.1	Detailed Design Analysis
II.2	Design Optimization
II.3	Sensitivity Analysis
II.4	Detail Design Review Meeting
II.5	Final Design and Detail Drawings
Task III	Reporting Requirements
III.1	Monthly Reports
III.2	Design Review Meetings I and II
III.3	Final Report

ES.2 PRELIMINARY DESIGN

ES.2.1 Description of System Concepts

Three candidate system concepts were prepared. Each are described below.

Candidate design No. 1. - As shown in Figure ES-2, this design satisfies the requirements and objectives of the program. This design requires a single diaphragm, two accumulators, and two check valves. One disadvantage of this concept is that the maximum hydraulic pressure is limited to approximately the maximum engine pressure.

Candidate design No. 2. - This is the simplest design with diaphragm/bellows interface that can provide the high pressure hydraulic output directly as shown in Figure ES-3 without using an inefficient hydraulic pump-motor combination.

Candidate design No. 3. - The design shown in Figure ES-4 is the best near-term candidate. It does not involve any major changes in the RE-1000 FPSE and even retains the solid piston. The gas isolation bladder seems much easier to design than diaphragms or bellows for design No. 1 or No. 2 since there will be practically no pressure differential across the bladder.

ES.2.2 Dynamic Stability and the Pump Design

An important consideration in the design of a hydraulic output mechanism for a FPSE is the dynamic stability of the combined system. Figure ES-5 shows a power load matching between an ordinary hydraulic pump and the RE-1000 FPSE assuming a constant frequency. Because the slope of the FPSE power curve at the matching point is higher than that of the hydraulic pump load, any deviation of the piston stroke from the matching point will be amplified by the surplus in power if the stroke should increase, or by the shortage in power if the stroke should decrease.

Consequently, the system consisting of the RE-1000 FPSE and an ordinary hydraulic pump is inherently unstable.

In order for a hydraulic output to be inherently stable, the power load curve near the match point should look like the one shown in Figure ES-6 where the slope of load curve is higher than the slope of the engine power curve. In this case, any deviation of stroke from the matching point will be corrected by the shortage

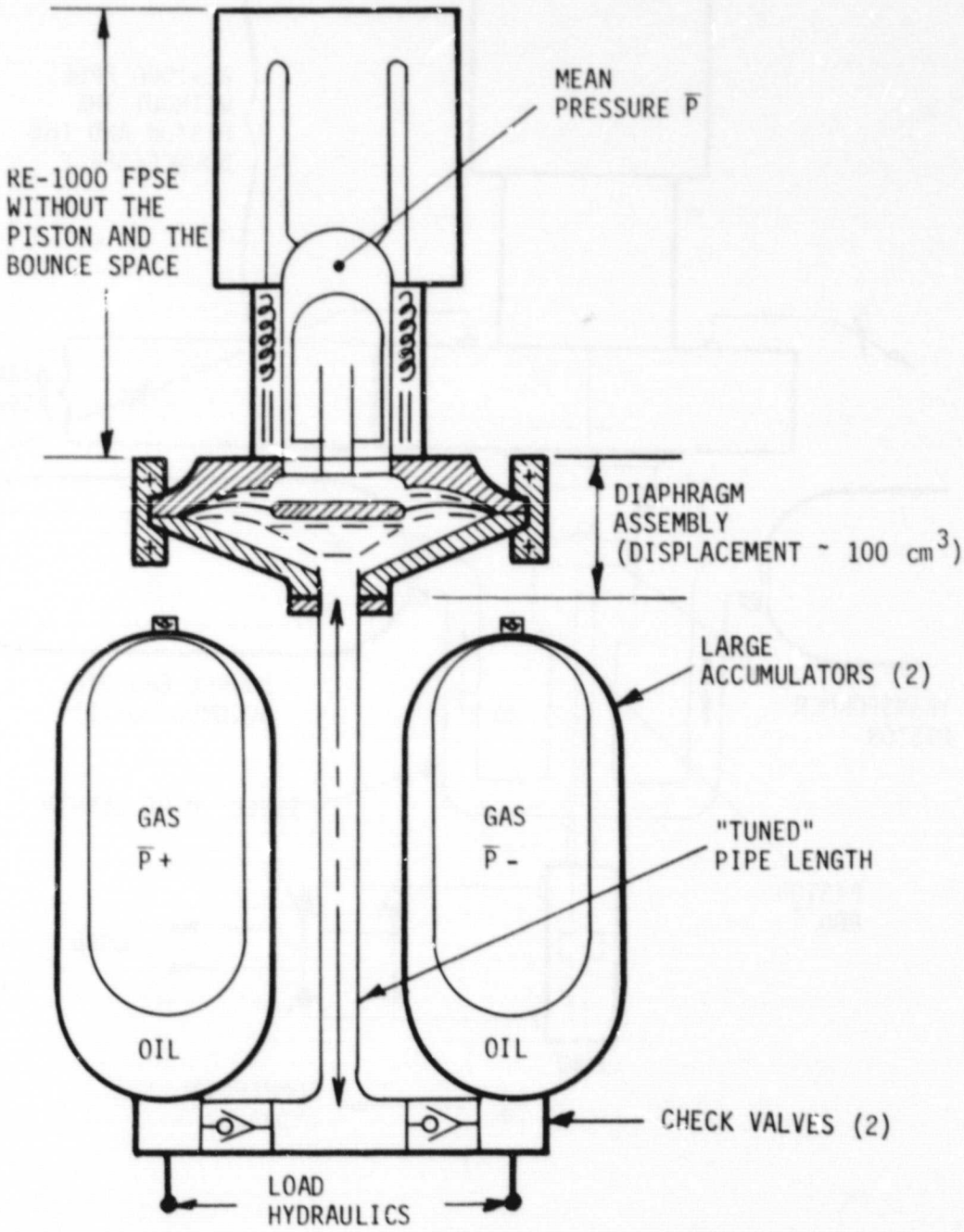

Figure ES-2. - Candidate design No. 1 with a diaphragm interface and a liquid piston driven null-center band pump output.

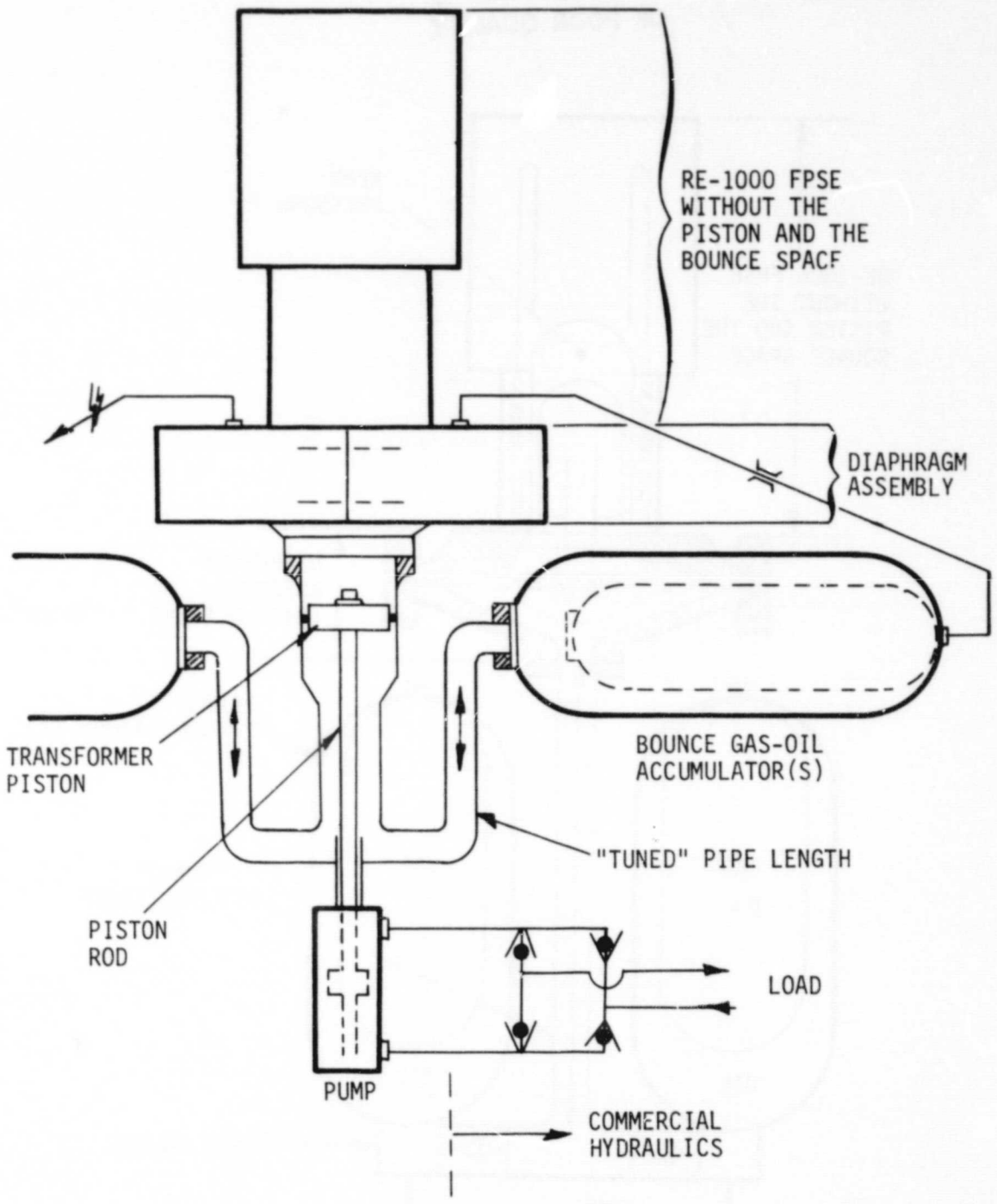

Figure ES-3. - Candidate design No. 2 with a diaphragm interface transformer piston, and a null-center band pump output.

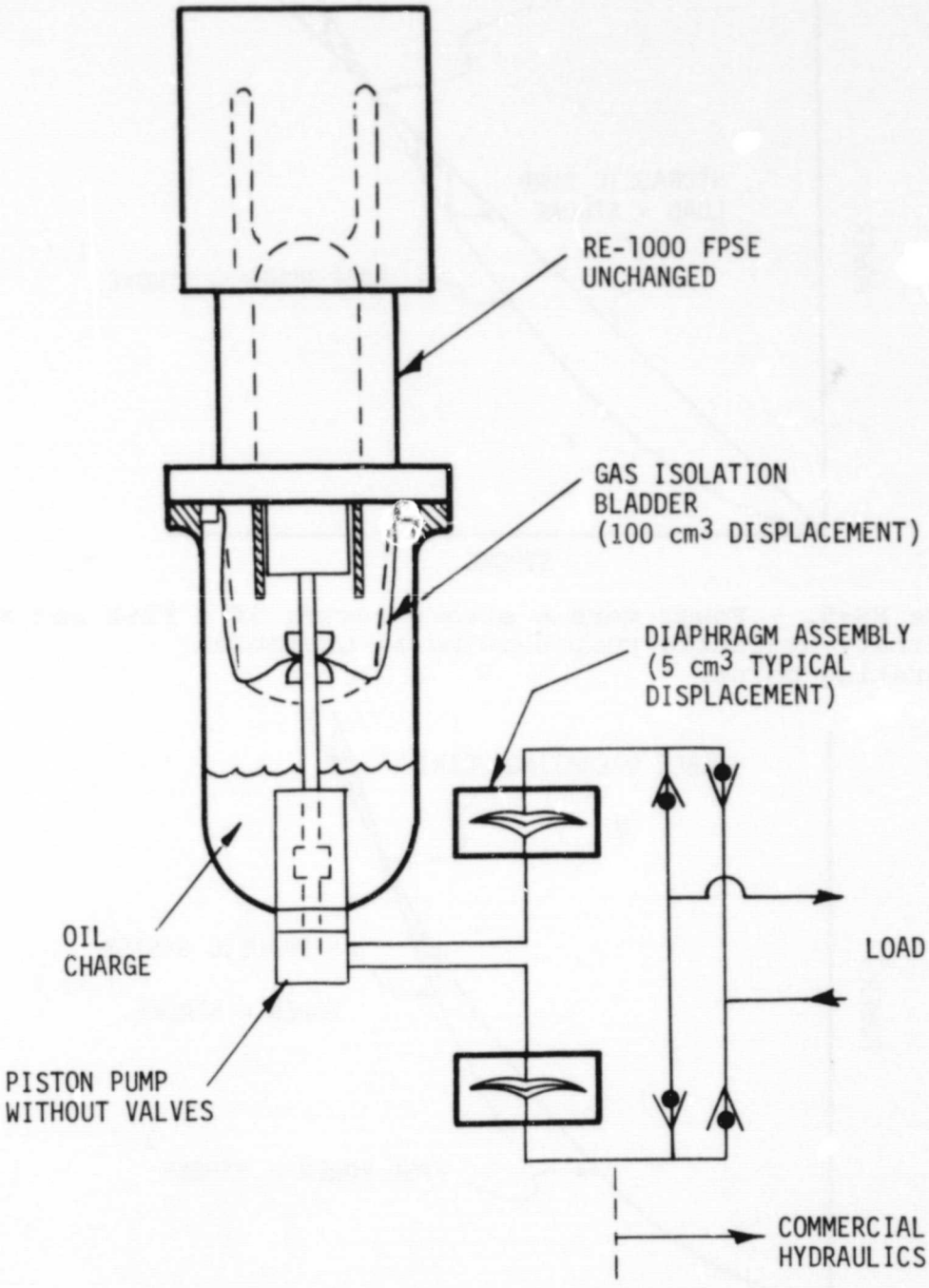

Figure ES-4. - Candidate design No. 3 with the engine piston, an isolation bladder, and a null-center band pump output.

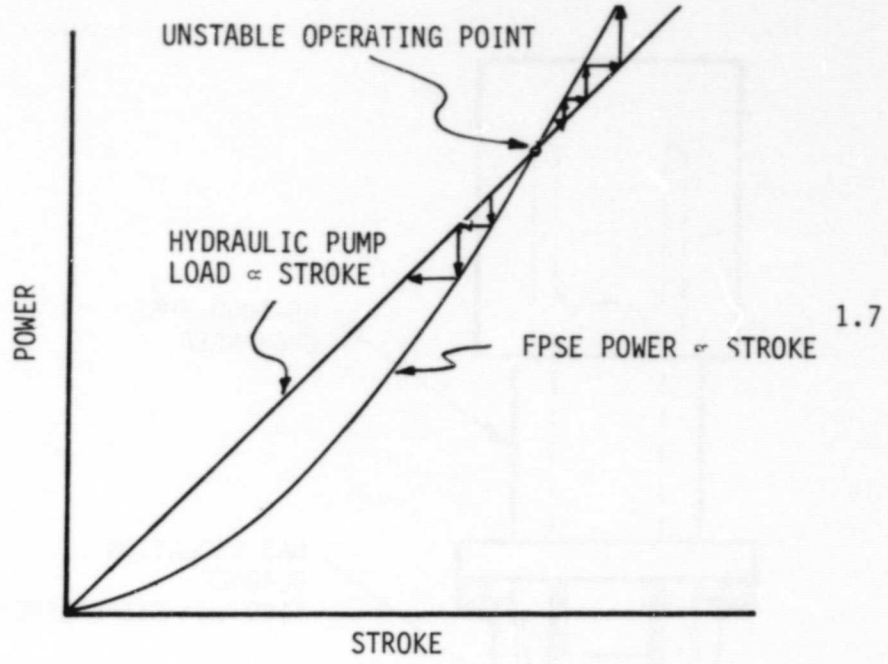

Figure FS-5. - Power versus stroke curves of a FPSE and an ordinary hydraulic pump showing an unstable operating point.

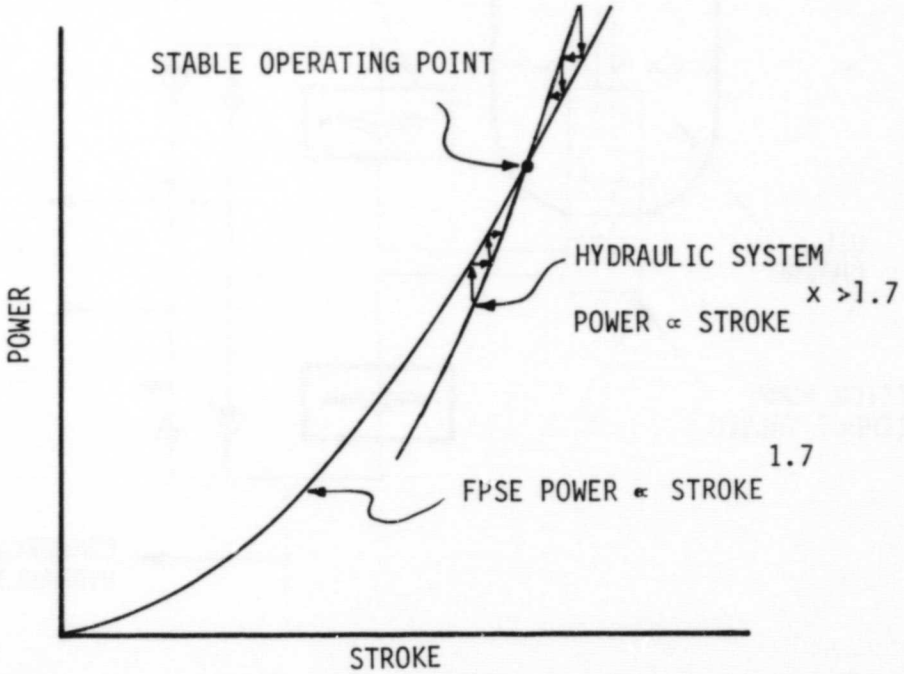

Figure ES-6. - Power versus stroke curves of a FPSE and an acceptable hydraulic pump showing a stable operating point.

in power if the stroke should increase, or by the surplus in power if the stroke should decrease.

The three hydraulic output methods shown in Figures ES-7, ES-8, and ES-9 satisfy the above criteria and are inherently stable. The design shown in Figure ES-7 is for the candidate design No. 1, whereas the designs shown in Figures ES-8 and ES-9 are applicable to both the candidate designs No. 2 and No. 3.

The volume displacement of the stabilizer diaphragm shown in Figure ES-7 is less than that of the main engine diaphragm. If the main diaphragm displacement is less than that of the stabilizer diagram, there will be no pumping. In other words, this pump has a dead band in the intermediate stroke region.

Figure ES-8 shows the schematic of a "double" acting hydraulic pump which also has a mid-stroke hydraulic dead band. The dead band is achieved by properly positioning port holes.

Figure ES-9 shows the schematic of a "single" acting pump. It uses essentially the same concept as the "double" acting pump except that it has a mean pressure reservoir.

ES.2.3 Comparison of System Concepts and Final Selection

Of the three candidate design concepts described in the previous section, the candidate design No. 1 was eliminated. The reasons for its elimination are:

- Limited pressure output.
- Low efficiency if a hydraulic motor pump is used for pressure boosting.

The remaining concepts to be examined were candidate design No. 2 having a flexible interface with the working gas (diaphragm or bellows), and the candidate design No. 3 with the piston retained. Table ES-2 presents a qualitative comparison of the concepts by listing their relative advantages and disadvantages.

The bellows version was discarded because of the following reasons:

- High projected cost in manufacturing and quality control.

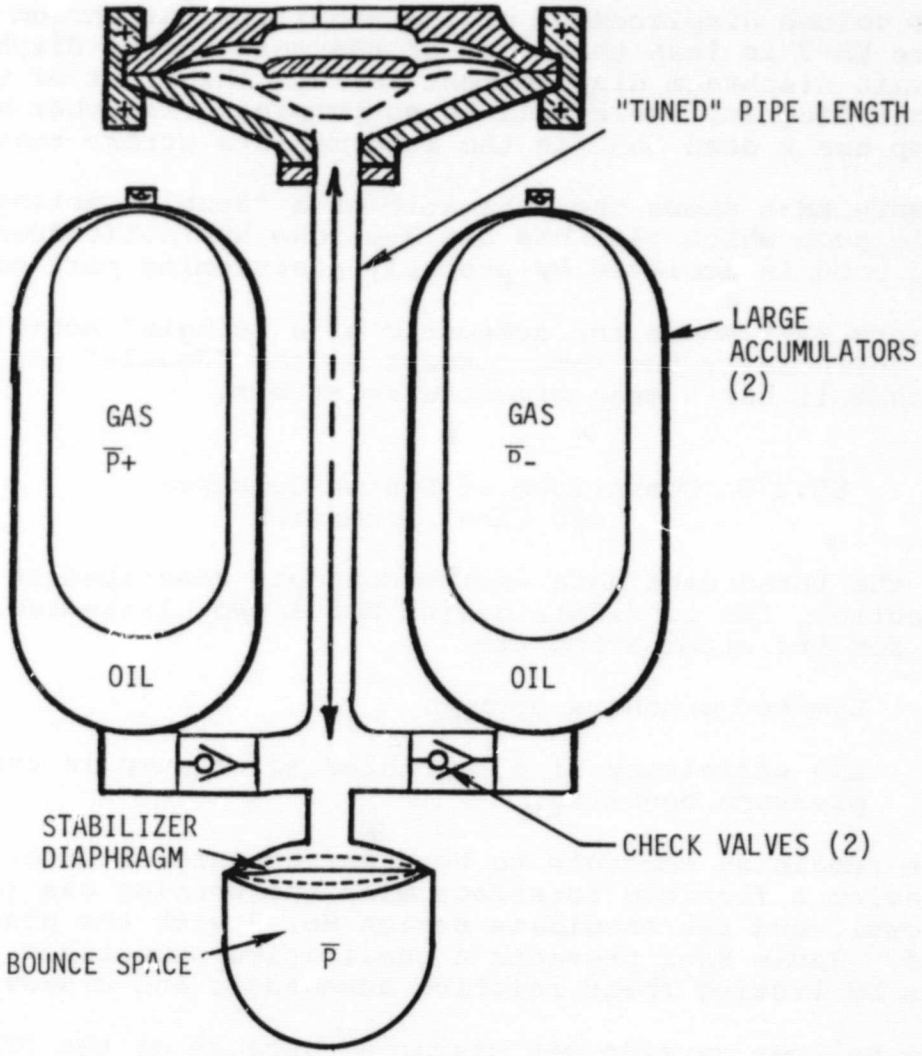

Figure ES-7. - Liquid piston driven hydraulic pump with a null-center band.

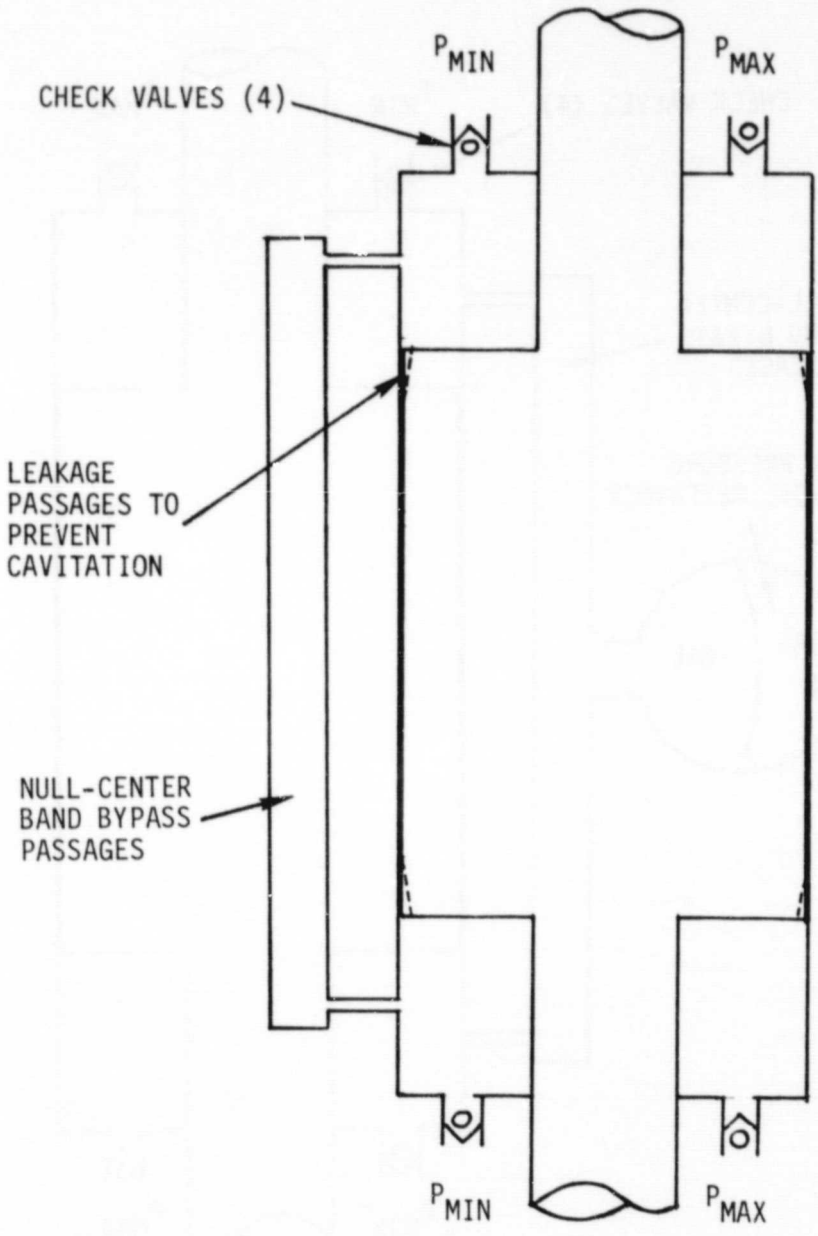

Figure ES-8. - Double acting hydraulic pump with a null-center band.

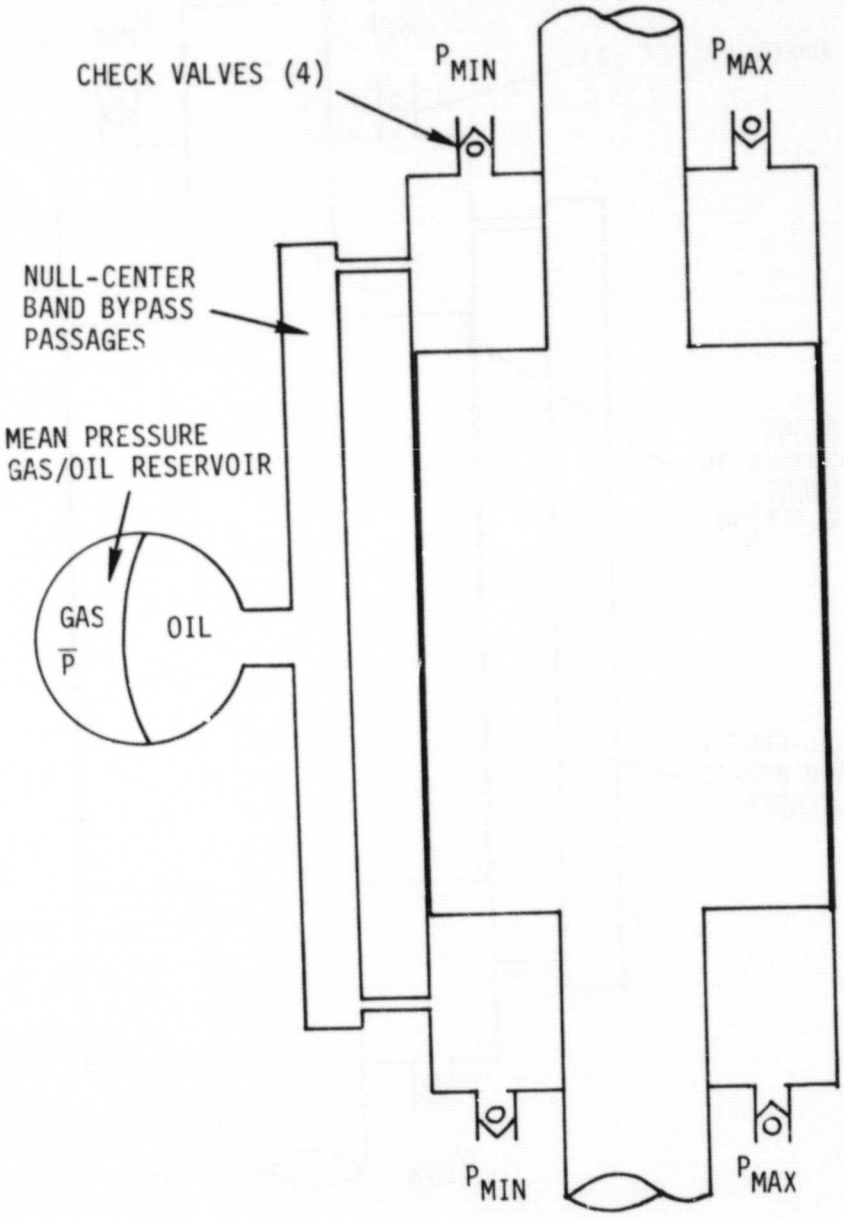

Figure ES-9. - Single acting hydraulic pump with a null-center band.

TABLE ES-2. - COMPARISONS OF CANDIDATE DESIGNS OF THE HYDRAULIC OUTPUT SYSTEM FOR RE-1000 FPSE

Parameter	Evaluation		
	Flexible interface version		
	Diaphragm	Bellows	Piston version
Thermodynamic performance	Possibly acceptable only after considerable modification of RE-1000, but still below piston version level at best	Difficult to predict, probably as high as diaphragm engine at best	Acceptable
Dynamic stability	Good	Good	Good
Cost	Medium	Very high	Low
Reliability and life	Good	Poor	Very good
Scaleability	Poor (requires multiple diaphragms or huge diaphragms)	Good (reasonable diameter) but very high cost due to tooling required	Very good
Modification of RE-1000 required	Medium	Considerable	Minimal
Provision for pressure loss protection	Reasonably easy in both directions	Possible only in nested condition	Easy in both directions
Start-up, stop load following	Good using dead band hydraulic equipment		
Quality control of components	Good	Very difficult	Very good
Availability of components	Reasonably easy to manufacture	Very difficult to manufacture	Very easy to manufacture
Fluid squeezing losses	Can be minimal	Difficult design problem to make it minimal	None
Ease of active space cooling of compression	Good	Good	Poor
Decision	Recommended	Not recommended	Recommended

- Difficulty of providing overpressure protection.
- Fluid squeezing loss problems.

Of the two remaining candidate designs, the diaphragm version was selected to be developed further. The rationale was that the diaphragm version would provide more opportunities for technical advancement than the piston version.

ES.2.4 Preliminary Dynamic and Thermodynamic Analysis

The objectives of the preliminary analyses were:

- To check the compatibility of the Foster-Miller designed hydraulic pumps with the RE-1000 FPSE and to determine if the overall system is dynamically stable.
- To obtain the performance trend for the RE-1000 FPSE integrated with the pump.
- To help the design effort by indicating necessary modifications as the design evolved.

ES.2.4.1 Dynamic analysis. - A FPSE dynamic analysis, which had been developed by Sunpower, was used to investigate the dynamic compatibility of the RE-1000 FPSE to particular hydraulic loads. The analysis utilizes simplified thermodynamics.

From the dynamic analysis, the following were learned:

- The system consisting of the RE-1000 FPSE and Foster-Miller designed hydraulic pump is dynamically stable.
- At high power output, the displacer collides with the piston. This can be prevented by shortening the piston or moving its position.
- The nonsinusoidal motion of the piston can be corrected by increased stored energy in the system.
- The analysis was for the piston version of the RE-1000 FPSE, but the trends should also apply to the flexible interface version with equivalent inertial energy.

ES.2.4.2 Thermodynamic analysis. - A number of computer simulations were run of the RE-1000 FPSE engine to determine the effects of increased heat transfer in the compression space resulting from

the substitution of a diaphragm for the current piston. The simulations employed Sunpower's third order code with constrained dynamics of piston and displacer.

The conclusions of the preliminary thermodynamic analysis were as follows:

- All components of the Stirling cycle must be considered together before any conclusions can be drawn regarding the merits of an increased heat transfer to approach isothermalization.

- Merely increasing the heat transfer in the compression space of a Stirling engine is not sufficient to guarantee an improvement in performance. The machine must be reoptimized in all its aspects before near isothermalization can be expected to yield a benefit.

- The heat transfer in the diaphragm area should be carefully investigated, because design and performance depend strongly on prediction of this phenomenon.

- Net heat transfer from, or cooling of the diaphragm compression space appears necessary to achieve good performance.

ES.3 DETAIL DESIGN

ES.3.1 Description of the Recommended Design

The final design incorporates the following:

- Modular sections and simple, accessible parts for research testing.
- Interchangeability with current RE-1000 FPSE output section without disturbing engine section.
- Either vertical axis hydraulic assembly, or horizontal assembly to demonstrate dynamic balancing better.
- Displacement sensors on all engine moving parts and hydraulic pump.
- Conservative design for low stress and low cost.

The design is described referring to Figure ES-10, which is a simplified schematic of the actual design. Basically the system operates as follows:

- Engine gas displaces oil trapped between the engine diaphragm and the bottom end of the transmission piston.
- The transmission piston displaces oil trapped on the other (top) end, thereby displacing the bounce gas diaphragm.
- No significant net power is transferred to this oil or the diaphragms, and the effective mass of this piston and oil is insufficient to provide the desired cyclic motion in combination with engine and bounce gas springs.
- Additional effective piston mass is provided in the counter balance assembly.
- The annular piston masses are forced by the surrounding trapped oil to move in opposite directions synchronously so that the entire engine system is effectively balanced dynamically.
- If only one mass is clamped to the piston rod and oil is free to flow around it in the same section, then unbalanced dynamic operation results.

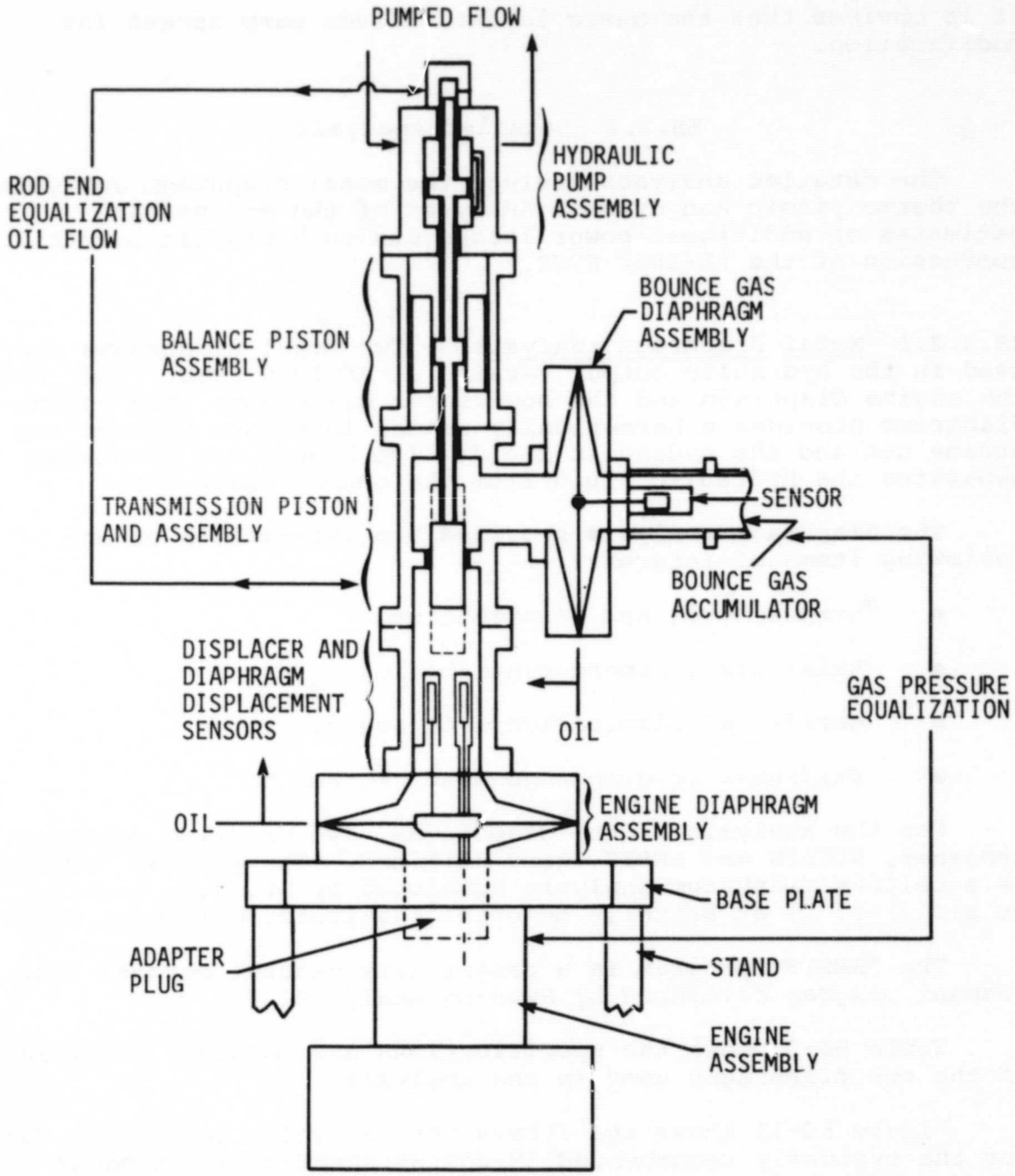

Figure ES-10. - Simplified schematic of the recommended hydraulic output system design.

- The piston rod transmits net power to the hydraulic oil pump, which is isolated from the diaphragm oil.

It is obvious that the basic layout affords easy access for modification.

ES.3.2 Detailed Analysis

The detailed analyses include the metal diaphragm analysis, the thermodynamic and dynamic analyses of the engine, and estimates of additional power losses due to hydraulic output conversion of the RE-1000 FPSE.

ES.3.2.1 Metal diaphragm analysis. - Two metal diaphragms are used in the hydraulic output version of RE-1000 FPSE. They are the engine diaphragm and the bounce gas diaphragm. The engine diaphragm provides a hermetically sealed interface between the engine gas and the hydraulic fluid. The bounce gas diaphragm separates the hydraulic fluid from the bounce space gas.

The diaphragm analysis provided the information on the following items of interest:

- Stress level and distribution.
- Axial displacement distribution.
- Meridional displacements of edges.
- Stiffness of diaphragm near TDC and BDC.

For the analysis of the diaphragms, two existing computer programs, NONLIN and ANSYS, were utilized. The program "NONLIN" is a bellows/diaphragm analysis developed by Dr. J.F. Lestingi, et al. (ref. 1) at Battelle Memorial Institute, Columbus, Ohio.

The "ANSYS" program is a proprietary general purpose finite element program developed by Swanson Analysis, Inc.

Table ES-3 shows the specifications and boundary conditions of the two diaphragms used in the analysis.

Figure ES-11 shows the stress versus cycles to failure data for the typically recommended AM 350 SS sheet of 1.016 mm in thickness. The maximum stresses of the diaphragms are 100 ∿ 110 MPa which gives the safety factor of at least five with respect to the endurance limit of 590 MPa for AM 350 SS.

TABLE ES-3. - SPECIFICATIONS AND BOUNDARY CONDITIONS FOR THE DIAPHRAGM ANALYSIS, NONLIN

Specifications	Engine Diaphragm	Bounce gas diaphragm
Outer diameter (cm)	20.32	20.32
Inner diameter (cm)	6.35	2.45
Thickness (cm)	0.0508	0.0508
Youngs Modulus, E (MPa)	2.069×10^5	2.069×10^5
Poisson's Ratio, ν	0.27	0.27
Boundary conditions		
Outer edge	Simply supported to the casing	Simply supported to the casing
Inner edge	Simply supported to the center plug which moves with the diaphragm	Axially clamped to and radially guided by the center plug which moves with the diaphragm
Volume amplitude at design point (cm^3)	40	40

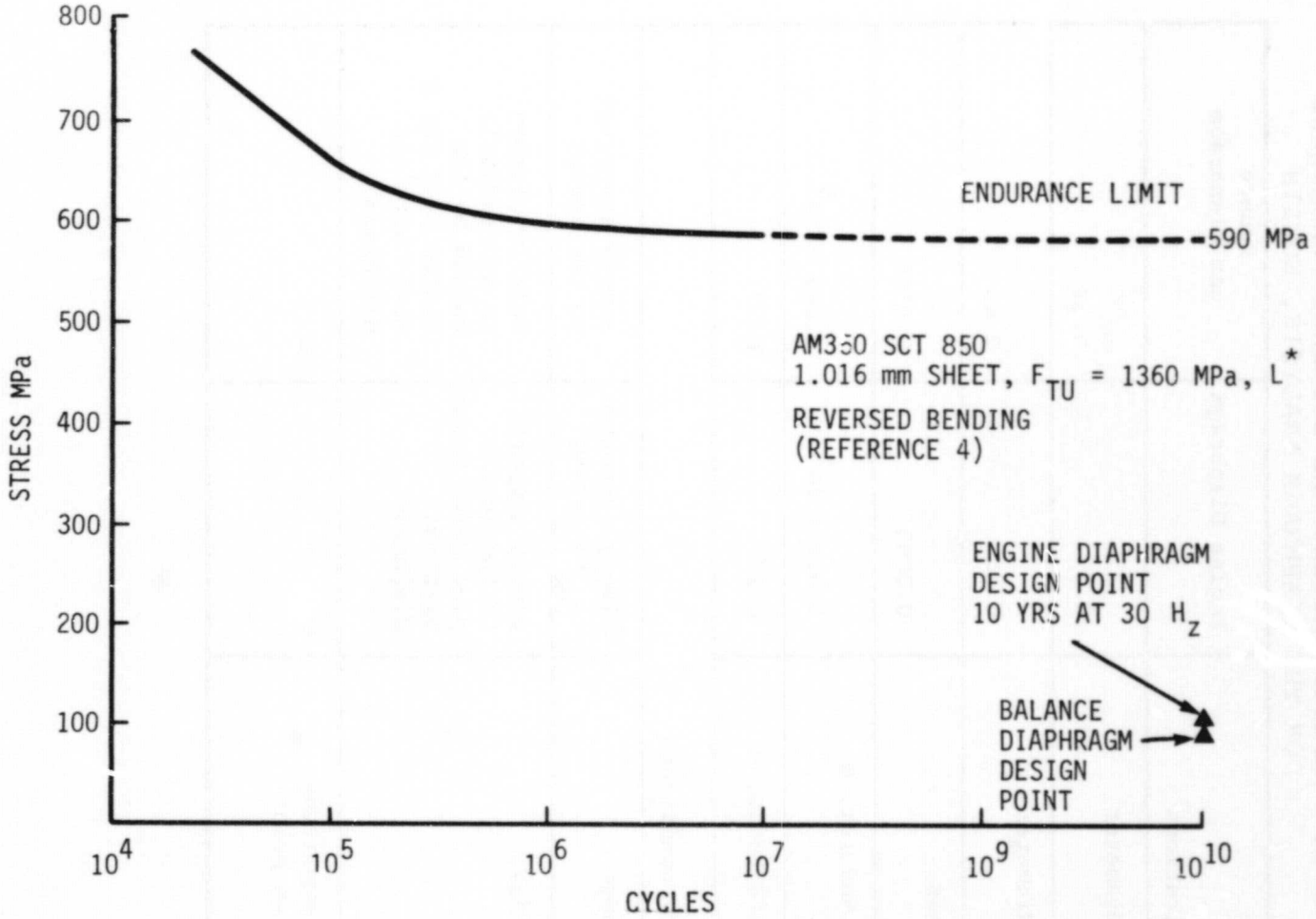

*ULTIMATE TENSILE STRENGTH IN LONGITUDINAL DIRECTION OF ROLLING.

Figure ES-11. - Stress versus cycles of failure for AM 350 SS sheet.

This means that as long as the diaphragms are fabricated without defects, they will last indefinitely under normal operating conditions. This probably is also true for many other more convenient sheet materials.

ES.3.2.2 Thermodynamic performance predictions. - For the detailed analysis of the hydraulic output Free Displacer Stirling engine, the Sunpower Third Order Stirling engine analysis was utilized. This has two modes of operation: the constrained mode uses predetermined dynamics of reciprocating components. The unconstrained mode simultaneously solves the dynamics and thermodynamics. The highly impulsive or step-function-like nature of the load necessitated the use of the unconstrained mode to closely simulate the actual processes of the engine. The less expensive, constrained mode analysis was used to obtain the performance trend and to perform a sensitivity analysis of important operating parameters.

Within the scope of the design program, there are two parameters significantly affecting the power output and the efficiency of the engine: the displacer phase angle and the cylinder or diaphragm-space heat transfer.

The displacer phase angle is closely linked to the overall engine dynamics. Varying the displacer phase angle will change the frequency slightly and the amplitudes of the piston and the displacer, the pressure wave phase angle, and consequently the engine output performance.

With the increased heat transfer area and the extremely narrow spaces in the diaphragm region of the compression space, estimation of the magnitude of the heat transfer has significant consequences in the predicted performance of the engine.

Hence, the analyses were performed iteratively with particular attention to the combined effect of displacer phase angle and the compression space heat transfer. Note that the diaphragm heat transfer analysis is original, based on limited related data; actual levels remain to be demonstrated as a significant part of the entire FPSE research program.

The results of the third order analysis included:

- The base-point, or reference simulations of the standard RE-1000 FPSE and the diaphragm piston engine.
- The sensitivity analysis of the diaphragm piston Stirling engine with respect to the cylinder heat transfer, h, the phase angle of the displacer, ϕ_d, and the pump load force, F_{load}.

- The predicted performance of the diaphragm piston Stirling engine.

Figure ES-12 illustrates the parametric effect of heat transfer in the compression space. Included in Figure ES-12 are P-V work, indicated efficiency and availability loss for the compression space as a function of the rate of heat transfer. The following observations were made:

- The P-V power near the adiabatic extreme (small hA) is higher than that of the isothermal extreme (large hA) This is because the mass flow in and out of the compression space for the near adiabatic case is higher than that of the near isothermal.

- The efficiency for the near isothermal case is much higher than that of the near adiabatic case.

- In the intermediate region between the adiabatic and the isothermal case, the efficiency and the power reduce to their respective minimum values. Unfortunately, the diaphragm engine appears to fall in this broad region, and there seems no obvious, simple way to avoid it.

Figure ES-13 shows the efficiency and power of the diaphragm engine with respect to the displacer phase angle based on constrained mode third order analysis. The maximum efficiency occurs near 60 deg and the maximum power occurs near 80 deg. Figure ES-14 shows a simple modification of the displacer rod which would increase the gas spring volume to achieve 8[illegible] phase angle.

In Table ES-4, the predicted engine performances are presented. They include the results from separate analyses of losses due to viscous friction, leakage, and pressure drop in the hydraulic section of the engine. The improvement of performance due to the simple displacer rod modification is notable. It is predicted that the hydraulic output Stirling engine, as designed, is capable of delivering 1.87 kW brake power at 29.7 percent efficiency.

Considering that this particular engine design is not yet optimized, the predicted level of performance looks promising.

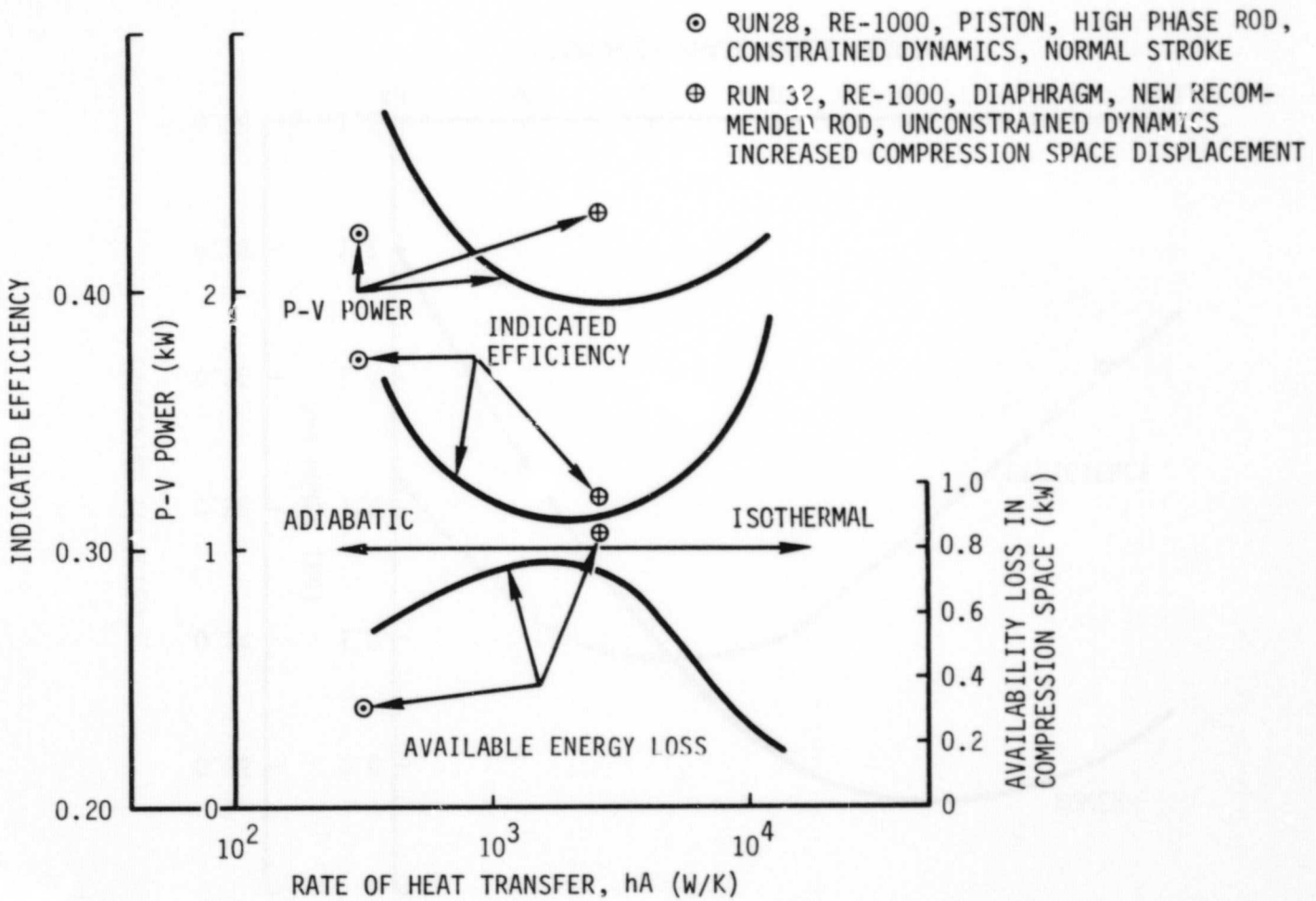

Figure ES-12. - Predicted performance of the Diaphragm Piston, Free Displacer Stirling engine as a function of heat transfer in the compression space.

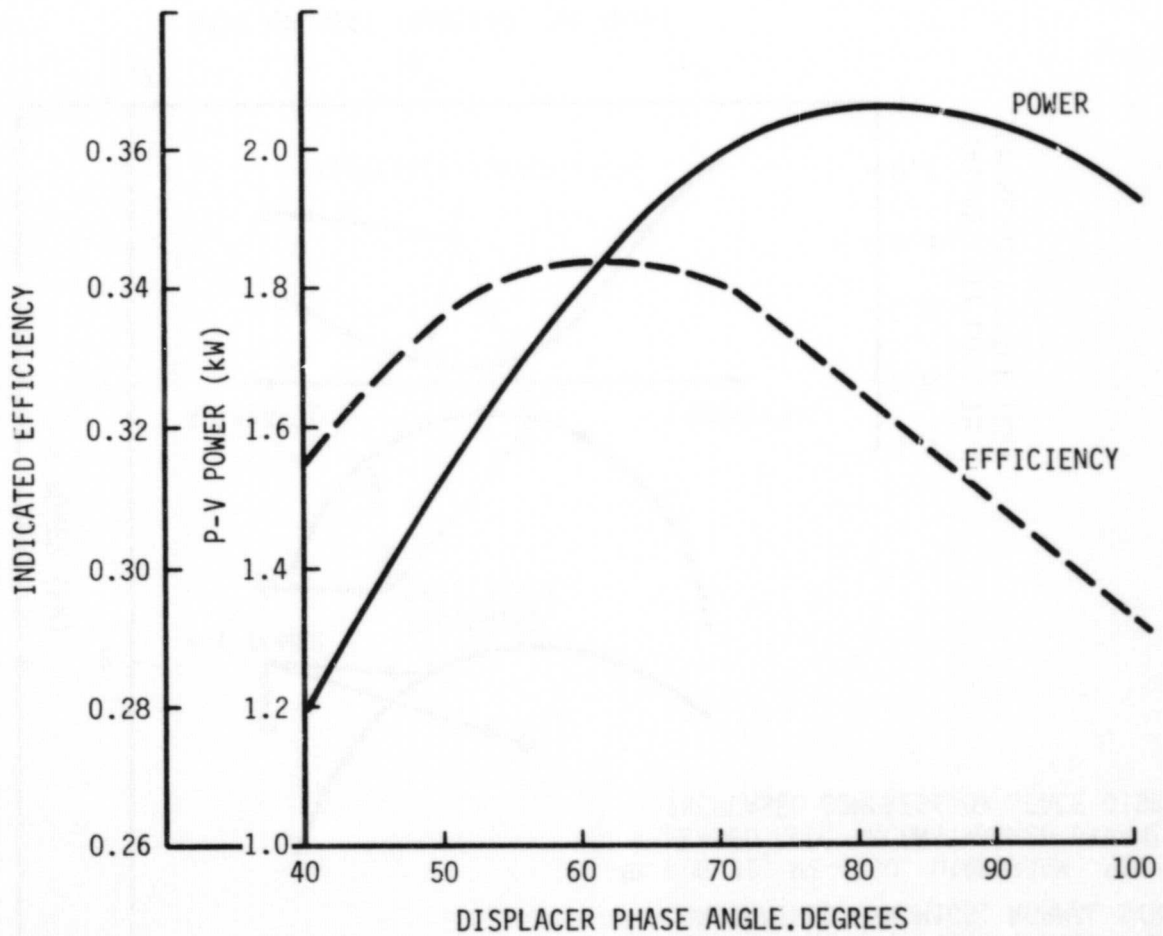

Figure ES-13. - Influence of displacer phase angle on the performance of the Diaphragm Piston, Free Displacer, hydraulic output Stirling engine.

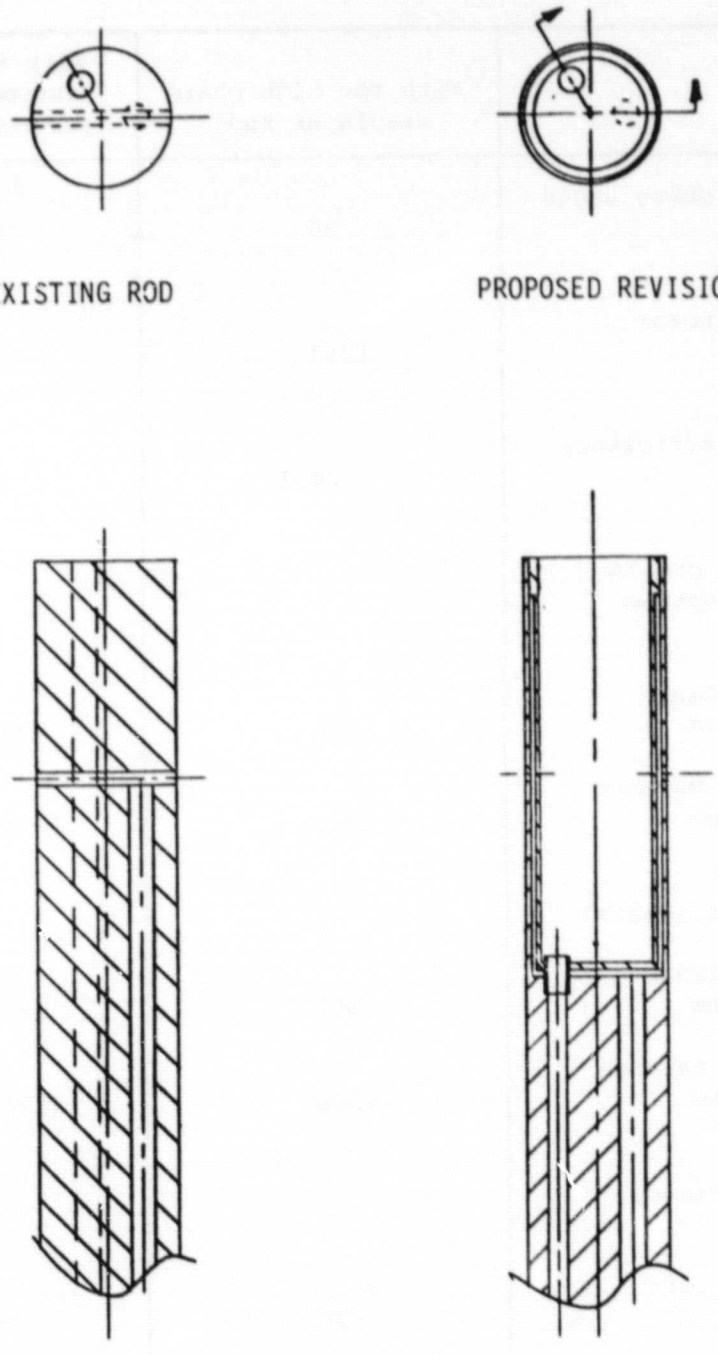

Figure ES-14. - Proposed displacer rod design to increase the gas spring volume.

TABLE ES-4. - PERFORMANCE PREDICTIONS OF DIAPHRAGM PISTON, FREE DISPLACER STIRLING ENGINE WITH NULL CENTER BAND HYDRAULIC PUMP OUTPUT

	With the high phase displacer rod	With the new recommended displacer rod
Displacer phase angle (degrees)	98	77
Indicated power (watts)	1210	2010
Indicated efficiency (percent)	24.2	32.0
Power loss due to hydraulic system (watts)		
With balance mechanism	212	212
Without balance mechanism	(142)	(142)
Brake power (watts)		
With balance mechanism	998	1798
Without balance mechanism	(1068)	(1868)
Brake Efficiency (percent)		
With dynamic balance	20	28.6
Without dynamic balance	21.4	29.7

1. INTRODUCTION

1.1 Background and Objectives

A free piston Stirling engine (FPSE) is a machine which executes a practical Stirling cycle without a crank mechanism. It was invented in the late 1950's by William Beale. The motion of the two reciprocating elements, the piston and the displacer is intimately related to the thermodynamics and fluid dynamics of the engine working gas.

The FPSE has many potential advantages over conventional kinematic Stirling engines. They are:

- Simplicity
- Freedom from leakage
- Potential self starting
- Low noise
- Long life.

A FPSE can provide electrical output by a linear alternator arrangement. It can also provide a hydraulic output by a hydraulic pump arrangement. A hydraulic power system coupled with a FPSE is a very attractive alternative for stationary or vehicular applications.

Sunpower, Inc., of Athens, Ohio, had designed and built a 1 kW FPSE having a load simulated by internal gas pumping the RE-1000 for research purposes at NASA-Lewis. Figure 1 shows the cutaway view of the RE-1000. The objective of the present program is to design a suitable hydraulic output mechanism for the RE-1000 to demonstrate analytically the feasibility of the hydraulic output FPSE.

1.2 Design Specifications

The present design of the hydraulic output mechanism has to satisfy the following requirements:

- The design should be easily integrable with the government-owned RE-1000 FPSE.
- Preferably minimal or no modification of the hot section of the RE-1000 should be required.

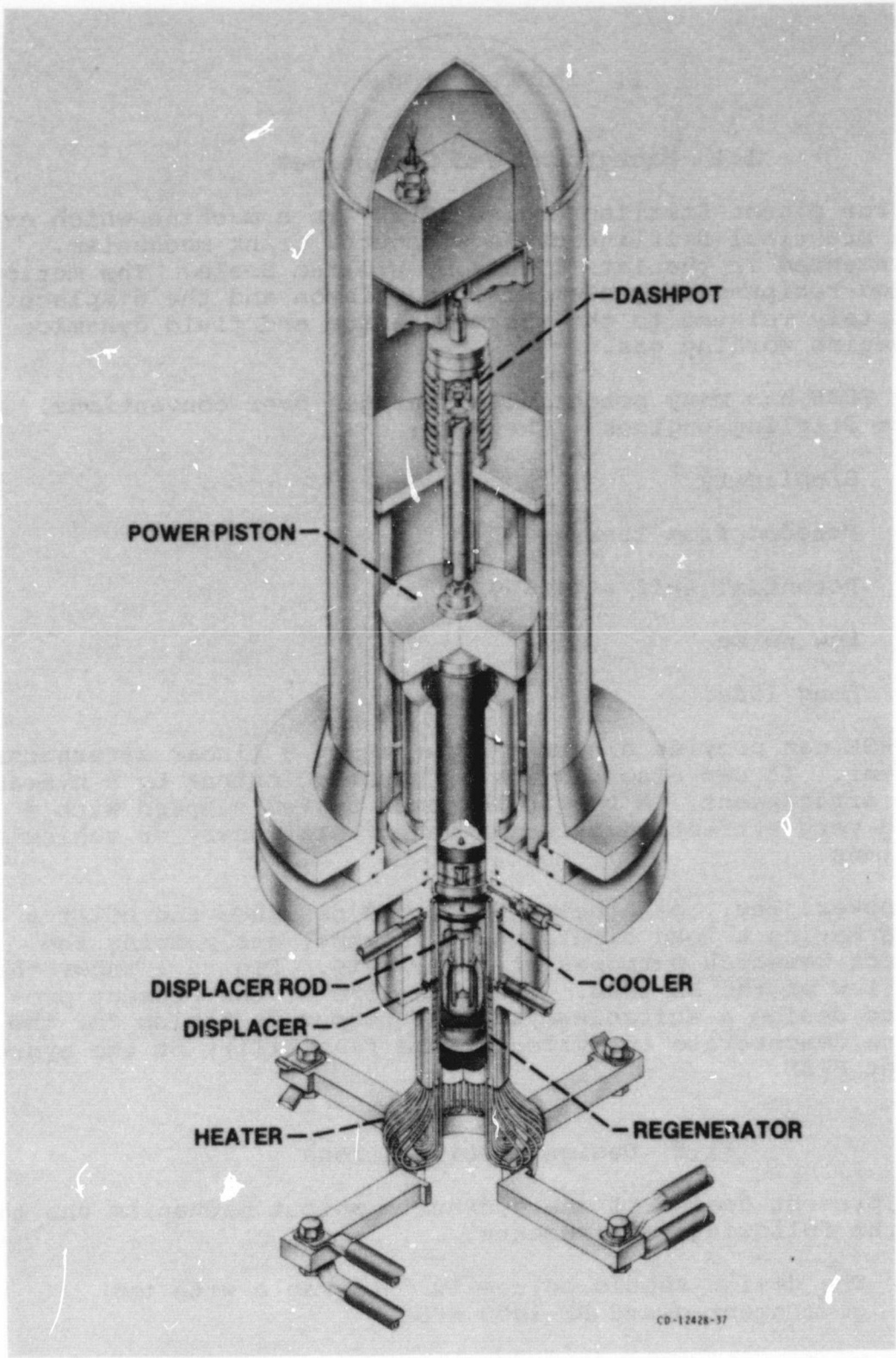

Figure 1. - Cutaway view of RE-1000 Free Piston, Free Displacer Stirling engine built by Sunpower.

- The RE-1000 FPSE should be coupled to the hydraulic fluid through a flexible hermetic interface.
- The following pressure and temperatures are to be used for design point.
  1. Heater tube temperature, 650°C
  2. Coolant temperature, 30°C
  3. Working gas charge pressure, 70 bar.
- The design should be scalable over the power range of 65 kW to 400 kW.
- The flexible interface should have a fatigue life in excess of 500 hr of operation for test purposes; yet have the potential to design for much longer lifetimes.

1.3 Program Description

The program consisted of three tasks. Table 1 shows each of the tasks divided into specific subtasks.

It is expected that a subsequent program will involve fabrication and initial hydraulic testing of components to be installed and tested on the RE-1000 at NASA-Lewis.

TABLE 1. - DESCRIPTION OF THE PROGRAM BY TASKS

Task I	Preliminary Analysis and Concept Selection
I.1	Preliminary Systems Analysis
I.2	Analysis and Design of Diaphragm/Bellows
I.3	Development of Three Candidate Design Concepts
I.4	Evaluation and Comparison
I.5	Design Review Meeting
Task II	Detailed Design
II.1	Detailed Design Analysis
II.2	Design Optimization
II.3	Sensitivity Analysis
II.4	Detail Design Review Meeting
II.5	Final Design and Detail Drawings
Task III	Reporting Requirements
III.1	Monthly Reports
III.2	Design Review Meetings I and II
III.3	Final Report

2. PRELIMINARY DESIGN

In this section, the candidate design concepts will be briefly described and be followed by the discussions of the system stability, pump design, trade-off studies, and the preliminary analyses

2.1 Description of System Concepts

Three system concepts are prepared. Each one will be described below.

Candidate design No. 1. - As shown in Figure 2, this design is the simplest one that satisfies the requirements and objectives of the program. This design requires a single diaphragm, two accumulators, and two check valves. One disadvantage of this concept is that the maximum hydraulic pressure is limited to approximately the maximum engine pressure. To overcome this disadvantage, an additional hydraulic pump-motor combination can be included; however, this will somewhat lower the overall efficiency of the system.

There seems to be no apparent obstacle to scale this design up to, say, 50 kW per cylinder. In order to provide a higher power output (up to 400 kW), multi-cylinder arrangements are necessary. In such cases, only a single set of high and low pressure accumulators will be needed, but the method of phasing the cylinders has to be devised.

Candidate design No. 2. - This is the simplest design with diaphragm/bellows interface that can provide the high pressure hydraulic output directly without the inefficient hydraulic pump-motor combination as shown in Figure 3. It is also scalable up to a reasonable size (50 kW per cylinder). In ganging up several cylinders together, a two cylinder unit has a definite advantage over other multi-cylinder units in that the two-cylinder arrangement eliminates the need for bulky bounce gas accumulators by using two cylinders hydraulically coupled out of phase by 180 deg. Other multi-cylinder units will require the means of maintaining proper phase angle between the cylinders.

Candidate design No. 3. - The design shown in Figure 4 is the best near-term candidate. It does not involve any major changes in the RE-1000 FPSE and even retains the solid piston. The gas isolation bladder seems much easier to design than diaphragms or bellows for design No. 1 or No. 2 since there will be practically no pressure differential across the bladder. Also, the high pressure, low volume transmission diaphragms are very

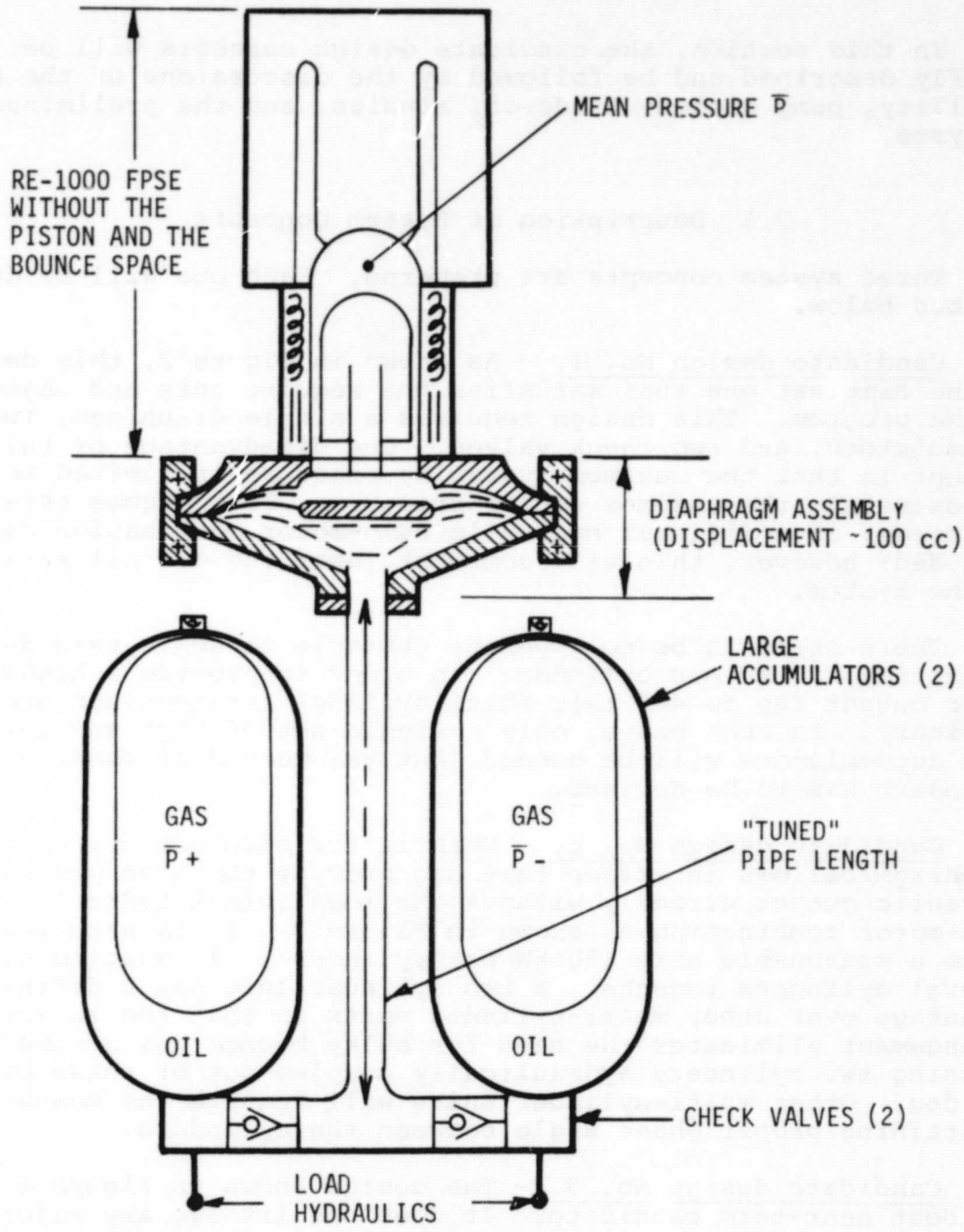

Figure 2. - Candidate design No. 1 with a diaphragm interface and a liquid piston driven null-center-band pump output.

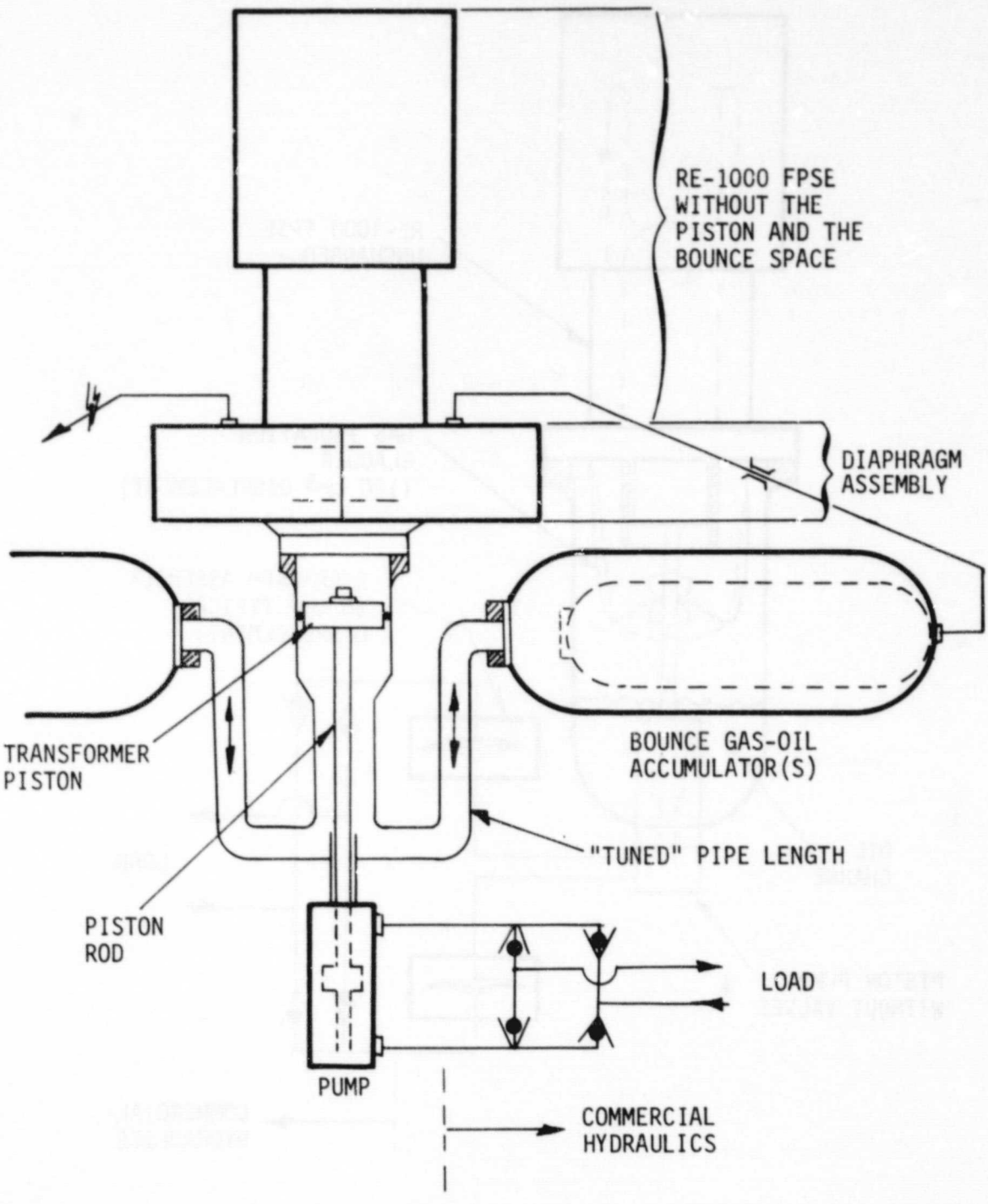

Figure 3. - Candidate design No. 2 with a diaphragm interface, transformer piston, and a null-center-band pump output.

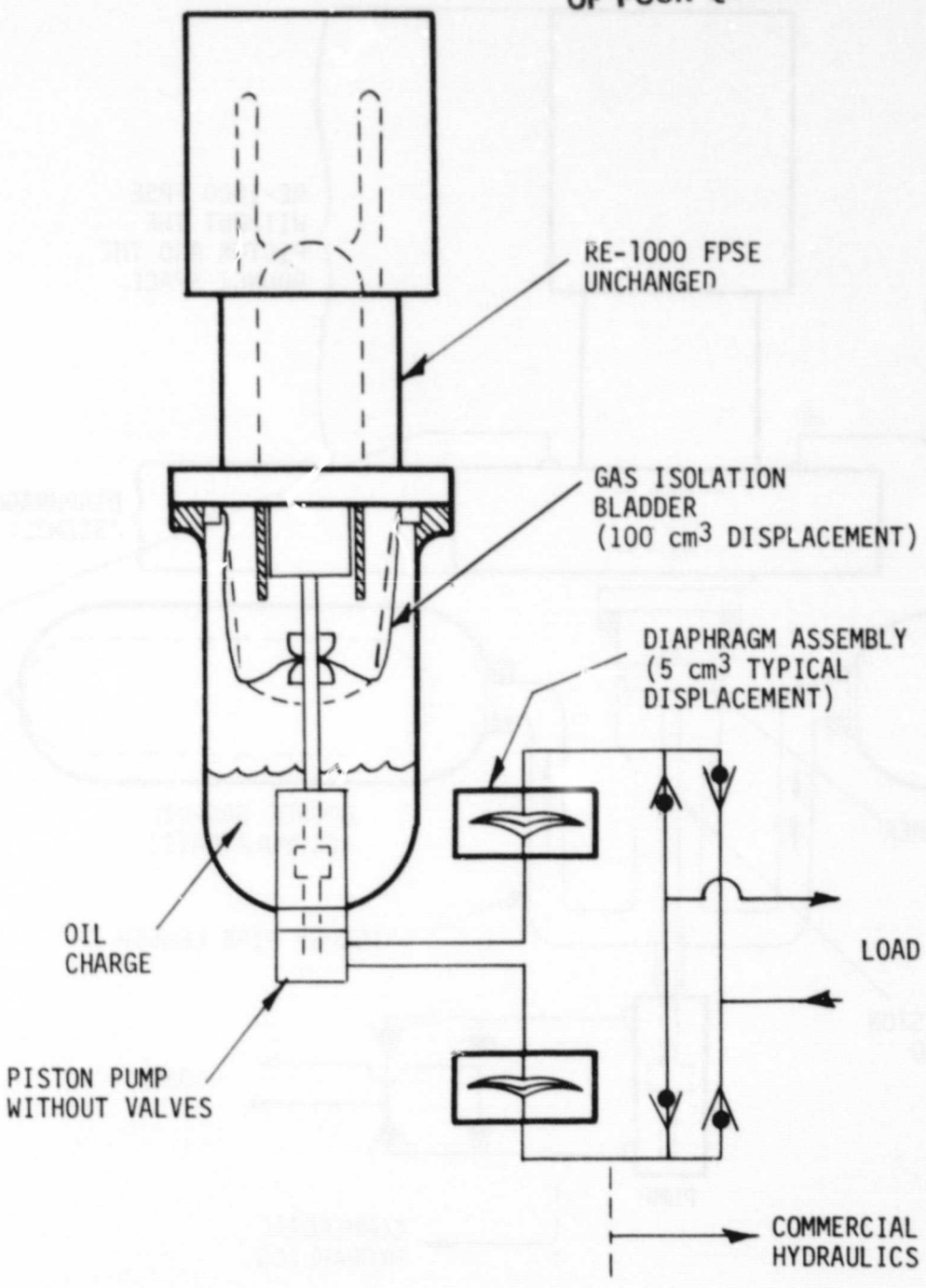

Figure 4. - Candidate design No. 3 with the engine piston, an isolation bladder, and a null-center-band pump output.

small in size and will cost much less than those for design No. 1 or No. 2. Compared to the other two candidate designs, this design will pose the fewest questions in scaling up among the three designs.

Again, the two cylinder arrangement will have definite advantages as in design No. 2; it will not require a large gas spring volume and will have an inherent phasing characteristic of the two cylinders if the gas spring volume is common to both.

2.2 Dynamic Stability and the Pump Design

An important consideration in the design of a hydraulic output mechanism for a FPSE is the dynamic stability of the combined system. Figure 5 shows a power load matching between an ordinary hydraulic pump and the RE-1000 FPSE assuming a constant frequency. Because the slope of the FPSE power curve at the matching point is higher than that of the hydraulic pump load, a small increment in stroke from the matching point will result in surplus power in the system which will cause an increase in stroke. The process repeats itself so that the stroke increases continuously until impact. Obviously, should the stroke decrease just a small amount from the matching point, the load absorbs more power than the engine puts out. This tends to load up the engine and shorten the stroke. The shortened stroke creates further power shortage. The process repeats itself so that the stroke decreases continuously until the engine stops.

Consequently, the system consisting of the RE-1000 FPSE and an ordinary hydraulic pump is inherently unstable. To make it stable requires a power/load feedback control system, which seems disadvantageous due to the complexity, cost, and poor response or inefficiency of typical Stirling engine control methods.

In order for a hydraulic output design to be inherently stable, the power load curve near the match point should look like the one shown in Figure 6 where the slope of load curve is higher than the slope of the engine power curve. In this case, any deviation of stroke from the matching point will be corrected by the shortage in power output if the stroke should increase or by the surplus in power if the stroke should decrease.

The three hydraulic output methods shown in Figures 7, 8, and 9 satisfy the above stability criteria and are inherently stable. Figure 10 shows the dynamic characteristics for the design of Figure 7. The design shown in Figure 7 is for the candidate design No. 1, whereas the designs shown in Figures 8 and 9 are applicable to both the candidate designs No. 2 and No. 3.

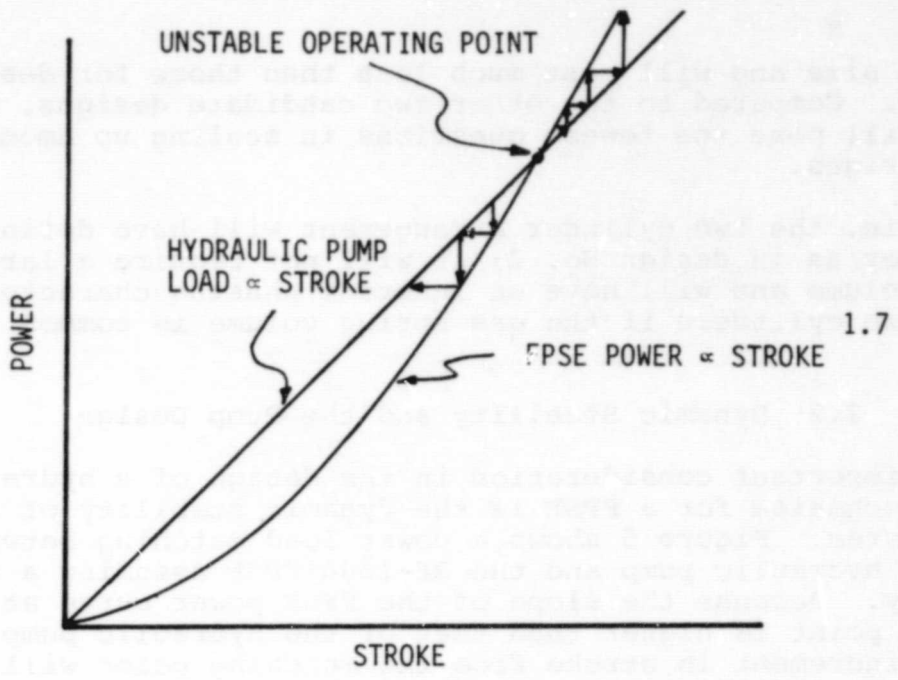

Figure 5. - Power versus stroke curves of a FPSE and an ordinary hydraulic pump showing an unstable operating point.

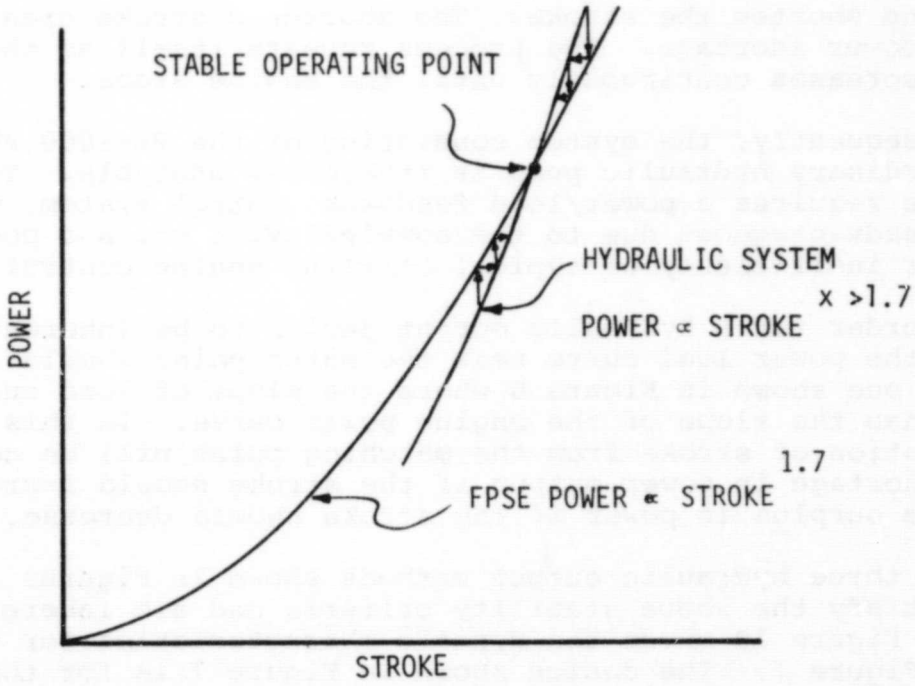

Figure 6. - Power versus stroke curves of a FPSE and an acceptable hydraulic pump showing a stable operating point.

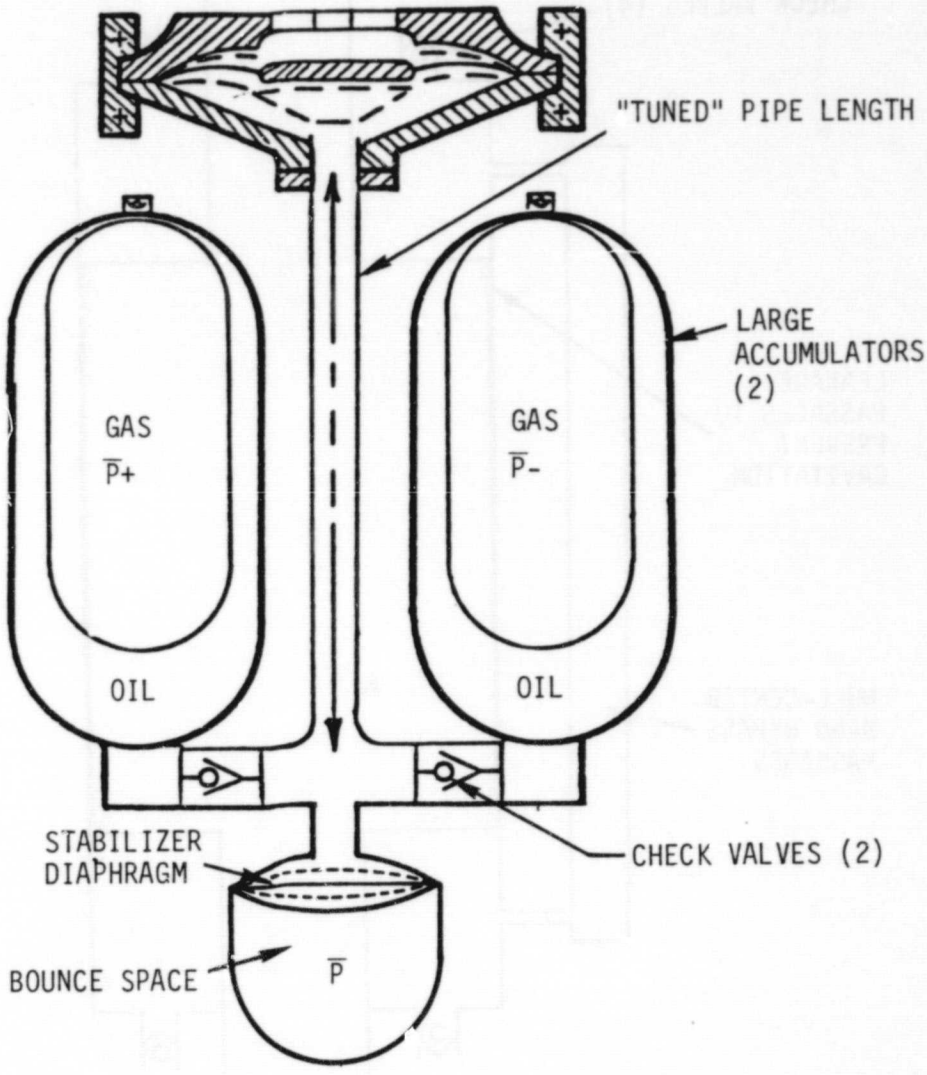

Figure 7. - Liquid piston driven hydraulic pump with a null center band.

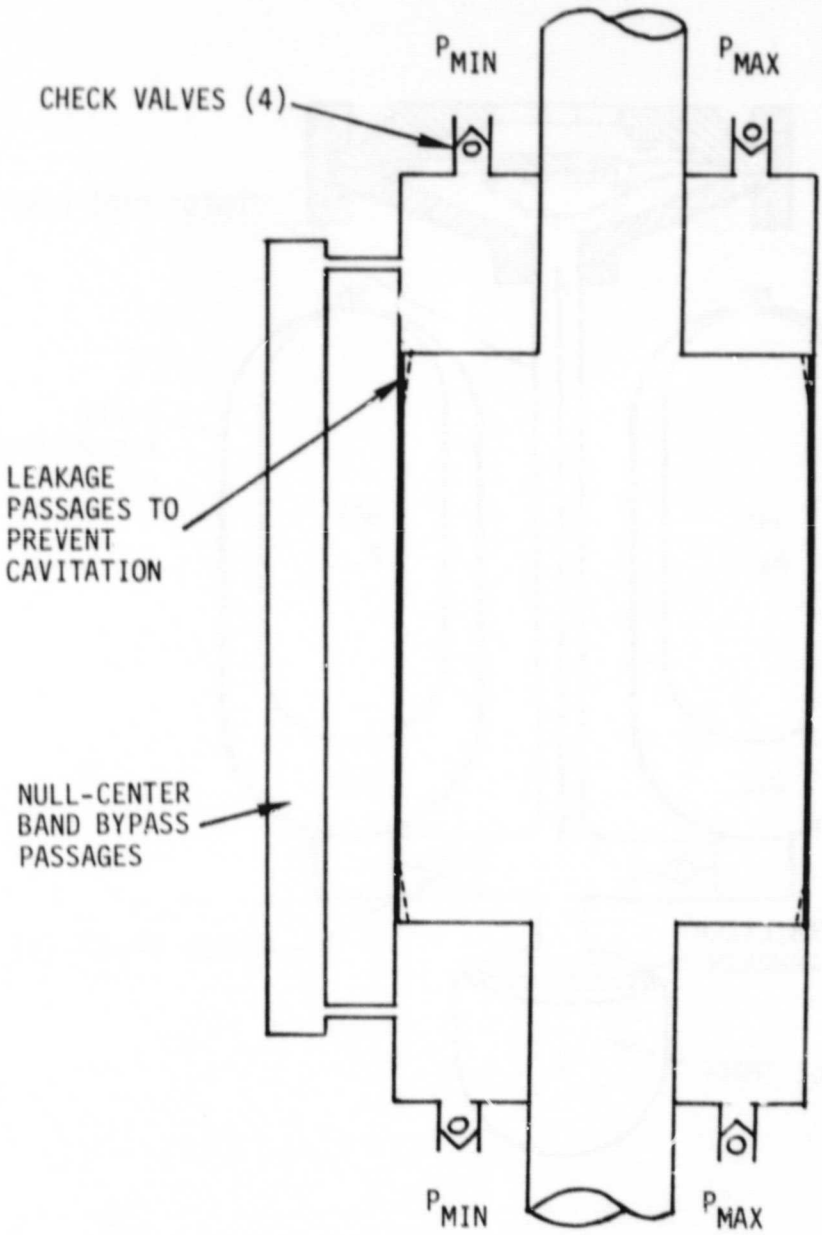

Figure 8. - Double acting hydraulic pump with a null center band.

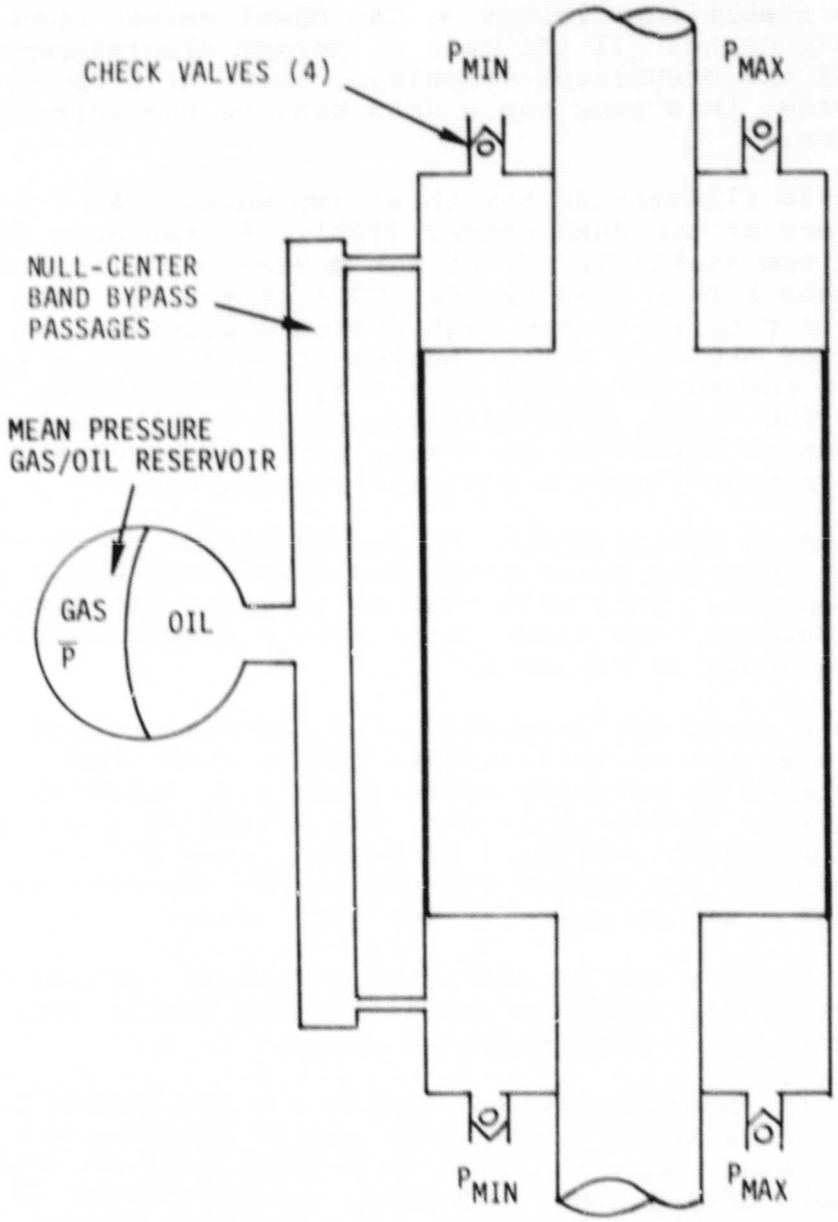

Figure 9. - Single acting hydraulic pump with a null center band.

The volume displacement of the stabilizer diaphragm snown in Figure 7 is less than that of the main engine diaphragm. When the volume displacement of the main engine diaphragm surpasses that of the stabilizer diaphragm, the check valves open, and the pump starts pumping. If the main diaphragm displacement is less than that of the stabilizer diaphragm, there will be no pumping. In other words, this pump has a dead band in the intermediate stroke region.

Figure 10 illustrates how this pump works. At $t = t_1$, both diaphragms are at top dead center (TDC). As the main diaphragm moves down, the stabilizer diaphragm moves down also, until the latter reaches bottom dead center (BDC) at $t = t_2$. The main diaphragm starts pumping to the high pressure reservoir at $t = t_2$ until it reaches its BDC at $t = t_3$. Between $t = t_3$ and $t = t_4$, both diaphragms move toward TDC until at $t = t_4$ the stabilizer diaphragm reaches its TDC first. The main diaphragm starts suction from the low pressure reservoir at $t = t_4$ until it reaches its TDC at $t = t_5$. This constitutes a complete pumping cycle.

The loading function for the liquid piston shown in Figure 10 contains not only the power absorbing components but also some spring components. This will tend to increase the frequency of the FPSE. However, the system will have a stable matching point like the one shown in Figure 6.

Figure 8 shows the schematic of a double acting hydraulic pump which also has an intermediate stroke dead band. The dead band is achieved by properly positioning port holes so that within a certain stroke amplitude, the device will not pump. The leakage passages indicated by broken lines are to prevent cavitation during the sudden suction in the opposite chamber when the piston begins to cover the port hole.

Figure 9 shows the schematic of a single acting pump. It uses essentially the same concept as the double acting pump except that it has a mean pressure reservoir.

Figure 11 shows the load function for the double or single acting pump in relation to the pump piston displacement. For the single acting pump, the load is proportional to $(P_H-P_L)/2$. For the double acting pump, the load is proportional to P_H-P_L. This means the double acting pump will be much smaller in size than the single acting pump for the same capacity.

In Figure 11, at $t = 0$, the piston is at the midstroke position. At $t = t_1$, the piston covers the port hole and begins

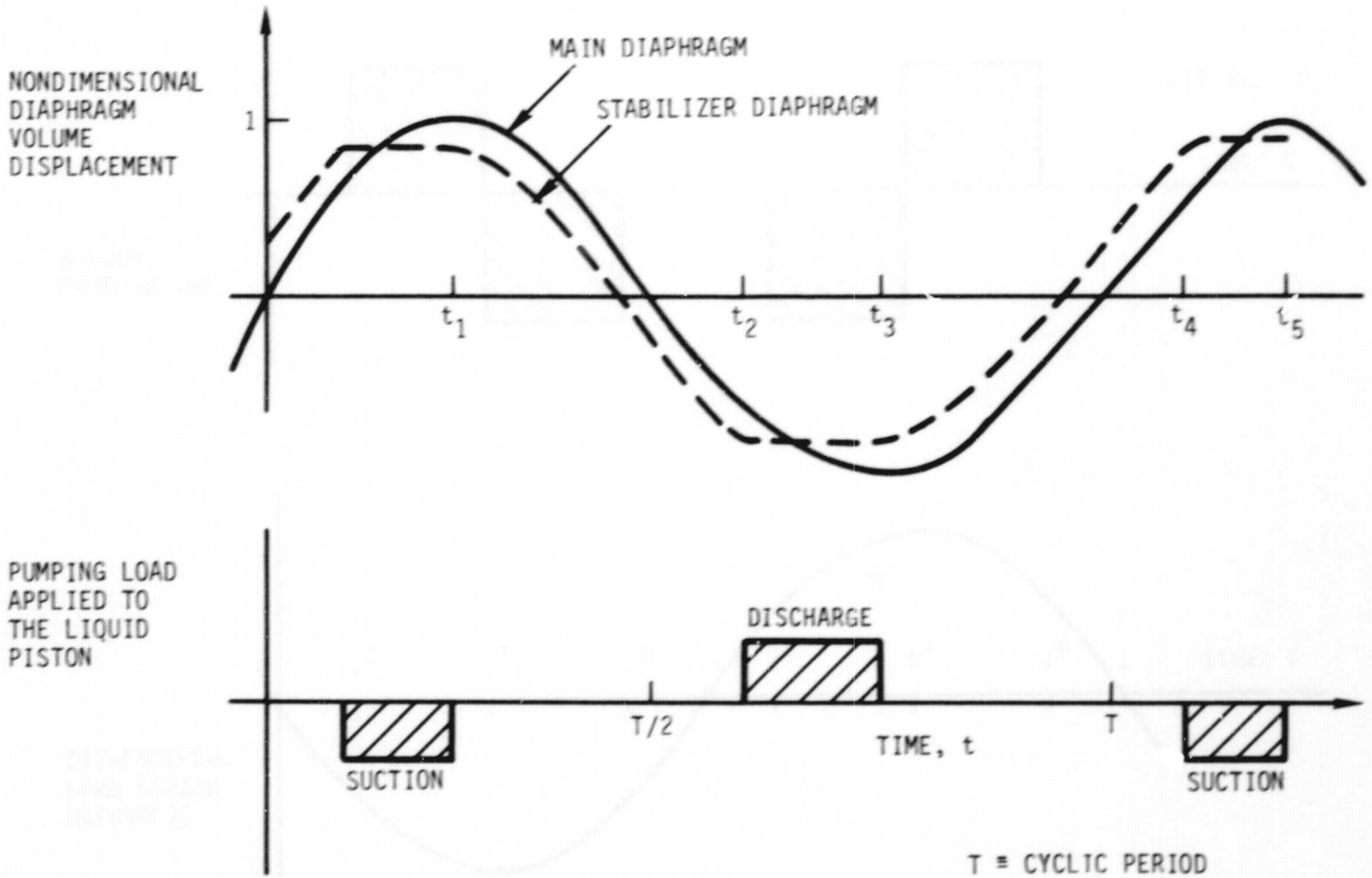

Figure 10. - Volume displacement and loading versus time for the liquid piston driven hydraulic pump with a null center band.

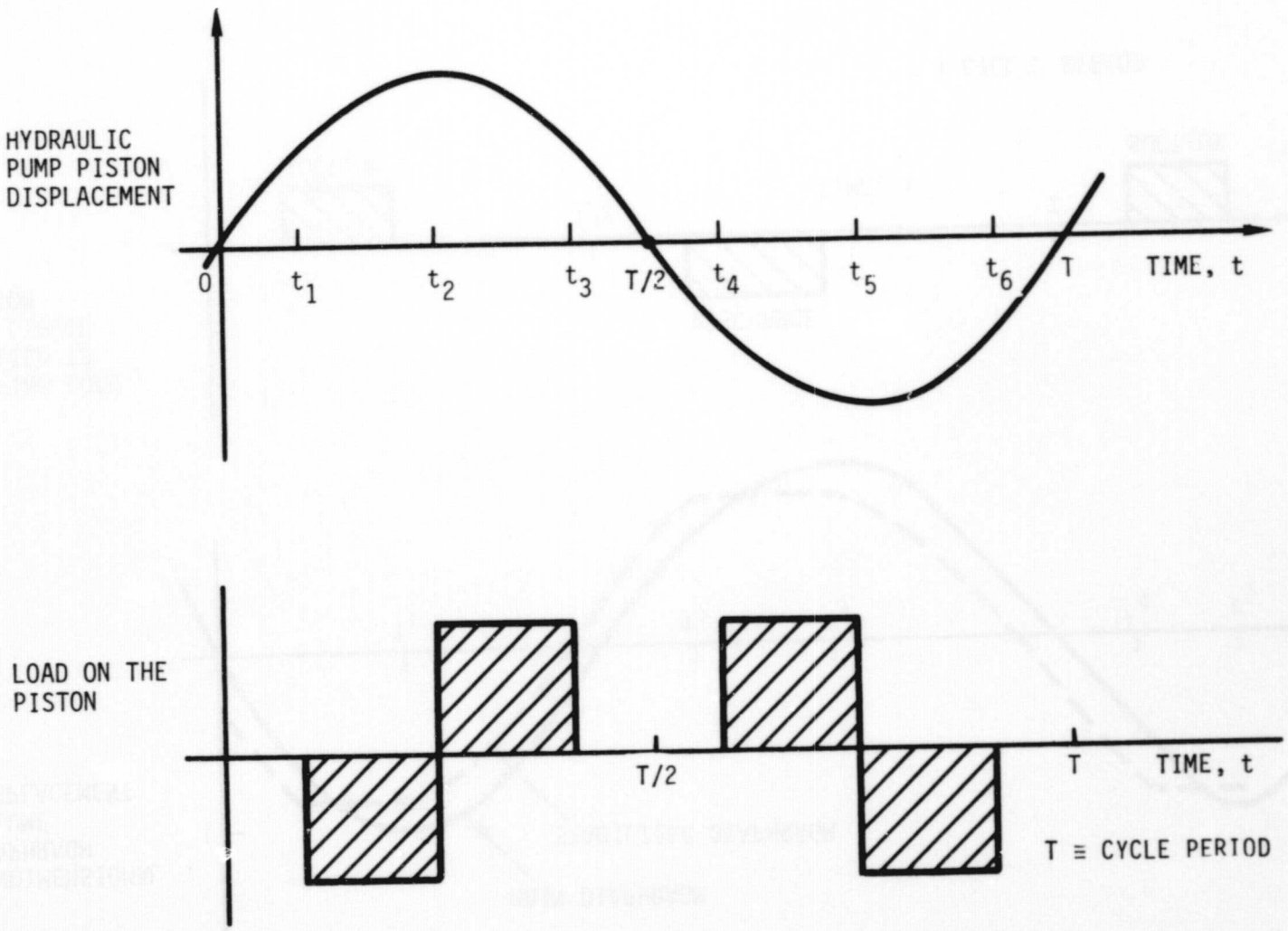

Figure 11. - Piston displacement and load versus time for the single and double acting pumps.

to pump to the high pressure (P_H) reservoir until the piston reaches TDC at $t = t_2$. As the piston moves away from TDC, it draws in from the low pressure (P_L) reservoir until at $t = t_3$ when the port hole is uncovered and the suction process stops. Similar processes occur as the piston travels in the opposite direction. The loading function shown in Figure 11 does not contain any spring components as were present in the liquid piston case.

Figure 12 shows the power matching between a FPSE and the hydraulic output methods presented in Figures 7, 9, and 10. The dead band width is dependent on the location of the port holes or the relative magnitude of the stabilizer diaphragm displacement. The slope of the idead load curve is directly proportional to the effective bore area of the pump and the accumulator pressure.

In Figure 13 are presented the various power loss mechanisms and their relative magnitudes for the proposed hydraulic pumps. The leakage control method to prevent cavitation in the double acting pump should not be a significant source of inefficiency. In order to design an efficient hydraulic output system, all of these losses have to be carefully controlled.

2.3 Comparison of System Concepts and Final Selection

Of the three candidate design concepts described in the previous section, the candidate design No. 1 was discarded. The reasons for its elimination are as follows:

- Limited pressure output
- Low efficiency if a hydraulic motor is used.

The remaining concepts to be examined were candidate design No. 2 having a flexible interface with the working gas (diaphragm or bellows), and the candidate design No. 3 with the original piston retained. Table 2 presents a qualitative comparison of the concepts by listing their relative advantages and disadvantages. The items of comparison are approximately in descending order of importance.

2.3.1 Bellows version. - A bellows in the present application has to satisfy a very difficult set of requirements, which include the following:

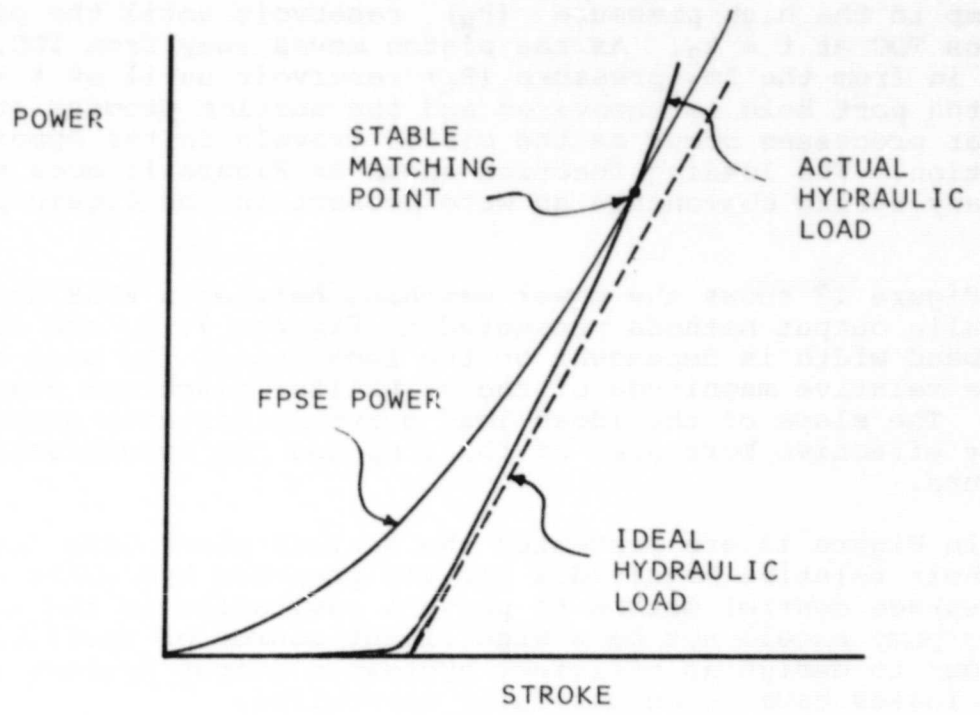

Figure 12. - Power load matching between a FPSE and the proposed hydraulic output system design.

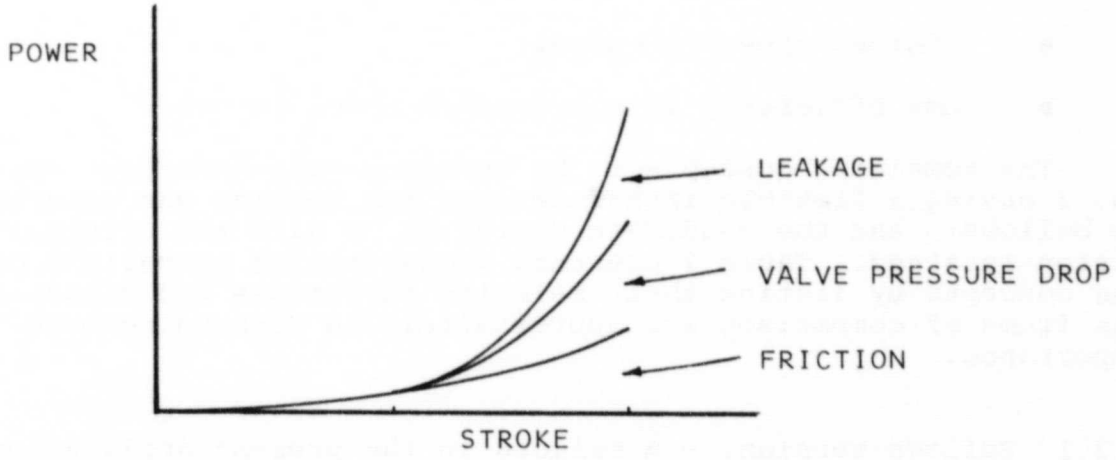

Figure 13. - Power losses in the proposed hydraulic output system design - not to scale.

TABLE 2. - COMPARISONS OF CANDIDATE DESIGNS OF THE HYDRAULIC OUTPUT SYSTEM FOR RE-1000 FPSE

Parameter	Evaluation		
	Flexible interface version		
	Diaphragm	Bellows	Piston version
Thermodynamic performance	Possibly acceptable only after considerable modification of RE-1000, but still below piston version level at best	Difficult to predict, probably as high as diaphragm engine at best	Acceptable
Dynamic stability	Good	Good	Good
Cost	Medium	Very high	Low
Reliability and life	Good	Poor	Very good
Scalability	Poor (requires multiple diaphragms or huge diaphragms)	Good (reasonable diameter) but very high cost due to tooling required	Very good
Modification of RE-1000 required	Medium	Considerable	Minimal
Provision for pressure loss protection	Reasonably easy in both directions	Possible only in nested condition	Easy in both directions
Start-up, stop load following	Good using dead band hydraulic equipment		
Quality control of components	Good	Very difficult	Very good
Availability of components	Reasonably easy to manufacture	Very difficult to manufacture	Very easy to manufacture
Fluid squeezing losses	Can be minimal	Difficult design problem to make it minimal	None
Ease of active space cooling of compression	Good	Good	Poor
Decision	Recommended	Not recommended	Recommended

- High frequency.
- Low dead volume or clearance volume.
- Low gas/oil flow losses.
- Overpressure protection in nested condition as well as in fully extended position.

A leading manufacturer of metal bellows, who also markets bellows type compressors, was consulted about the possible use of metal bellows in the hydraulic output applications. None of the existing bellows designs could meet all of the above requirements. Also, it was learned that non-standard bellows might require a new die for fabrication, and the weldment geometry and stresses do not scale simply. (Formed bellows are impractical for this purpose due to large size and/or clearance volume).

The bellows version was discarded because of the following reasons:

- High projected cost in manufacturing and quality control.
- Poor scalability.
- Difficulty of providing overpressure protection.
- Fluid squeezing loss problem.

Therefore the final choice has to be either the candidate design No. 2 with a diaphragm (diaphragm version) or the candidate design No. 3 (piston version). These two will be discussed further.

2.3.2 Diaphragm version. - The preliminary design of the diaphragm version has the following features:

- Annular diaphragm with simply supported edges; that is clamped between O-ring seals.
- Overpressure protection mechanism provided for both directions on both diaphragms.
- Minimal flow loss due to diaphragm and support structures.
- Active cooling of both gas side and oil side provided for engine diaphragm.

- Displacement transducers are on two diaphragms and engine displacer.

- Dynamic mass balancing having moderate hydraulic losses.

- Heavy, but low cost experimental version of diaphragm engine.

The diaphragm version will demonstrate four areas of interest: hydraulic output mechanism, diaphragm performance, mass balance, and hermetic gas/oil separation and gas containment. The risks involved with the diaphragm version are the relatively high cost to convert the RE-1000, potentially poor engine performance, and the large test program required to demonstrate system performance. The potential for poor performance exists primarily due to the generally inadequate state of the art with respect to cyclic heat transfer in the diaphragm gas compression space, as discussed in subsection 3.2.

2.3.3 Piston version. - The piston version has the following features:

- Only small amount of modification of RE-1000 required. Use existing piston, pressure vessel.

- Gas/oil separation achieved by a simple method of using a pre-stretched rubber tube or drum head clamped to piston rod.

- Rubber failures will not cause any immediate oil contamination of bounce space.

- All hydraulic components except piston and rod are located outside the hermetically sealed pressure vessel. Adaptation of check valves, hoses, etc., do not involve depressurization of the engine

The piston version would demonstrate two areas of interest:

- Hermetic gas/oil separation and oil containment.

- Hydraulic output mechanism.

The risks involved in selecting the piston version are minor compared to the risks of the diaphragm version. The risks associated with the piston version are related to the gas/oil separation bladder design and the small hydraulic diaphragm development. The advantages of the piston version are:

- Low development and production cost for conversion to hydraulic output.
- Minimal test program required.
- No change of engine performance (except what is generic to hydraulic output).

It was obvious that selecting the piston version over the diaphragm version would mean the least developmental effort and risks. However, both versions could be developed within reasonable cost and time.

It was decided to select the diaphragm version to be developed further. The rationale was that the diaphragm version would provide more opportunities for technical advancement. For example, the diaphragm version development program would provide the following:

- Modularized design for independent development of output components.
- Data on actively cooled, diaphragmed cold-end FPSE.
- High cyclic rate data on diaphragms.

2.4 Preliminary Dynamic and Thermodynamic Analysis

The objectives of the preliminary analyses were:

- To check the compatibility of the FMA designed hydraulic pumps with the RE-1000 and determine if the overall system is dynamically stable.
- To obtain the performance trend for the RE-1000 integrated with the pump.
- To help the design effort by indicating necessary modifications as the design evolved.

To achieve the objectives, Sunpower performed both dynamic and thermodynamic analyses. The results of the analyses will be presented here.

2.4.1 Dynamic analysis. - This subsection summarizes the results of dynamic analysis performed by Sunpower to investigate the dynamic compatibility of the RE-1000 to particular hydraulic loads.

The dynamic studies utilized a Sunpower developed pressure factor analysis. This analysis, while not intended to give exact numerical results, is a useful tool for predicting approximate engine dynamics and performance trends.

The general trends of the pressure factor analysis had been verified, in some cases, using the Sunpower third order analysis.

The RE-1000 now has two sets of displacer and rods. For the present analysis, the set designed for maximum power was used in determining the hydraulic load-engine compatibility. The RE-1000 with this set had run with a displacer stroke of 2.90 cm, a phase angle of 80 deg, and a frequency of 34.7 Hz. The hydraulic pump is designed to pump only if the stroke becomes larger than the dead band width of 2.748 cm.

The load function to simulate the pump load is similar to the one shown in Figure 11. Table 3 presents the results of the analysis. Cases No. 1 through No. 4 show the effect of the increasing load on the overall performance.

Figure 14 illustrates the effect of load force on the performance of the hydraulic output, RE-1000. The square wave load, with a center null band, has a tendency to slow down the motion of the piston near the extremes of its travel. This explains why the frequency decreased as the load force amplitude increased as shown in Figure 14.

It was also learned that the square wave load affects the dynamics of the piston and displacer significantly. The strokes of the piston and displacer change and their motions are distorted from sinusoidal. For case No. 1, the displacer collides with piston as indicated in Figure 15.

Because this displacer was designed for near resonant operation, decreasing frequency with load reduces the displacer and piston amplitudes. This was true for cases No. 2, 3, and 4 when there were no collisions predicted.

The displacer-piston collision during high power output can be prevented by shortening the length of the piston. The additional compression space volume should result in only a small reduction in engine power and frequency.

In an attempt to bring the piston displacer motion closer to a sinusoidal condition, the energy stored in the piston was increased by increasing the piston mass. Starting with case No. 5 through No. 8 in Table 3, the piston mass (M_p) was increased by 20, 50, 100, and 200 percent. A spring (K_p) was added to the piston

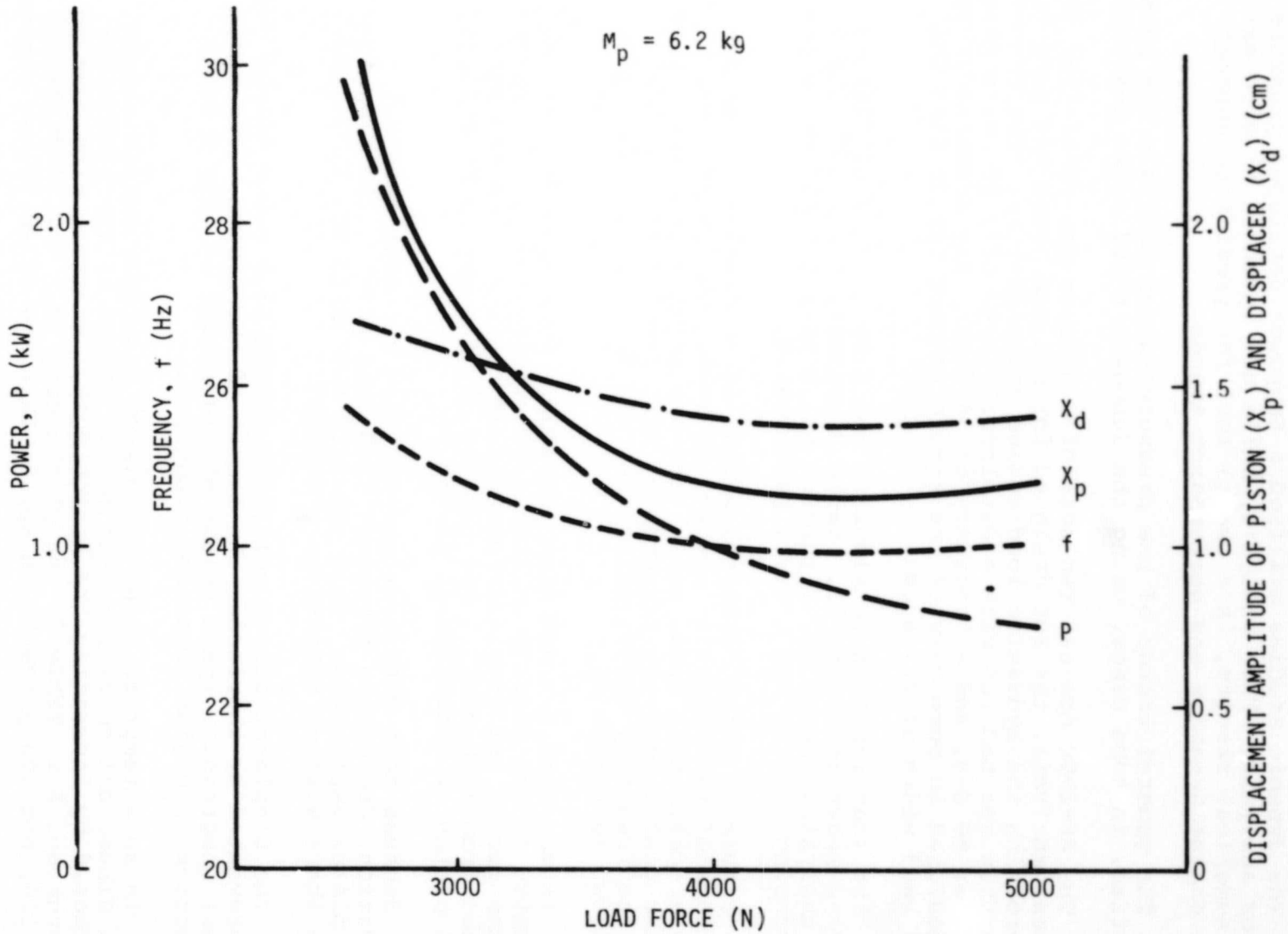

Figure 14. - Effect of the null center band hydraulic pump load on RE-1000 performance.

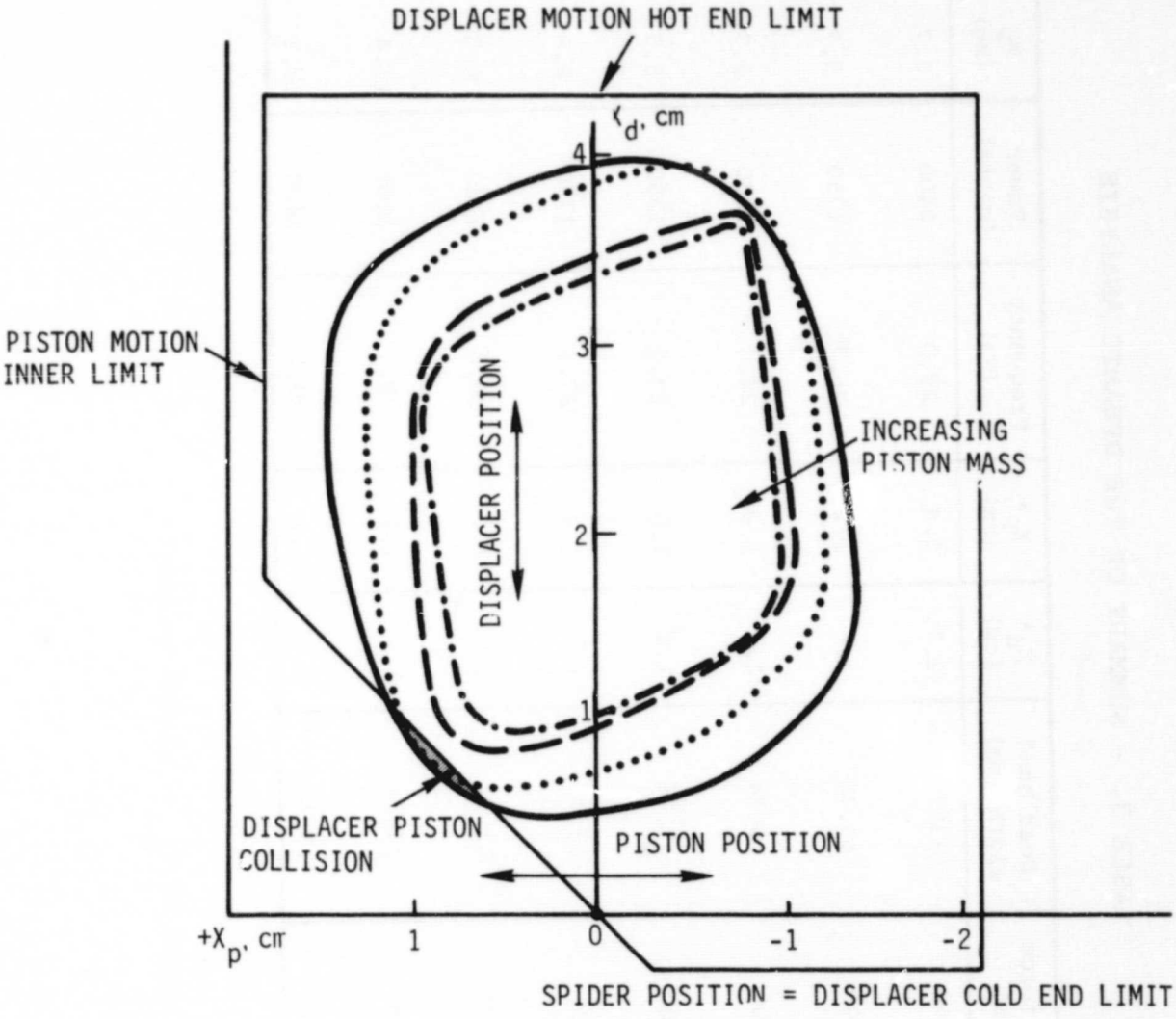

Figure 15. - Piston-displacer phase plots of the null center band, hydraulic-pump output Stirling engine for different piston masses.

TABLE 3. - SUMMARY OF THE DYNAMIC ANALYSIS

Run No.	Load force (N)	Dead band width (mm)	X_d* (cm)	X_p* (cm)	Frequency (Hz)	Power (watts)	M_p (kg)	K_p (10^4 N/m)
1	2900	13.74	1.7	1.4	29.0	2400	5.7	0
2	3200	13.74	1.6	1.2	26.7	1750	5.7	0
3	4000	13.74	1.4	1.0	24.0	1200	5.7	0
4	5000	13.74	1.4	1.0	23.0	1200	5.7	0
5	3200	13.74	1.6	1.2	27.0	1770	6.84	3.2
6	3200	13.74	1.6	1.2	28.0	1730	8.55	8.0
7	3200	13.74	1.5	1.1	28.5	1500	11.4	16.0
8	3200	13.74	1.4	1.1	29.0	1400	17.1	32.1

*X_d = displacer stroke/2; X_p = piston stroke/2

in each run sufficient to swing the additional mass at 26.7 Hz of case No. 5. The results are plotted in Figure 16. As the piston mass increased, the ratio of cyclic energy to stored energy became small. This means the shape of the load function would have less influence on the dynamics of the piston and displacer. Figure 17 clearly demonstrates this. The piston motion became much closer to sinusoidal and the frequency increased.

The dynamic analysis has been used to investigate the operation of the RE-1000 engine connected to a hydraulic load. The results were not intended for exact detail design, since the analysis itself is a simplified one. The trends, however, can be regarded as correct. The conclusions from the dynamic analysis are:

- The system consisting of the RE-1000 FPSE and FMA designed hydraulic pump is dynamically stable.
- At high power output, the displacer collides with the piston. This can be prevented by shortening or moving the piston.
- The nonsinusoidal motion of the piston can be corrected by increased stored energy in the system (spring/mass).
- The analysis was for the piston version of the RE-1000, but the trends should also apply to the flexible interface version.

2.4.2 Thermodynamic analysis. - A number of computer simulations were run of the Sunpower RE-1000 FPSE engine to determine the effects of increased heat transfer in the compression space resulting from the substitution of a diaphragm for the current piston. The simulations were done with Sunpower's third order code with constrained dynamics of piston and displacer. Tables 4 and 5 summarize the important input and output of these simulations. The code specifies a constant heat transfer coefficient in the compression and expansion spaces. The wall temperatures of the two spaces are assumed constant during the duration of an engine cycle. They can be held fixed or adjusted between cycles to approach a temperature which gives no net heat exchange between gas and wall over the course of a cycle. The cylinder heat transfer coefficient is based on data of Taylor (ref. 1). Cylinder heat transfer computed in this way has given performance predictions in close agreement with test data on the current version of the RE-1000 FPSE.

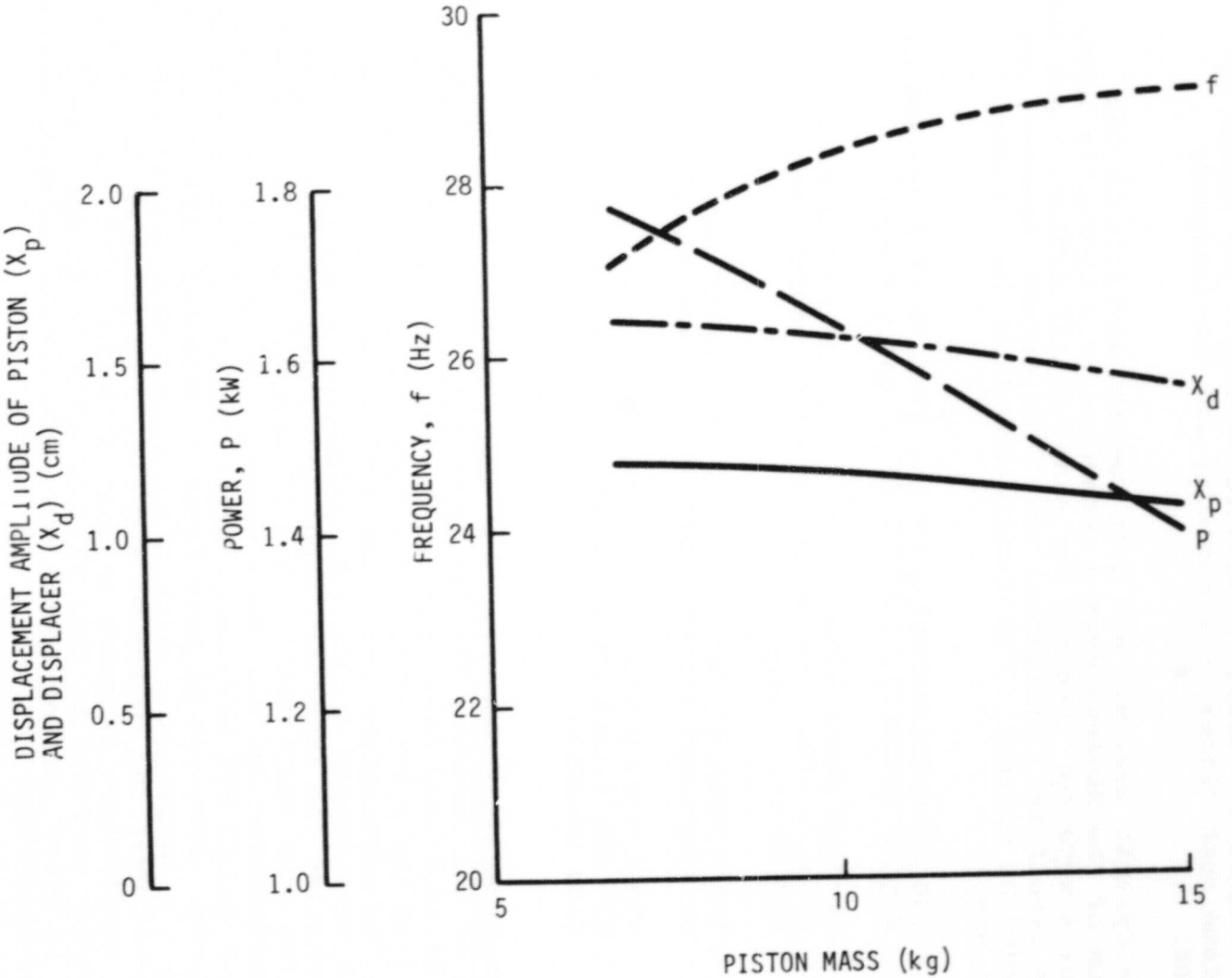

Figure 16. - Effect of increasing the piston mass on RE-1000 with null center band hydraulic load.

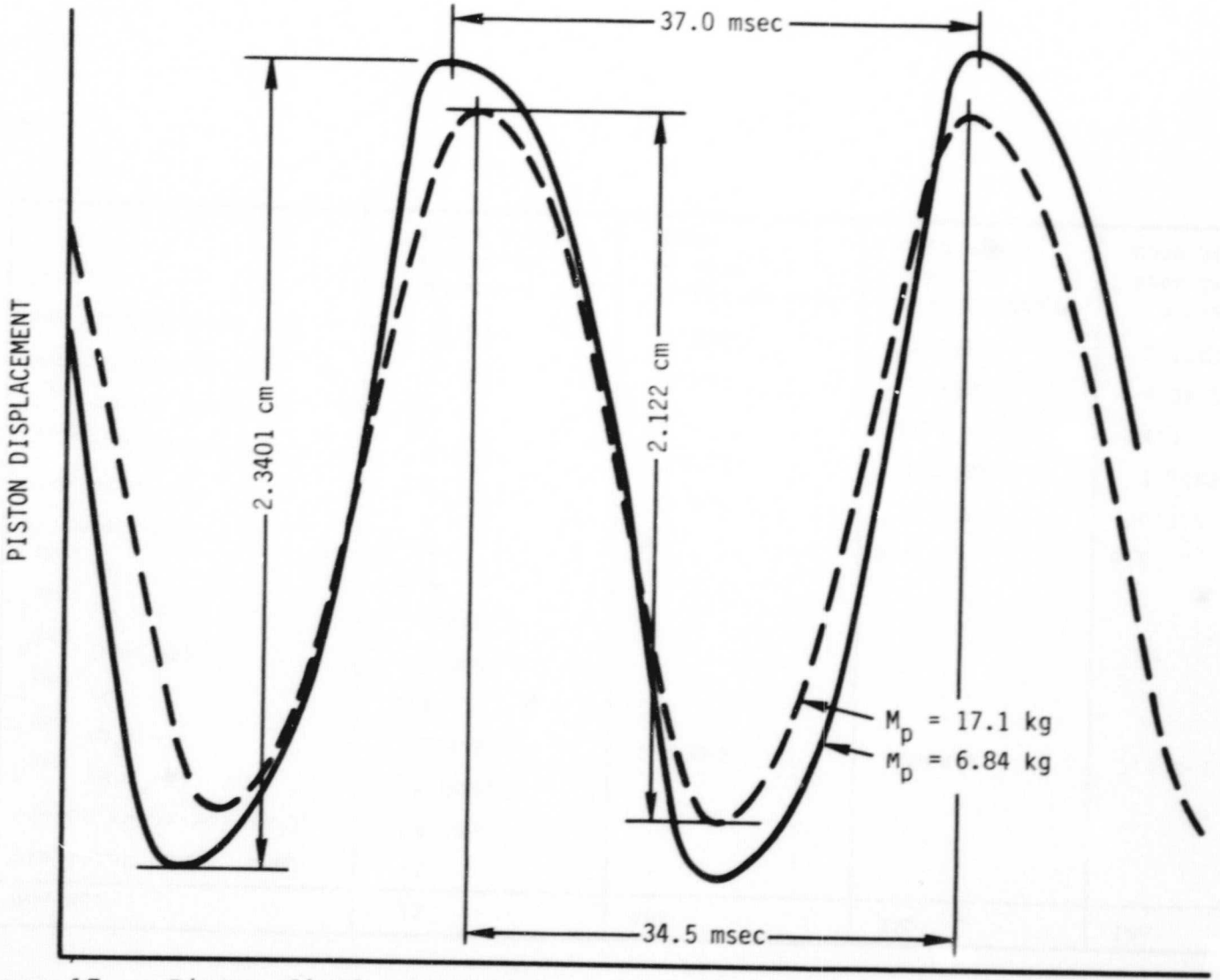

Figure 17. - Piston displacement versus time plot of RE-1000 with the null center band hydraulic load for two different piston masses.

TABLE 4. - EFFECT OF INCREASING THE COMPRESSION SPACE HEAT TRANSFER ON THE PERFORMANCE OF RE-1000 FPSE WITH THE LOW PHASE ANGLE DISPLACER ROD

Run No.	11	18a	18b	18c
Displacer phase (deg)	41			
Piston swept vol (m^3)	58.8E-6			
h_{cmp} (W/m^2-K)	6.97E4			
S_{cmp} (m^2)	2.57E-3	2.48E-2	4.96E-2	7.44E-1
T_{cmp} (K)	323			
h_{exp} (W/m^2-K)	4.86E4			
S_{exp} (m^2)	2.57E-3			
T_{exp} (K)	813			
PV power (W)	1185	809	844	876
Indicated η	0.387	0.303	0.317	0.328
P_{cmp} amplitude (N/m^2)	9.32E5	7.69E5	7.27E5	7.16E5
P_{cmp} phase (deg)	24.8	20.6	23.3	24.7
Regen enthalpy flux (W)	4.03E2	4.12E2	4.22E2	4.25E2
Sum pumping loss (W)	1.21E2	1.10E2	1.13E2	1.15E2
Remarks	Reference run low phase angle desigr.	Diaphragm area in comp space	2 × diaphragm area in comp space	3 × diaphragm area in comp space

TABLE 5. - EFFECT OF CYLINDER HEAT TRANSFER ON THE PERFORMANCE OF RE-1000 FPSE WITH THE HIGH PHASE ANGLE DISPLACER ROD

Run No.	20a	19	20b	21	22	23	24
Displacer phase (deg)	80						
Piston swept vol (m^3)	58.8E-6				70.6E-6	80.1E-6	
h_{cmp} (W/m^2- K)	1.36E5						
S_{cmp} (m^2)	2.57E-3	2.48E-2					
T_{cmp} (K)	320	326	326	313	313	313	334
h_{exp} (W/m^2-k)	5.68E4						
S_{exp} (m^2)	2.57E-3		2.48E-2	2.57E-3			
T_{exp} (k)	839	826	824	843	835	830	829
PV power (W)	2094	1538	1440	1623	1884	2056	1897
Indicated η	0.353	0.278	0.303	0.329	0.333	0.326	0.308
P_{cmp} amplitude (N/m^2)	1.31E6	1.03E6	9.92E5	1.06E6	1.22E6	1.37E6	1.33E6
P_{cmp} phase (deg)	26.3	24.9	24.9	25.9	20.7	17.1	16.0
Regen enthalpy flux (W)	1077	1031	1078	1048	1060	1049	1037
Sum pumping loss (W)	391	332	374	336	350	364	352
Remarks	Reference run, high phase angle design	Diaphragm area in comp space	Diaphragm area in comp space and exp space	Diaphragm area in comp space, cooled wall	Diaphragm area in comp space, cooled wall, increased stroke	Diaphragm area in comp space, cooled wall, increased stroke	Diaphragm area in comp space, floating wall increased stroke

The following is the nomenclatures for Tables 4 and 5:

Displacer phase	Phase lead of displacer over piston
Piston swept vol	Total volume swept in compression space
h_{cmp}	Film coefficient in compression space
S_{cmp}	Heat transfer surface in compression space
T_{cmp}	Mean wall temperature in compression space
h_{exp}	Film coefficient in expansion space
S_{exp}	Heat transfer surface in expansion space
T_{exp}	Mean wall temperature in expansion space
PV power	Indicated working gas power
Indicated η	PV power divided by heat input to heater
P_{cmp} amplitude	Amplitude of compression space pressure
P_{cmp} phase	Phase lag of compression space pressure behind piston
Regen enthalpy flux	Net enthalpy transport through regenerator
Sum pumping loss	Summation of pumping power for cooler, regenerator and heater

Table 4 gives results for the RE-1000 design with a 41 deg displacer phase angle. Table 5 gives results for a redesigned version of the RE-1000 FPSE with an 80 deg displacer phase angle. In both cases the increased heat transfer in the compression space was modeled by maintaining the identical film coefficient of the RE-1000 piston engine but increasing the surface area by the frontal area ratio of diaphragm to piston (9.66), or some multiple thereof, consistent with Taylor's correlation parameters.

Admittedly, this approach is a crude one because it uses heat transfer data from ordinary internal combustion engines for a diaphragmed Stirling engine with quite different geometry and thermodynamics.

Tables 4 and 5 show the performance of the diaphragm engine to be lower than that of the piston engine. This is principally due to a reduction in working gas pressure amplitude and phase lag with respect to the piston, both brought about by isothermalization in the diaphragm space. A secondary effect is the interaction between the compression space and cooler due to an elevated average temperature in the compression space.

A reduction in pressure amplitude is important because it reduces the specific power of the machine which, with nearly constant parasitic losses (pumping losses, regenerator enthalpy flux, etc.), also reduces efficiency. The reason pressure amplitude decreases can be understood by noting that the pressure change in a gas space per piston motion is less with nearly isothermal conditions than with nearly adiabatic conditions.

Calculations were made to increase pressure amplitude by simply increasing piston stroke (Table 4, runs 22, 23, 24). The pressure amplitude and power could be brought up to the reference level for the RE-1000 by this means but the efficiency was still low by a few percentage points. The reason for this seems to be due to the reduced phase angle of the pressure wave referred to the piston or diaphragm. This apparently resulted from a change in the temperature swing in the compression space. The phasing of the working gas flow through the heat exchangers is also affected. This can result in subtle heat transfer losses in the heat exchangers and reduced efficiency. It appeared that this problem could be overcome by optimizing the displacer motion in conjunction with increased piston stroke.

Considering heat transfer in the compression space, if the walls of this space are considered quasi-adiabatic (Table 5, runs 19, 20a, 20b, 24) (no net heat exchange with the working gas), the mean cycle temperature of the compression space becomes higher than the cooler space wall temperature by as much

as 20°C. A thermodynamic loss occurs when the compression space gas enters the cooler. Hence, efficiency can be improved by active cooling of the compression space walls. Indeed, (Table 5, runs 21, 22, 23), when the compression space wall temperature is lowered to the cooler space wall temperature, efficiency rises somewhat.

Even after increasing piston stroke and actively cooling the compression space wall, (Table 5, run 23) the efficiency of the diaphragm version RE-1000 could not be brought back up to the piston version base level efficiency (Table 5, run 20a). While at first surprising, this result is plausible in terms of the arguments presented above.

The conclusions of the preliminary thermodynamic analysis are:

- All components of the Stirling cycle must be considered together before any conclusions can be drawn regarding the merits of an increased heat transfer to approach isothermalization.

- Merely increasing the heat transfer in the compression space of a Stirling engine is not sufficient to guarantee an improvement in performance. The machine must be re-optimized in all its aspects before near isothermalization can be expected to yield a benefit.

- The heat transfer in the diaphragm area should be carefully investigated, because design and performance depend strongly on prediction of this phenomenon.

- Net heat transfer from, or cooling of the diaphragm compression space appears necessary to achieve good performance.

3. DETAIL DESIGN

3.1 Description of the Recommended Design

3.1.1 General description. - With the preliminary design approach selected, it remained to produce a detail design consistent with the developmental program envisioned. For this the design incorporates:

- Modular sections and simple, accessible parts for research testing.
- Interchangeability with current RE-1000 FPSE output section without disturbing engine section.
- Either vertical axis hydraulic assembly, or horizontal for best demonstration of dynamic balancing.
- Displacement sensors on all engine moving parts and easily optional on hydraulic pump.
- Conservative design for low stress and low cost.

The design is described referring to Figure 18, which is a simplified schematic of the actual design. Basically the system operates as follows:

- Engine gas displaces oil trapped on one end of the piston (bottom).
- The piston displaces oil trapped on the other (top) end, thereby displacing the bounce gas diaphragm.
- No significant net power is transferred to this oil or the diaphragms, and the effective mass of this piston and oil is insufficient to provide the desired cyclic motion in combination with engine and bounce gas springs.
- Additional effective piston mass is provided in the counter balance assembly.
- The annular piston masses are forced by the surrounding trapped oil to move in opposite directions synchronously so that the entire engine system is effectively balanced dynamically.

- The annular piston mass counterbalance can be removed, and equivalent mass added to the piston rod, with oil free to flow around it, in order to demonstrate simple unbalanced dynamic operation similar to the normal RE-1000.

- The piston rod transmits net power to the hydraulic oil pump, which is isolated from the diaphragm oil.

It is obvious that the basic layout affords easy access for modification. Detail problems in design, and the solutions offered, will be described piece-by-piece, from the bottom up, as it were, referring to detail drawings.

3.1.2 Engine diaphragm assembly. - The engine diaphragm assembly interfaces with the RE-1000 mounting plate (Sunpower part: pressure vessel bottom plate). No changes to the RE-1000 FPSE are required except for two through-holes in the plate for separate water coolant input-output, and possibly a different displacer rod (for improved performance, see subsection 3.2.2).

Figure 19 is a sectional layout of the diaphragm assembly. A machined plug occupies the central hole in the plate vacated by piston version parts. This plug is the primary adapter between the existing RE-1000 and the hydraulic output assembly, so it performs several functions. First, it conducts working gas between the engine cooler and the diaphragm space, and it conducts coolant water in order to function like the engine cooler, thermodynamically. Secondly, it adapts the mechanical assembly to hold the displacer rod in place, to fit the existing overboard gas seal or O-ring, and to provide passage for the displacer LVDT sensor rod. Figure 20 is a two-view of this plug. The piece is made of aluminum, favorable for heat transfer and machining. The lower end has lugs to fill the otherwise dead volume of the displacer rod spider. The drilled gas passages are similar to those of the RE-1000 FPSE cooler, sized for low dead volume, flow friction, and cyclic thermal losses.

Above the mounting plate is the lower half of the engine diaphragm support, a turned plate with milled slots. Figure 21 is a two-view of the part. Mounting seal and shoulders suit the existing mounting plate. At the inner diameter is a gas seal with the central plug; this and the lower outer seal contain the coolant water. The water enters and distributes radially, flows semi-circumferentially in grooves around the support plate and central plug, and exits on the opposite radius. The plate is aluminum for heat transfer and machining.

The upper surface of the plate is contoured axi-symmetrically to fit the extended shape of the diaphragm. In addition, there are radially milled small slots, tapered to zero depths outward,

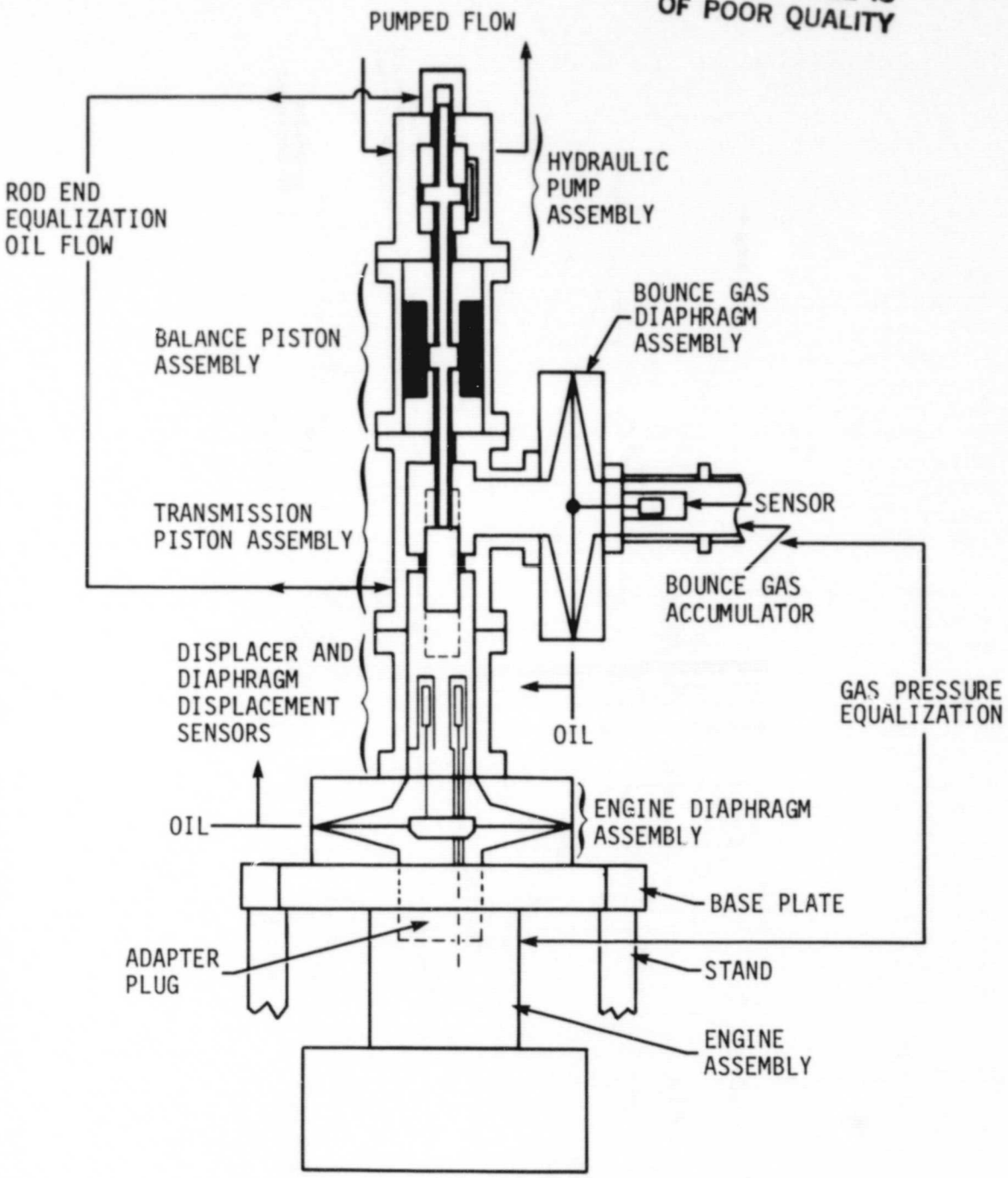

Figure 18. - Simplified schematic of the recommended hydraulic output system design

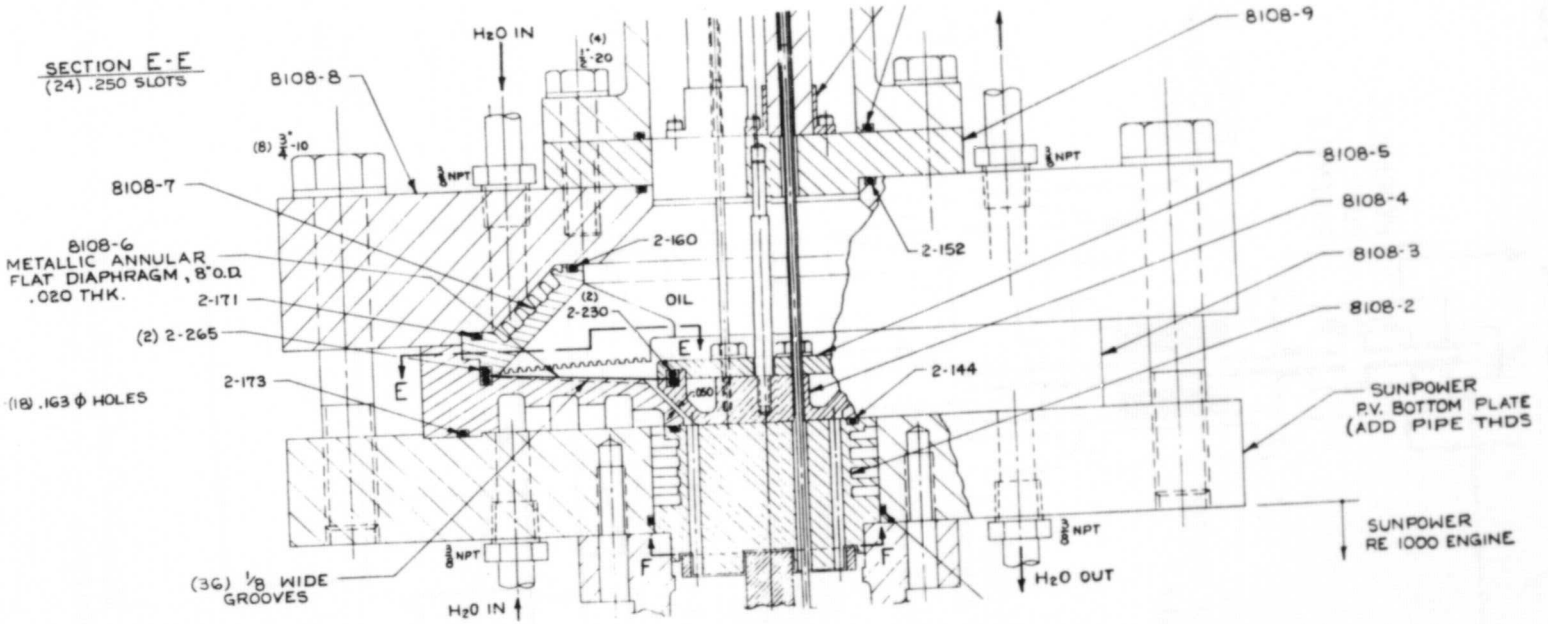

ORIGINAL PAGE IS
OF POOR QUALITY

Figure 19. - Sectional layout of the diaphragm assembly (dimensions in United States customary units)

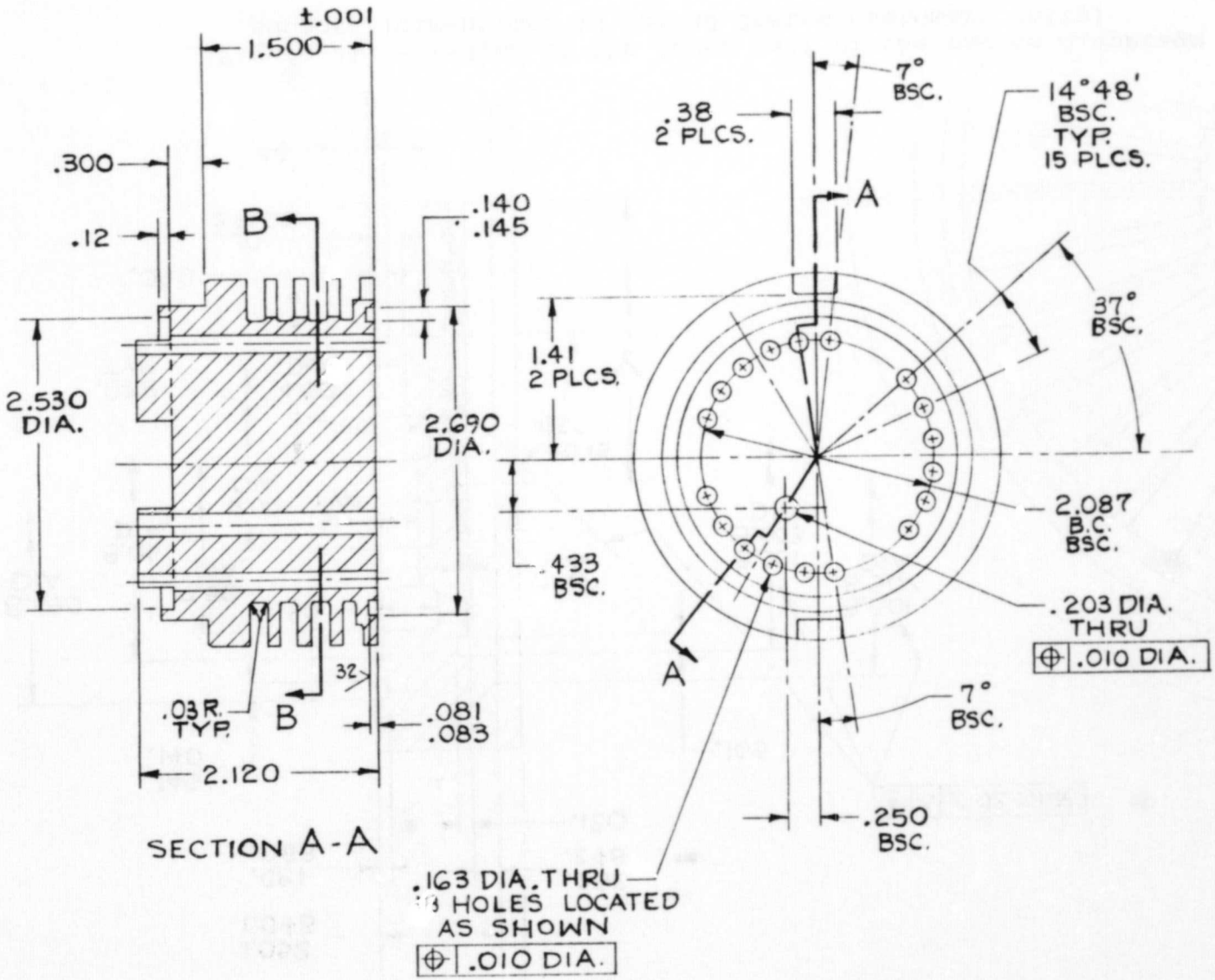

Figure 20. - 2-View of the adapter plug with cooling passages (dimensions in United States customary units)

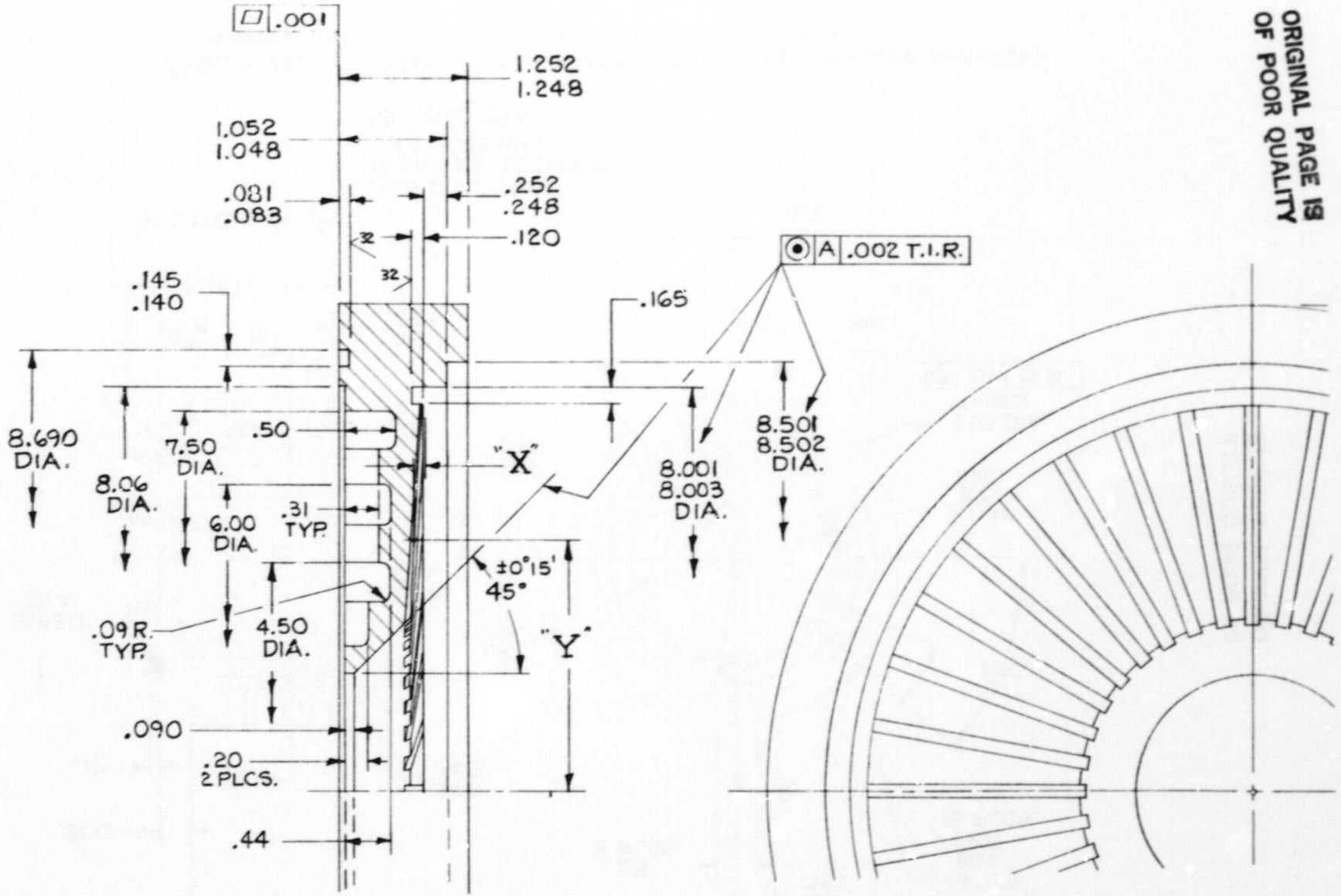

Figure 21. - 2-View of the lower half of the engine diaphragm support (dimensions in United States customary units)

to provide for gas flow distribution with low flow resistance when the diaphragm to support clearance is very low, that is, at maximum cyclic downward excursion. The "disked" contour is NC (numerical control) machined to specified depth versus radius coordinates and the unsupporting slot spans are small so that the diaphragm should not be damaged due to impact, sudden loss of engine pressure, or high oil pressure.

The diaphragm itself is flat, annular (20.32 × 6.35 × 0.0508 cm), and supported at its edges by clamped elastic seals, O-rings. This design has many advantages:

- Structurally meridional bending and direct stresses are effectively nil at the edges, and the flexed shape offers large displacement for a given stress limit.
- The diaphragm can be relatively thick and "springy" instead of "floppy" or delicate, still with moderate bending stresses mid span.
- It cannot be simpler or less demanding for fabrication. Welding and forming are not required, only sheet stock having moderately high endurance limit strength (say, above 200 MPa for present purposes).

Perhaps most important, the flat diaphragm offers the simplest shape for control of the varying gap between the diaphragm and its stroke limiting or support members. Good performance depends on achieving close clearance but free fluid flow; diaphragm waviness or floppiness complicates achieving this. Possible radial temperature gradients (less than 20°C) will not cause significant additional stress, and "oil canning" effects are far overpowered by gas-oil pressure differentials.

The flat annular diaphragm having flexibly clamped edges, sometimes referred to as simply supported or articulated edges, has not been fully proven, but it has been used initially successfully in at least one Stirling engine application, by Cooke-Yarborough (ref. 1), as well as for rotary seal backup members by FMA. Refinement of design is expected to involve primarily the details of O-ring properties and clamping groove section.

The diaphragm is clamped from above, the oil side, by an extensively machined plate or annular ring, shown in Figure 22. In addition to sealing and supporting the diaphragm, it serves to distribute and cool the oil and, hence, the diaphragm, which receives heat from gas compression (about 700W predicted, see Table 7, Run No. 29). This part is also made of aluminum for good heat transfer and machining. The bottom surface is not only contoured to support the diaphragm but it also is slotted radially and grooved circumferentially to allow free oil flow even when the diaphragm is resting on it.

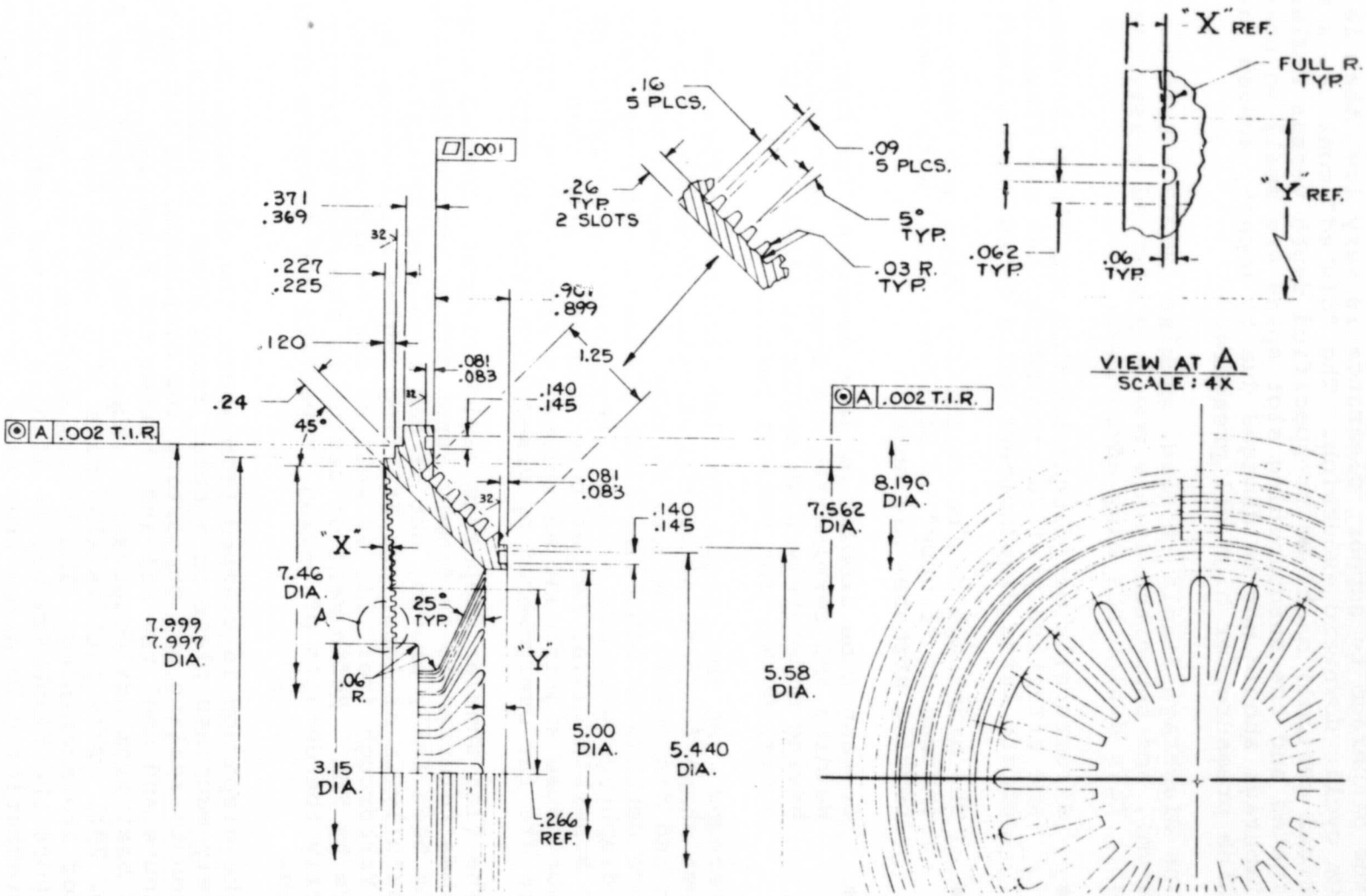

Figure 22. - 2-View of the upper half of the engine diaphragm support (dimensions in United States customary units)

In addition the radial fingers formed by the slots also support the central plug piston of the diaphragm on the top. The slots, grooves, and plug piston supports are configured so that the diaphragm is not over-stressed even when full gas pressure is applied with no opposing oil pressure.

Heat flows from the diaphragm to the fingers due to the cyclic convection of the oil in the immediate vicinity. Heat then flows through the thick fingers to the circumferential water cooled grooves on the upper, outer surface of the diaphragm support piece. The primary thermal resistance is in the oil, and this is practically minimal.

The diaphragm support pieces are clamped to the RE-1000 mounting plate by a simple steel flange ring using the existing bolt circle. Pressure vessel codes are satisfied with respect to existing bolt and seal design.

Central to the diaphragm is a light aluminum plug piston that serves to support the inner edge of the diaphragm, particularly in the down position; to guide the cyclic gas flow; to guide the diaphragm in axi-symmetric displacement, without "cocking"; and to provide for displacement sensor rods. The diaphragm displacement is sensed directly using an LVDT rod, slug, and coil immersed in the oil.

Assembly of the diaphragm parts is not unusually critical; a proper sequence of vertical stacking and care will avoid damage to the light parts such as the diaphragm, O-rings, and LVDT stems (e.g.: assemble diaphragm with center plug, install diaphragm unit and O.D. O-rings on lower support and RE-1000, install upper diaphragm support, upper pressure head, and last the support spider-ring with stationary LVDT parts).

The displacer motion is also sensed directly with an LVDT, but the rod and plug are enclosed in a thin nonmagnetic steel tube fixed to the plug piston and closed at the upper end. Thus although the displacer slug is in the gas and the LVDT coil is in the oil, the direct signal is not suppressed and hermetic separation is maintained.

The LVDT coils are mounted on a ring having a central bridge that also serves to guide the plug piston rods. The assembly is enclosed in a simple spool piece having an electrical carry-through fitting.

It is envisioned that the entire diaphragm and transducer assembly is assembled conveniently by sequential vertical stacking.

3.1.3 Transmission piston assembly. - Figure 23 is a drawing of the transmission piston and its housing, which is central between the engine diaphragm, bounce gas diaphragm, and balance piston assemblies. Operation is rather obvious: the power piston effectively has engine pressure on one end and nearly constant bounce pressure on the other, and the rod transmits force to the balance and pump sections. Passages are large relative to the piston so that flow losses and inertance of the transmission oil is low. Leakage past the piston and rod is minimized by close clearance, which is simpler and more predictable than sealing rings for this research hardware.

Note two items: first, the pressure force on opposite ends of the piston rod area itself is equalized by a flow connection or tube connecting the lower oil space to the top of the hydraulic pump assembly, as shown in Figure 18. Secondly, the output piston assembly can be mounted with the piston rod axis horizontal, because the flanges for the oil flow passages are identical. With the piston rod horizontal, the radial facing flange of the piston assembly is mounted on the engine diaphragm and sensor assemblies, and the bounce gas diaphragm is mounted to the axial end of the piston assembly. Thus the bounce diaphragm appears in about the same place as shown in Figure 18 but the hydraulic assembly is cantilevered out to the other side. This configuration has advantages for demonstrating the effects of piston dead-weight and inertial imbalance as compared to vertical piston motion.

3.1.4 Bounce gas diaphragm assembly. - This assembly basically consists of the diaphragm, two support plates, and two flat flanges acting as clamps and pressure vessel, as shown in Figure 24. The diaphragm as well as its seals and supports is basically the same as that of the engine. Differences are that there is no need for either a large central plug piston or oil cooling, because there is easy access to the one LVDT transducer and there is not substantial gas circulation or cyclic compression. The diaphragm should operate roughly midway between the support plates, and the oil side plate has circumferential grooves as well as radial slots to minimize flow losses.

The gas pressure vessel attached to the assembly is optional, providing the correct volume. An obvious choice is the vessel from the RE-1000 piston version with an adapter flange.

3.1.5 Balance piston assembly. - The concept is not novel of providing inertial balance using two masses moving oppositely due to hydraulic coupling. The simplest arrangement for doing so with minimal hydraulic losses is shown in Figure 25. Both of the pistons, one central, one annular, have the same area; so their displacements are equal but opposite. Oil circulates only a short distance and at low velocity. The oil is effectively

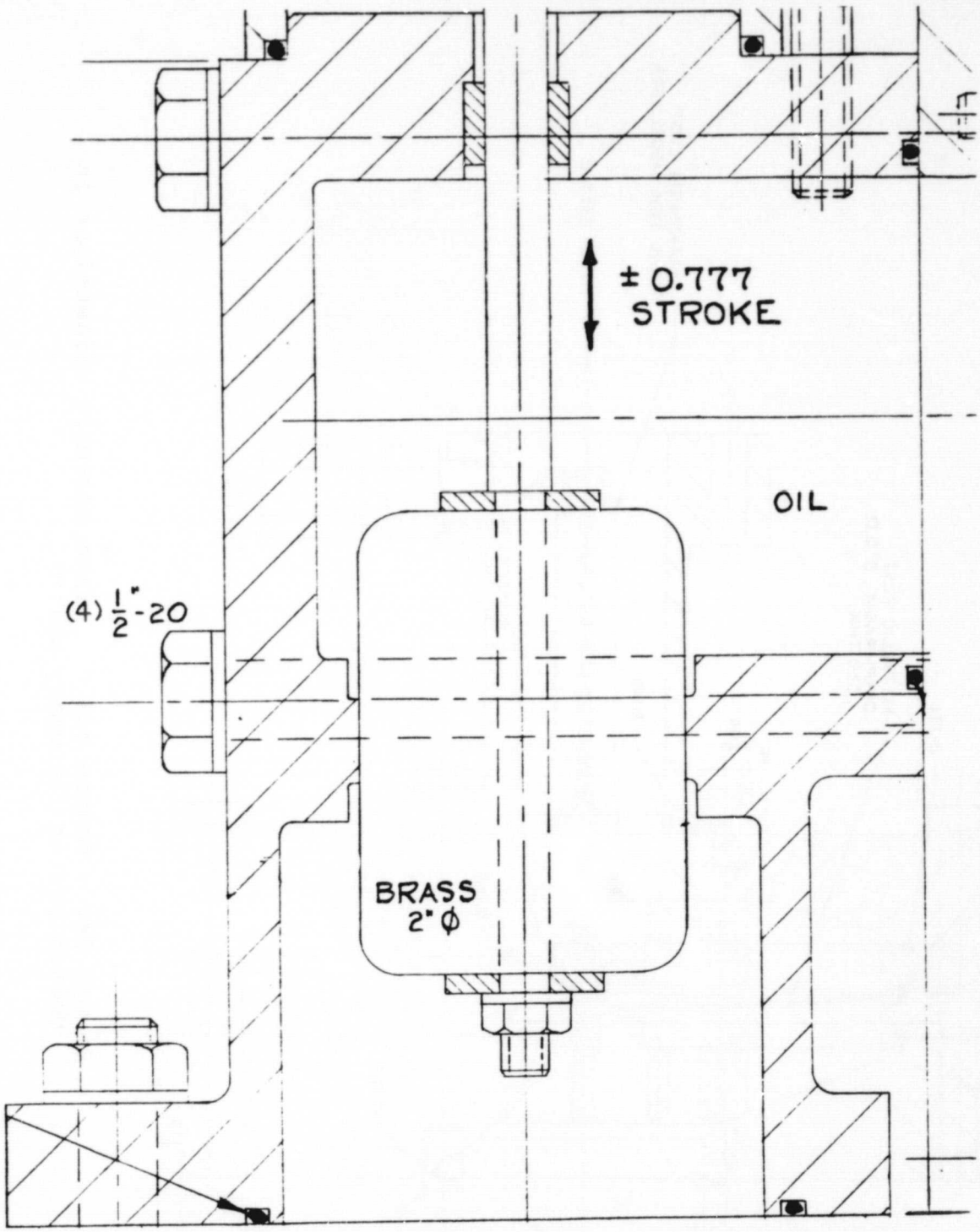

Figure 23. - Transmission piston and its housing
(dimensions in United States customary units)

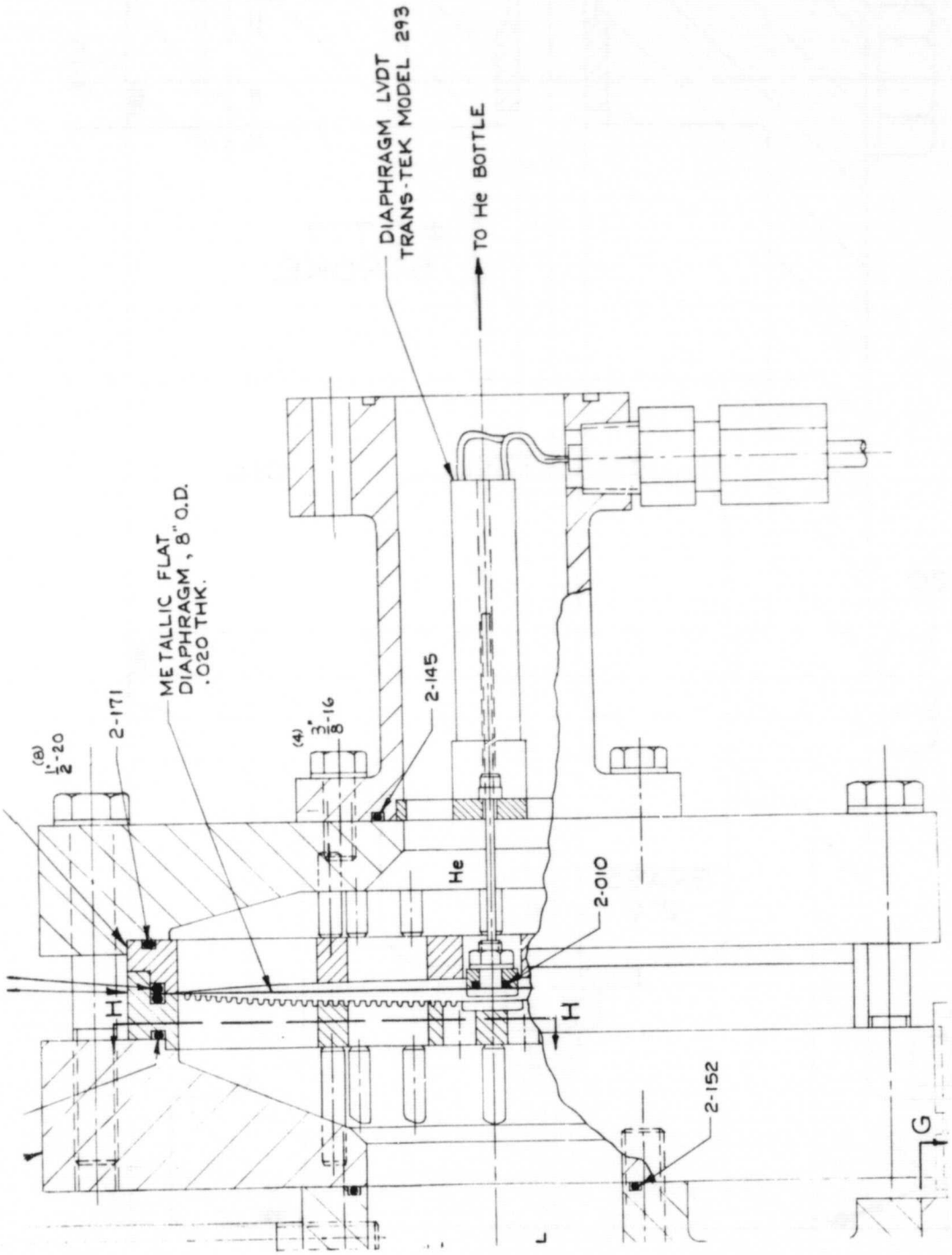

Figure 24. - Bounce gas diaphragm assembly (dimensions in United States customary units)

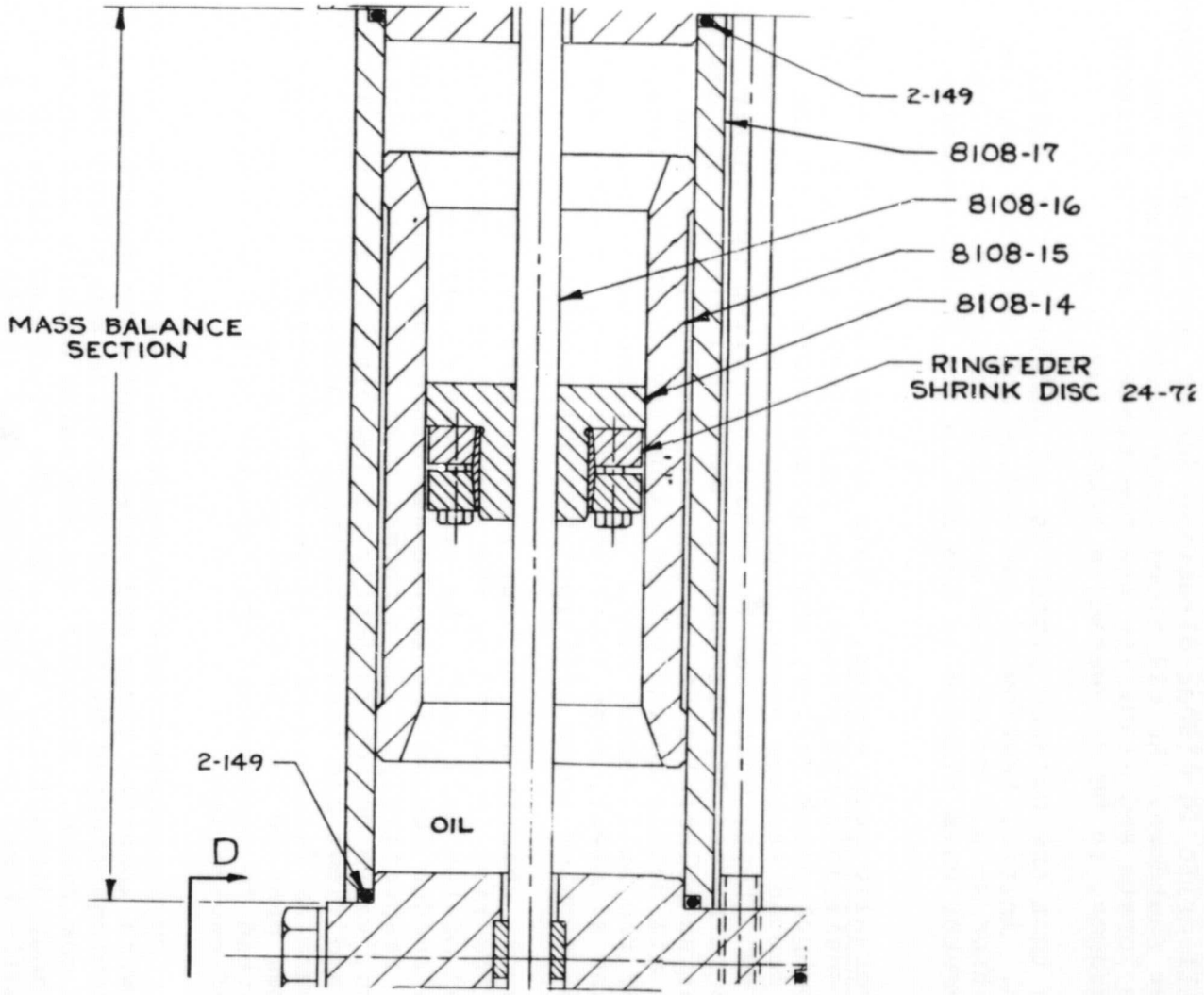

Figure 25. - Annular piston mass counter balance assembly (dimensions in United States customary units)

segregated dynamically in the upper and lower spaces due to small piston clearances that minimize leakage.

Clearances and land lengths are selected to minimize viscous and leakage power (subsection 3.2) but there will be enough leakage past the pistons and rod bushings so that the annular piston will drift in either direction during operation, and downward after shutdown. An oil bleed compensation system is necessary to locate and stabilize the positions of all the pistons and diaphragms, to be discussed in subsection 3.1.7.

Note that the balance piston is not necessary for engine operation. Initial testing of the engine and vertical pump rod configuration should be carried out using an appropriate single small-diameter mass clamped to the rod in the balance section.

3.1.6 Hydraulic pump system. - This system consists of the rod having a small integral piston, the pump block, two sets of input and output check valves, small accumulators local to the block, a pumped storage accumulator, and an oil sump. All but the last two items, which can be remote and sized optionally, are shown in Figure 26, with several sectional views. The design and operating principles of the pump are basically the same as almost all double acting piston pumps having check valves, except for the null center band. As described previously this is the simplest, most inherently stable way to start and run a FPSE coupled to an efficient hydraulic output.

However, this is not without risk of penalty, depending on design. The risk is caused by the fact that at the beginning or the end of the null band, the piston has significant velocity, causing a sudden demand for intake and discharge flows to stop or start, respectively. (In a normal pump having harmonic piston motion, valve action is mostly at low piston velocity, TDC and BDC, and flows accelerate smoothly). Consequently, the present pump is designed with large flow passages, light valves, and minimum passage lengths to the attached accumulators, all of which tend to accommodate the "spurts" of flow with minimal hammer and cavitation.

The pump is constructed of a monolithic block having drilled passages with inserted plugs and valve modules to direct the flow. Bushings trapped by the end caps guide the piston and rod, which are one piece. Accumulators and valve modules are accessible without dismantling the pump. The discharge valve is a typical ball-check, sprung and guided. The intake valve is a "thumbtack" shape to achieve the necessary orifice area and yet lightness to admit flow from an atmospheric sump without destructive cavitation.

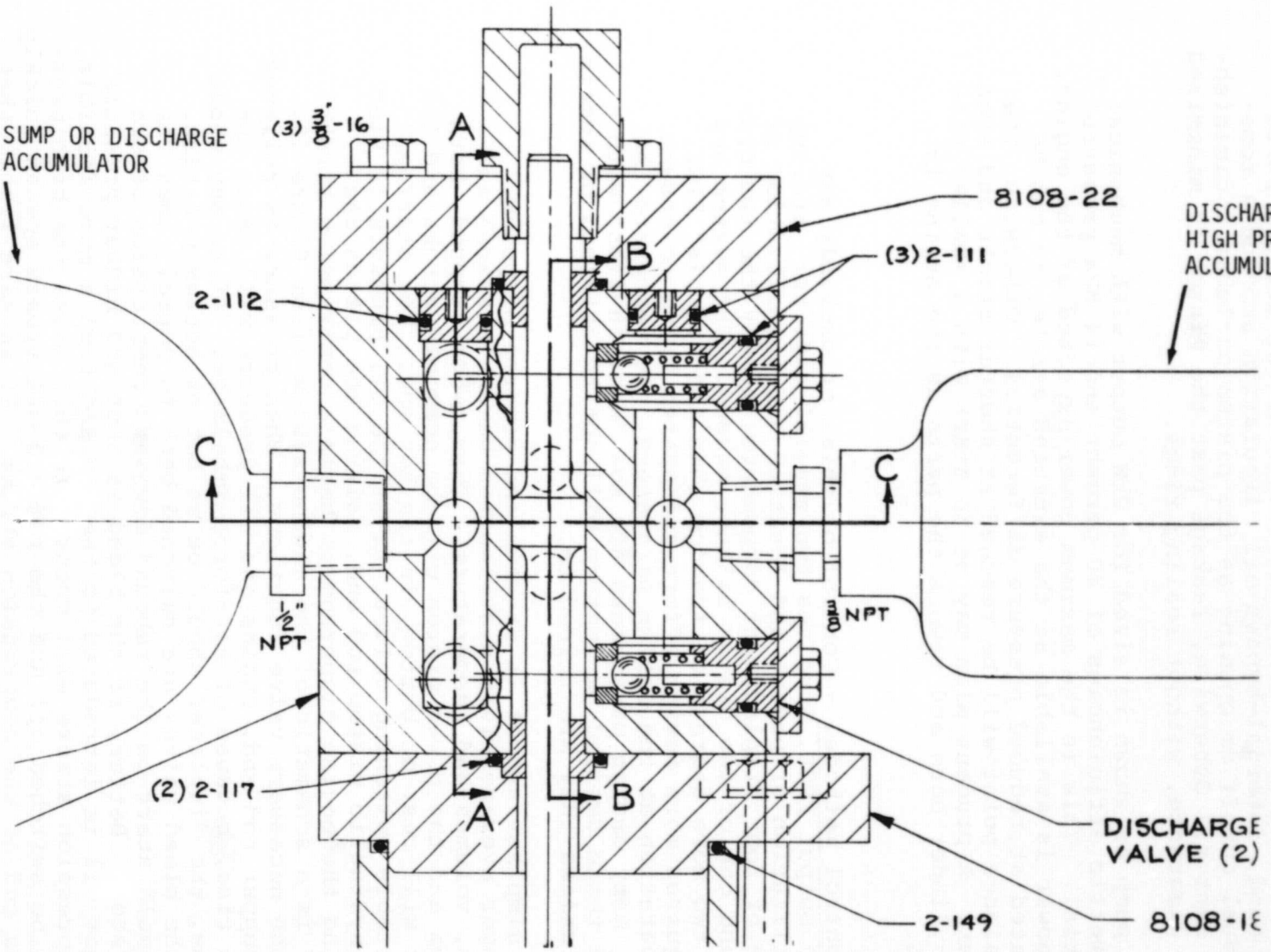

ORIGINAL PAGE IS OF POOR QUALITY

Figure 26. - Hydraulic pump system (dimensions in United States customary units)

The cross ports are drilled such that the piston is always guided and laterally pressure-balanced in its bore, and there is ample overstroke distance. In addition, the drilled ports for null band, internal-bypass oil circulation provide a somewhat gradual cutoff or opening as the piston occludes a diminishing port sector. Otherwise, leakage past the piston is minimized by close clearance, without sealing rings.

The pump as shown is sized for 2kW output with mechanical and volumetric efficiencies of 80 percent and 14 MPa pressure differential. This is the maximum power expected of the engine. If less power is available at the expected stroke, it can be accommodated at reduced pressure differential. Otherwise, the engine balance point will be reached at shorter stroke and even less power. A prudent plan may be to start with a smaller piston and cylinder bore and rework the parts as the engine is optimized.

3.1.7 Control methods. - Control of this, or probably any hydraulic output FPSE, involves two general aspects: startup and stabilization of power; and location and stabilization of all three or four displacement components, namely the two diaphragms and one or two piston balance masses. The system has at least two more degrees of freedom than the "simple" FPSE, so it requires more design effort and system means to ensure stable operation at the design parameters. We reiterate the obvious: many design parameters are not "cast in iron" with a FPSE, and these desired parameters will not be obtained or remain constant unless they are forced to.

The simplest aspect is startup and control of power, *given* proper average fluid distribution parameters such as pressures, volumes and temperature. Then, when stopped, both diaphragms and the power piston will be near mid-stroke and the displacer will rest on bottom, in the hot end. For startup, using suitable switching valves, first the oil pressure is bled from the hydraulic piston rod end, raising the piston and positioning the engine diaphragm to begin a compression stroke. Figure 27 is a schematic of the engine system (from Figure 18) showing the necessary valve functions. When pressure is relieved from the upper rod end, engine gas-oil pressure will cause the piston to rise, because of net-force imbalance. After any short dwell time, the displacer should be at hot or bottom position. Then if the bleed valves are switched back to normal, then the engine should start on the rebound downward compression stroke of the piston. Better, if the bleed is shut and higher pressure accumulator oil is introduced to the rod end then a more forcible rapid compression stroke will occur. In this case, the high pressure must be switched off and the rod end oil bypass opened quickly before the end of the compression stroke. It appears likely that

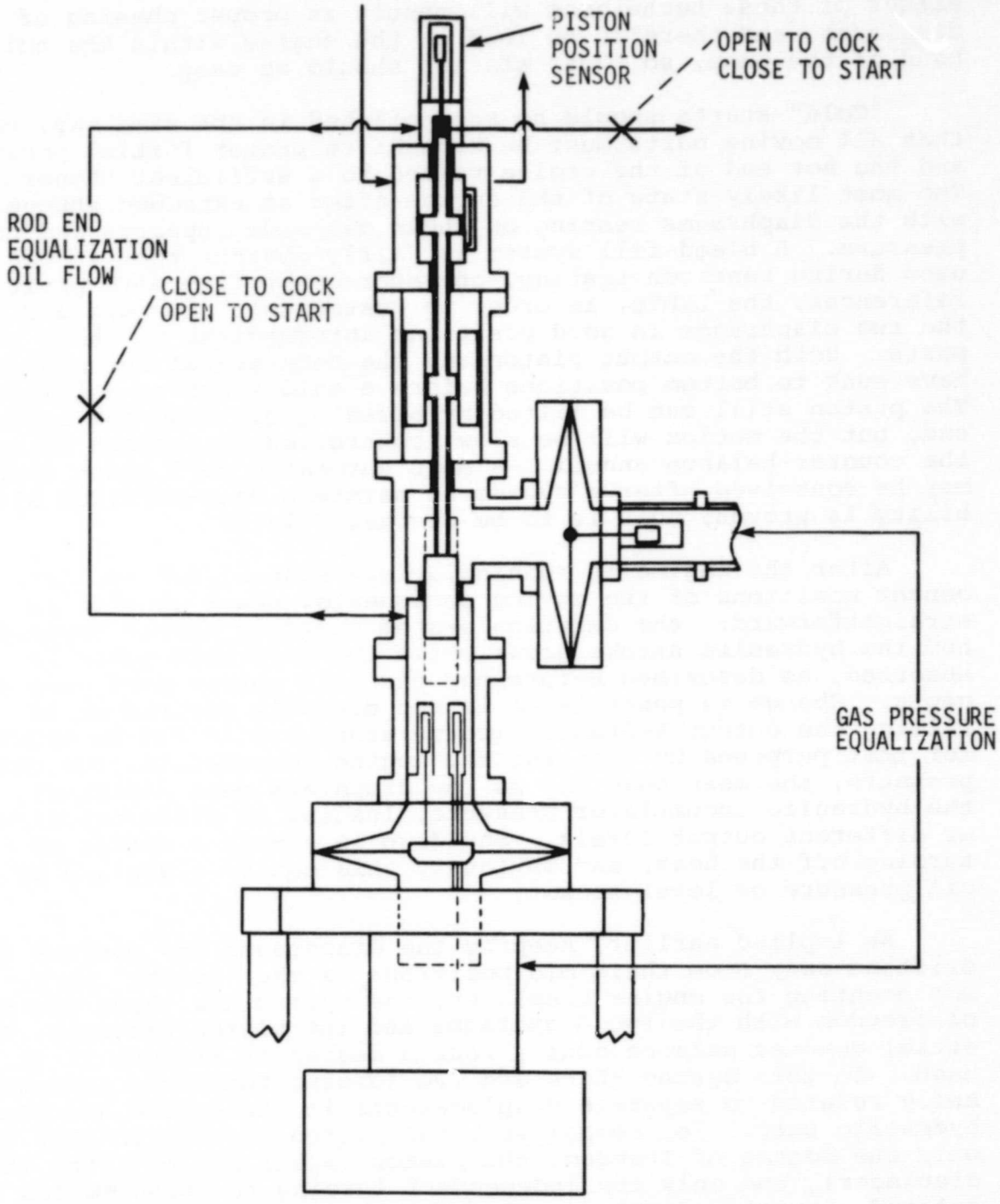

Figure 27. - Valves for lifting piston and starting engine

either of these techniques will result in proper phasing of the displacer, and there is no load on the engine within the null band of the pump, so "hot" startup should be easy.

"Cold" starts should be accomplished in the same way, except that all moving parts must be brought to proper initial positions, and the hot end of the engine raised to a sufficient temperature. The most likely state of the engine after an extended shutdown is with the diaphragms resting on their oil-side supports and no oil pressure. A bleed-fill system is fairly obvious that it can be used during research testing, operator controlled with position references, the LVDTs, in order to restore oil pressure and place the two diaphragms in good positions intermediate to their supports. Both the output piston and the counter-balance piston will have sunk to bottom positions before a cold start is attempted. The piston still can be lifted by bleeding oil from the upper rod end, but the motion will be slow, controlled by leakage through the counter-balance annuli. A more automatic cold start sequence may be conceived after a system to maintain mean-position stability is proven; this is to be discussed later.

After the engine is running, *given* stable, average or center positions of the moving components, power control is straightforward: the existing system controls heater temperature and the hydraulic stroke grows until the available power is absorbed, as described before for the null center band pump concepts. Change in power level is not normally desired while filling the output hydraulic accumulator, but it can be provided for test purposes by changing the engine temperature, the charge pressure, the mean dead volume (by diaphragm mean position), or the hydraulic accumulator pressure, leading to different strokes at different output levels. Shutdown is simply a matter of turning off the heat, and obviously this can be signalled by an oil pressure or level sensor.

As implied earlier, keeping the diaphragms and pistons from drifting away from their mid positions is the "tricky" part. Not counting the engine displacer, the system has three degrees of freedom with the two diaphragms and the piston assembly. The inertial counter balance adds a fourth degree of freedom if it is used. In this system there are two forcing functions independently related to separate displacements in the engine and the hydraulic pump. For comparison, the piston version RE-1000 has only one degree of freedom, the piston (again not counting the displacer), and only one independent forcing function, which is related to piston displacement. The piston acts directly on the engine working gas as well as the gas in the output damper. In the hydraulic output version the engine gas displacement is separated from the hydraulic pump displacement by an independently varying (i.e.; unknown inter-chamber leakage) volume of oil that acts to transmit force and motion.

The only possible control advantage of the hydraulic diaphragm version is that there is no leakage between the gas spaces except that provided in a control system. On the other hand, there is uncertainty concerning many factors: the directional bias forces of the diaphragms as they approach their supports, the bias force leading to drift of the hydraulic piston, and the net leakage of the pump oil to the transmission oil. With respect to first order effects, there are neither bias nor centering forces in the output transmission system itself, except for the piston weight, and there is no oil leakage bias (7 MPa transmission oil, 14 MPa accumulator, open sump). The primary bias, the piston weight, can be balanced permanently with the appropriate additional pressure (charge mass) in the engine versus that in the bounce space.

Consequently, the *tentative* conclusion is that with the engine and bounce gas hermetically isolated, the positional drift of all parts will be slow enough for operator response. Referring to the three position sensors, we recommend the following control method for *initial* testing: adjust the gas balance in order to control engine diaphragm position and balance the vertical piston force; adjust the balance of oil on either side of the transmission piston in order to center the output piston; inject or bleed oil from the balance space in order to maintain transmission oil volume and, hence, bounce gas diaphragm position, given that the engine diaphragm mean position is constant. Engine diaphragm position will vary *primarily* only with engine temperature, or effective "reduced" volume per mass. A system of bleed-check valves to provide these control functions is shown in Figure 28. This system has not been sized because the prediction of drift due to obscure secondary effects is difficult.

Systems to automatically control the positions of the hydraulic transmission parts have been conceived but not designed in detail. The tentatively preferred scheme is shown in Figure 29. It consists first of oil bleed valve spools attached to both diaphragms; they dump oil when a diaphragm approaches too near its gas-side support, thereby preventing impact and providing continuous operation with minimal dead volume in the engine gas compression diaphragm space. Secondly, a limited amount of oil flows from the high pressure accumulator into the cylinder annulus around the output piston. Bleed passages between the oil on opposite sides of the piston are modulated by the piston position so that a time-average bias in the leakage flow tends to center the piston. (This "centering-port" method is often used with gas leakage to stabilize free piston engines internally.) Similar bleed-bias ports are required to maintain approximate centering

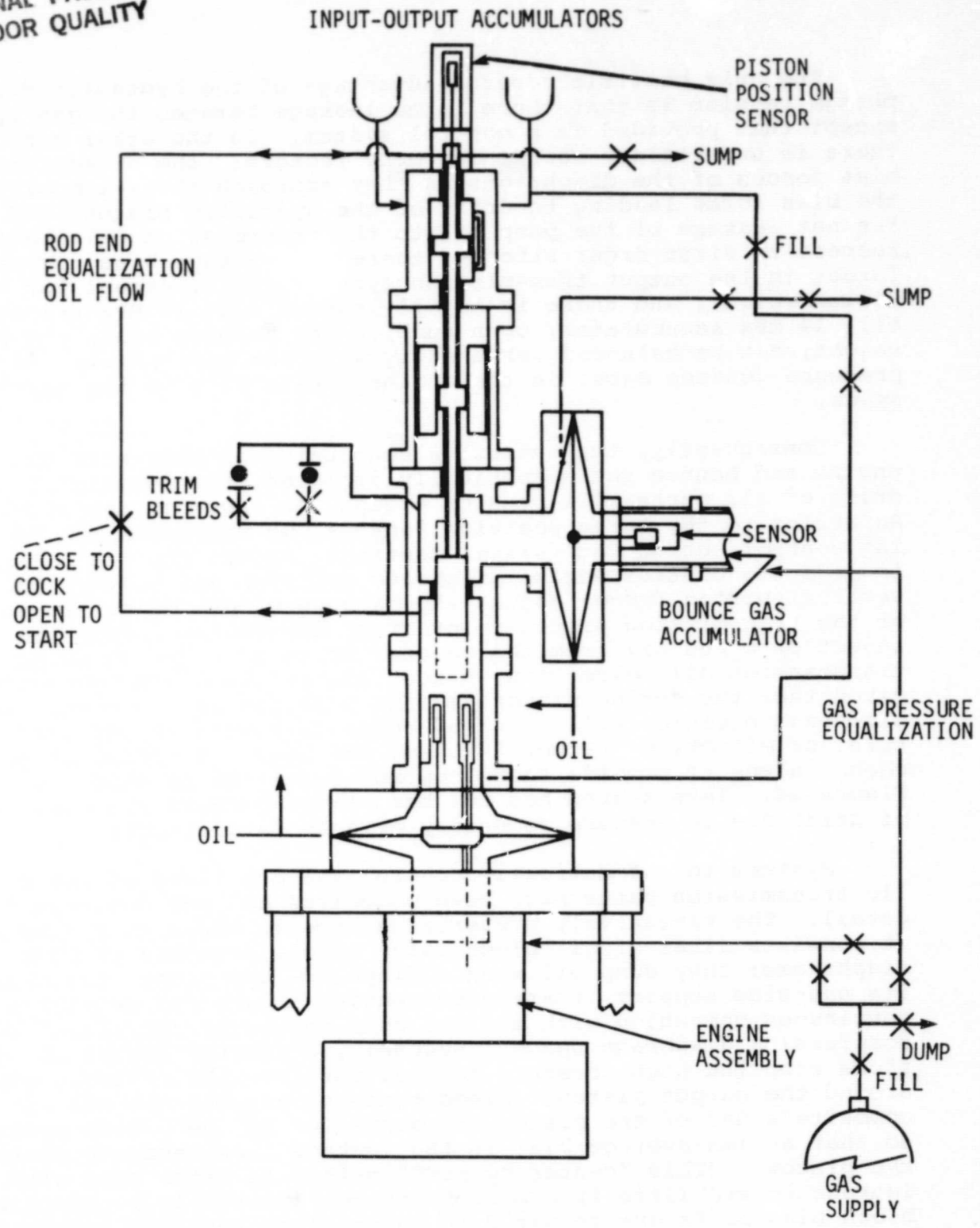

Figure 28. - Plumbing system for setup and manual trim control of engine using sensor information

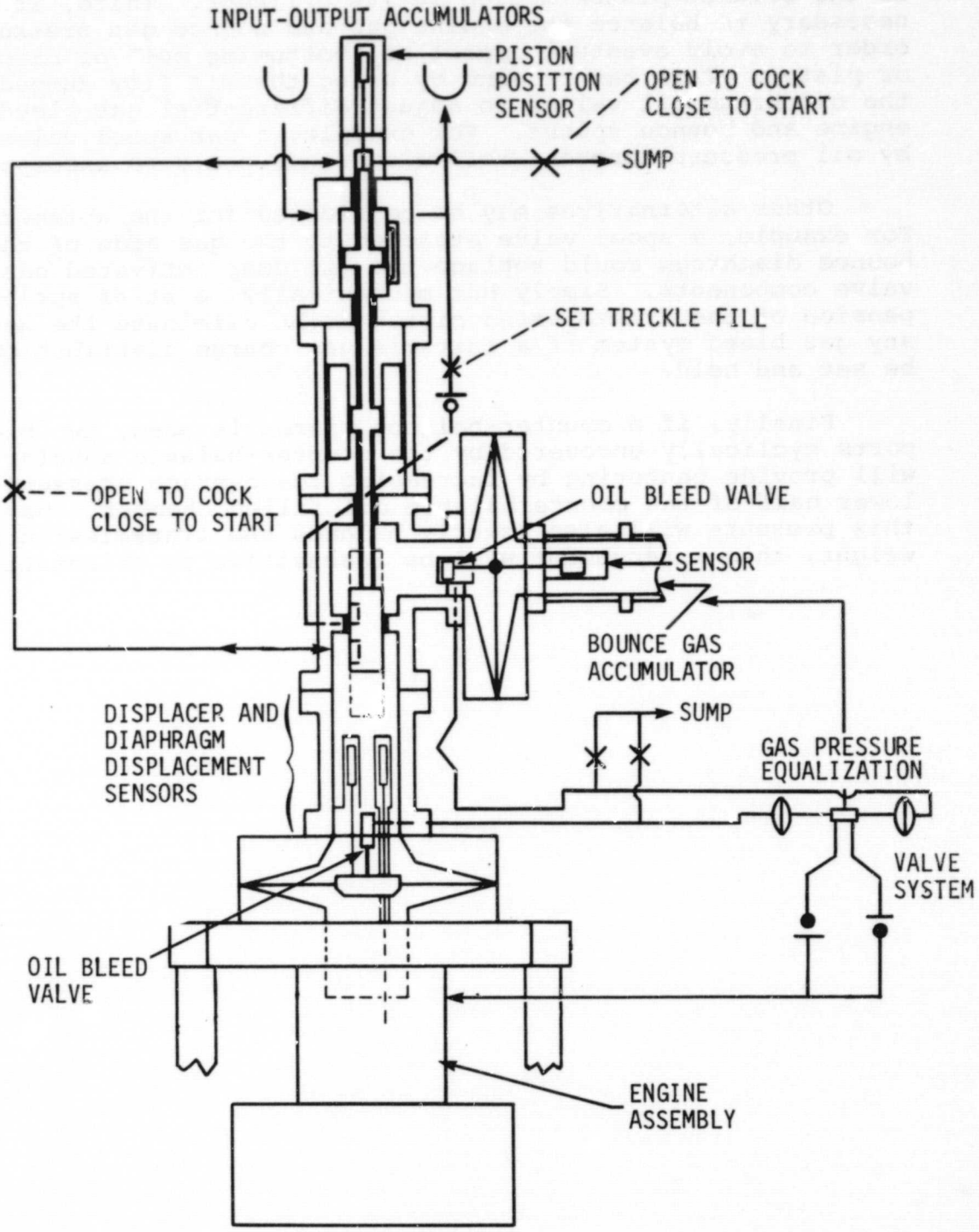

Figure 29. - Schematic of automatic position control for hydraulic output components

of the balance-piston motion in its cylinder. Third, it appears necessary to balance the engine gas and bounce gas pressures in order to avoid eventual impact or "bottoming out" of diaphragm or piston. This can be done by using the oil flow dumped from the diaphragm oil valves to adjust differential gas bleed between engine and bounce spaces. For example, a gas spool valve actuated by oil pressure through small diaphragms could be incorporated.

Other alternatives may be considered for the automatic system. For example, a spool valve attached to the gas side of the bounce diaphragm could replace the oil dump activated gas bleed valve components. Simply but mechanically, a stiff spring suspension of the transmission piston might eliminate the need for any gas bleed system if a suitable gas charge distribution could be set and held.

Finally, if a counter-balance piston is used, two bleed ports cyclically uncovered by the counter-balance annular piston will provide centering by increasing the average pressure in the lower half of the counterbalance oil filled chamber. Because this pressure will also exactly balance the transmission piston weight, this arrangement will be insensitive to orientation.

3.2 Detailed Analysis

This section describes the analyses performed in parallel with detail design of the hydraulic output system for the RE-1000 FPSE. The detailed analyses include the metal diaphragm analysis, the thermodynamic and dynamic analyses of the engine, and estimates of additional power losses due to hydraulic output conversion of the RE-1000 FPSE.

3.2.1 Metal diaphragm analysis. - Two metal diaphragms are used in the hydraulic output version of RE-1000 FPSE. They are the engine diaphragm and the bounce gas diaphragm. The engine diaphragm provides a hermetically sealed interface between the engine gas and the hydraulic fluid. The bounce gas diaphragm separates the hydraulic fluid from the bounce space gas.

The diaphragm analysis will provide the information on the following items of interest:

- Stress level and distribution - this information is required for the design of the edge sealing and supporting method. It will also be used to ensure that the maximum stress of the diaphragm remains well below the endurance limit of the diaphragm material.

- Axial displacement distribution - this information will be used to design the over-pressure protection supports. The squeezing and trapping of gas or oil between the diaphragm and the supports should be prevented by careful contouring of the support structures.

- Meridional displacements of edges - this is critical information for design of the edge sealing and supporting. Especially, if the O-ring seals are used for the edge sealing, the meridional displacement of edges will cause the O-rings to roll back and forth radially. This rolling distance should be short to prevent the fatigue failure of the O-ring material.

- Stiffness of diaphragm near TDC and BDC - the program NONLIN can analyze only static loading case. The dynamic effect was approximately accounted for by introducing a static force applied at the inner edge. The magnitude of the force was set equal to the inertia force of the center plug mass oscillating at design point conditions. The stiffness of the diaphragm (k) and the center plug mass (m) introduce a natural

frequency equal to $(1/2\pi)\sqrt{k/m}$. In order to prevent (high frequency oscillation) of the diaphragm at its TDC and BDC, the above natural frequency should be designed to be much higher than the engine frequency.

For the analysis of the diaphragms, two predeveloped computer programs, NONLIN and ANSYS, were utilized. The program "NONLIN" is a bellows/diaphragm analysis developed by Dr. J.F. Lestingi, et al. (ref. 2) at Battelle Memorial Institute, Columbus, Ohio. It is based on a multisegment numerical integration of a set of simultaneous nonlinear first order differential equations. This program is capable of analyzing linear elastic axisymmetric and nonsymmetric deformations, and nonlinear axisymmetric deformations of bellows and diaphragms.

The "ANSYS" program is a proprietary, general purpose finite element program developed by Swanson Analysis, Inc. The program is available through a commercial computer network.

FMA obtained the program NONLIN through the courtesy of Battelle Institute, Ohio. NONLIN was used for the actual analysis of the diaphragms. ANSYS was used only to check the results from NONLIN in the initial stage of the analysis effort.

Initial sizing of the diaphragms was done by approximate calculations combining the Belleville spring analysis (ref. 3) and simple bending theory for flat plates. Table 6 shows the specifications and boundary conditions of the two diaphragms used in the analysis. The specifications given here represent the final diaphragm designs for the hydraulic output RE-1000 FPSE.

The results of the diaphragm analysis are presented graphically in Figures 30 through 37. Brief discussions of each follow.

Figure 30 shows the diaphragm center deflection as a function of the pressure loading on the diaphragms. A flat annular diaphragm has a very low stiffness near the mid position. The stiffness increases rapidly as the diaphragm is deflected away from the mid position. Beyond a certain point, the diaphragm stiffness becomes almost constant as shown in Figure 30. Because of the rapidly increasing stiffness, the program NONLIN required a very small load step in order to achieve convergence. A 0.254 mm thick diaphragm was initially analyzed. As shown in Figure 30, the 0.254 mm diaphragm had such a low stiffness that only 1380 Pa pressure differential was required for the design point displacement of 80 cm^3. The stiffness in this case was so low that even a small radial pressure gradient due to fluid squeezing would cause the diaphragm to deform locally in a totally unpredictable way. That is why the thickness was increased to 0.508 mm in which case the diaphragms were stiff enough to avoid unwanted local deformations.

TABLE 6. - SPECIFICATIONS AND BOUNDARY CONDITIONS FOR THE DIAPHRAGM ANALYSIS, NONLIN

Specifications	Engine diaphragm	Bounce gas diaphragm
Outer diameter (cm)	20.32	20.32
Inner diameter (cm)	6.35	2.54
Thickness (cm)	0.0508	0.0508
Young's modulus (MPa)	2.069×10^5	2.069×10^5
Poisson's ratio, ν	0.27	0.27
Boundary conditions		
Outer edge	Simply supported to the casing	Simply supported to the casing
Inner edge	Simply supported to the center plug which moves with the diaphragm	Axially clamped to and radially guided by the center plug which moves with the diaphragm
Volume amplitude at design point (cm^3)	40	40

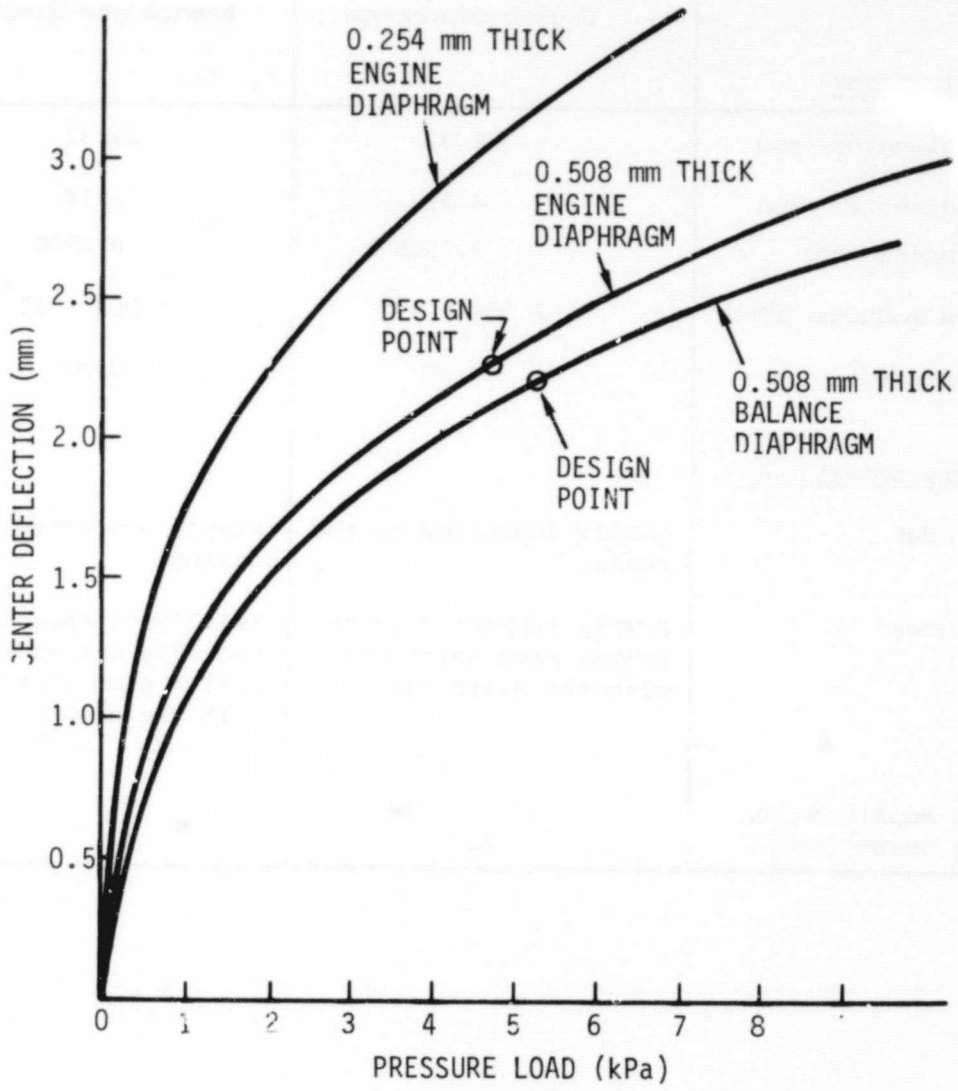

Figure 30. - Center deflection versus pressure loading of the diaphragms.

Figure 31. - Displacement distribution of the engine diaphragm at design point.

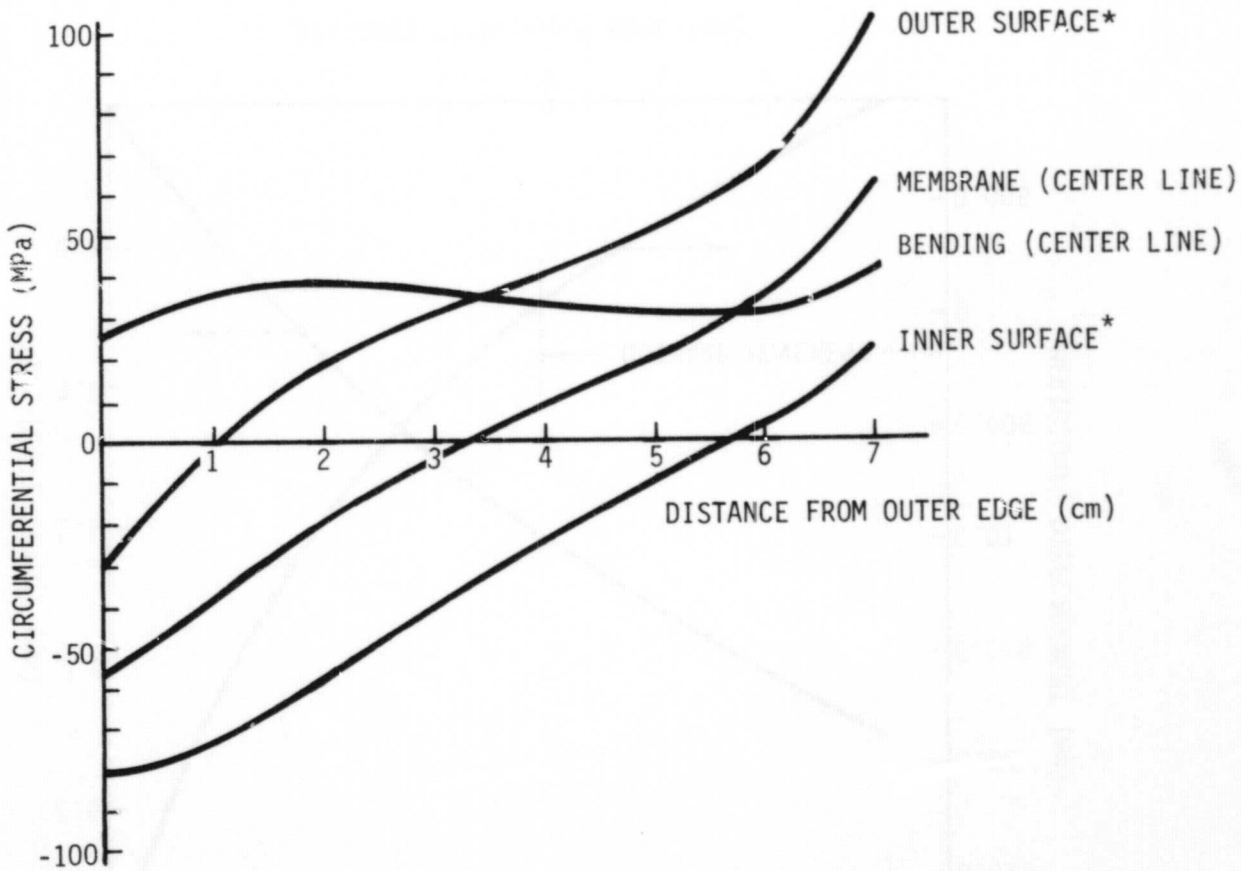

*Outer surface refers to the surface where the pressure load is applied. Inner surface refers to the opposite surface.

Figure 32. - Circumferential stress distribution of the engine diaphragm at design point.

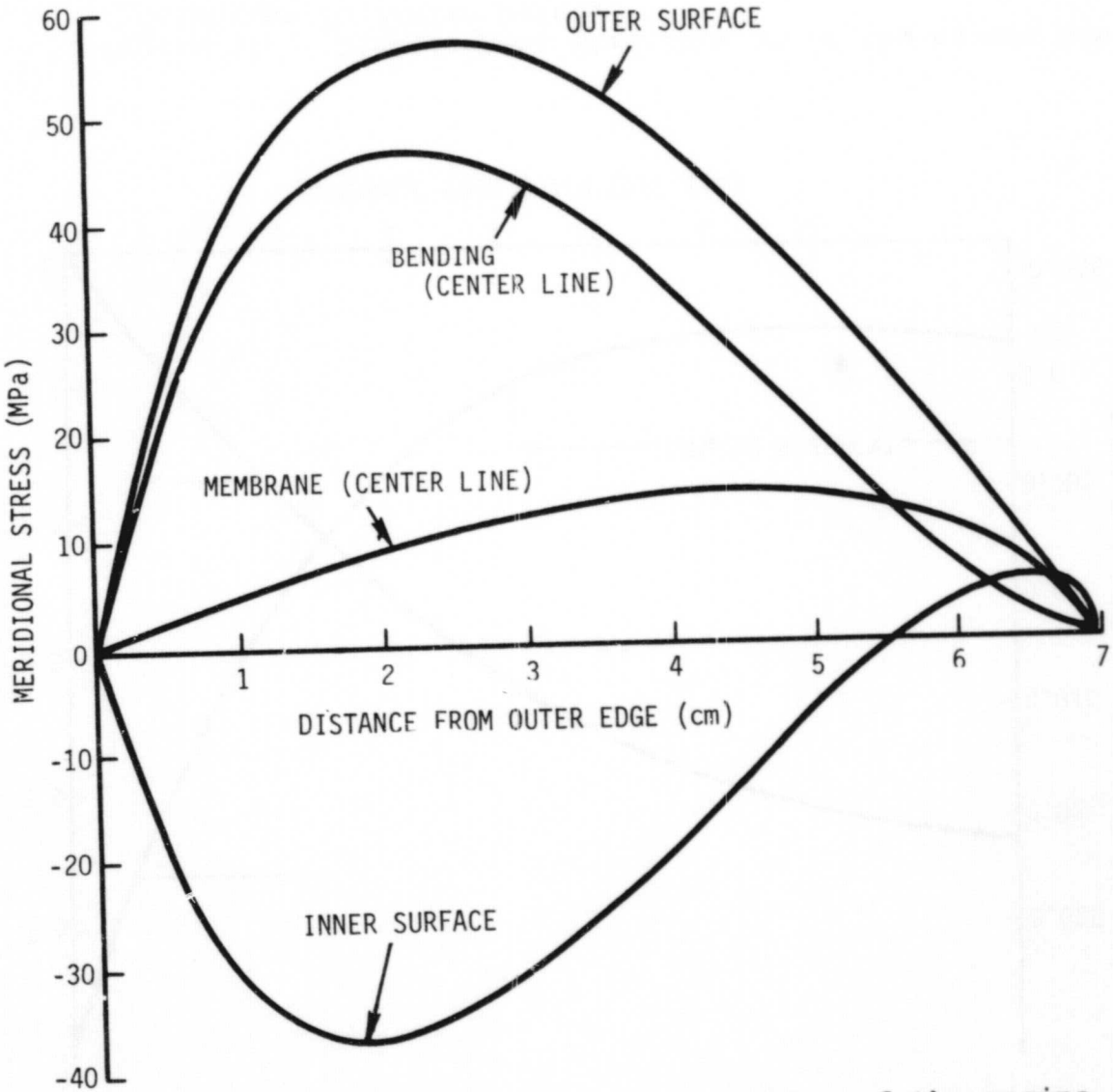

Figure 33. - Meridional stress distribution of the engine diaphragm at design point.

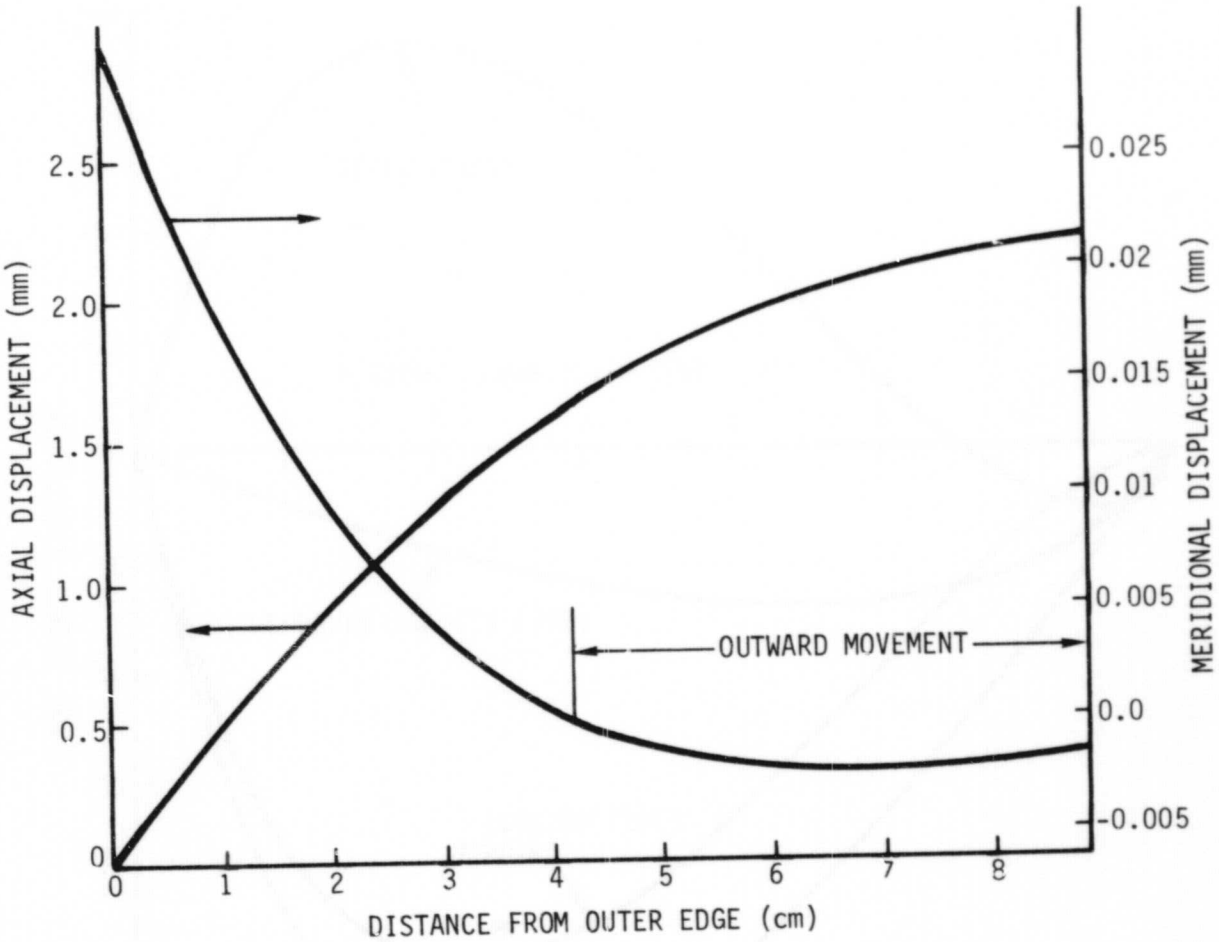

Figure 34. - Displacement distribution of the bounce gas diaphragm at design point.

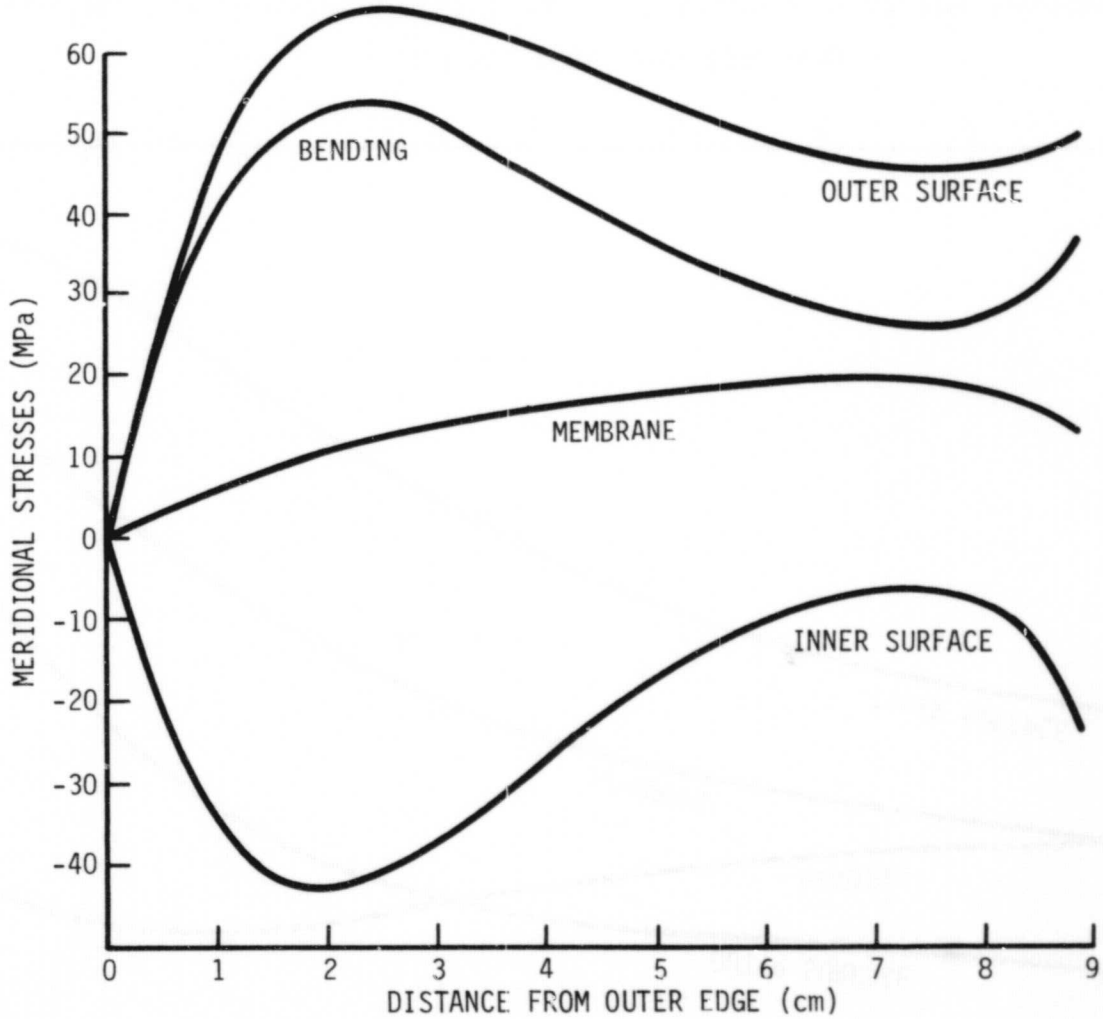

Figure 35. - Meridional stress distribution of the bounce gas diaphragm at design point.

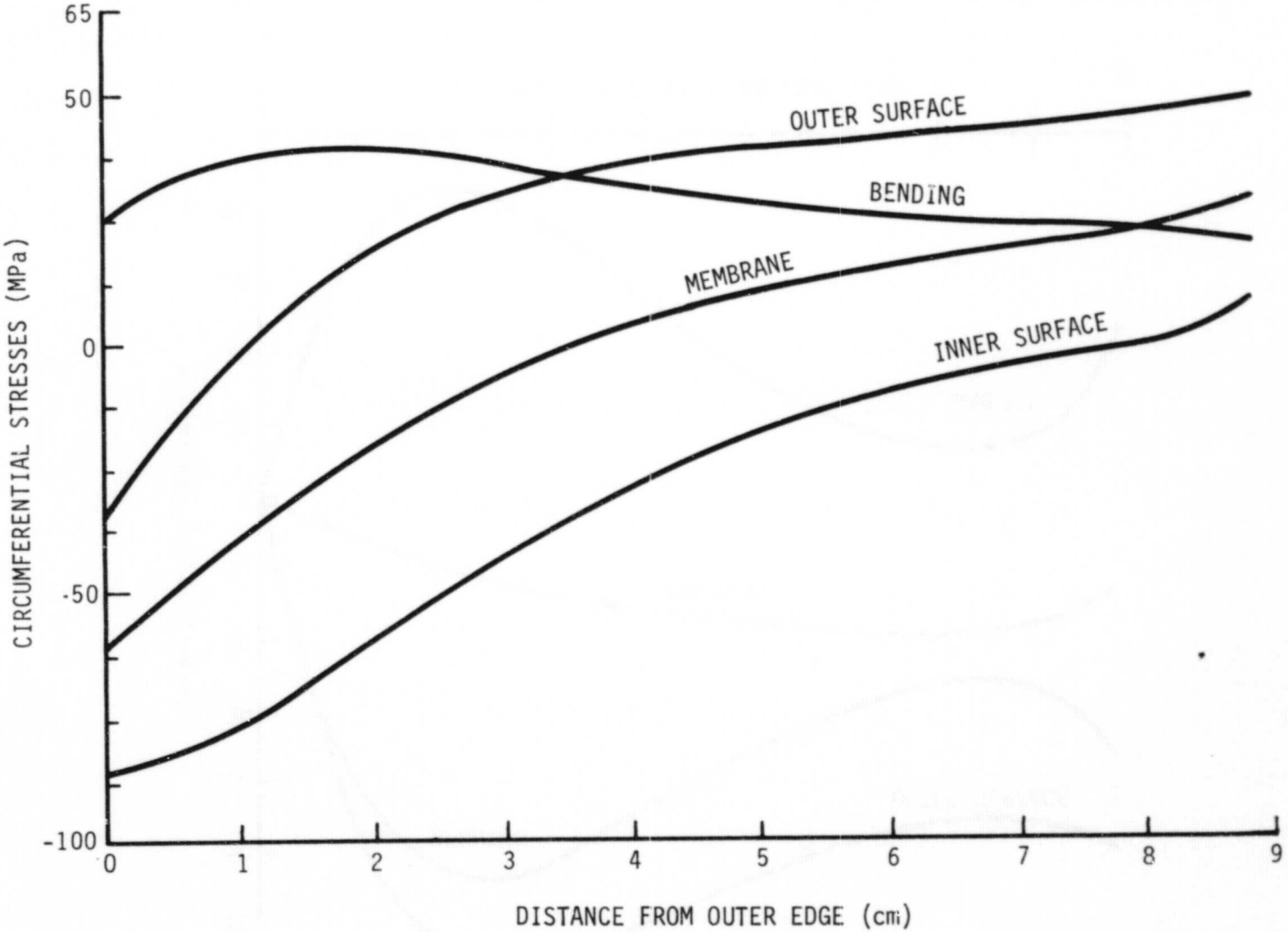

Figure 36. - Circumferential stress distribution of the bounce gas diaphragm at design point.

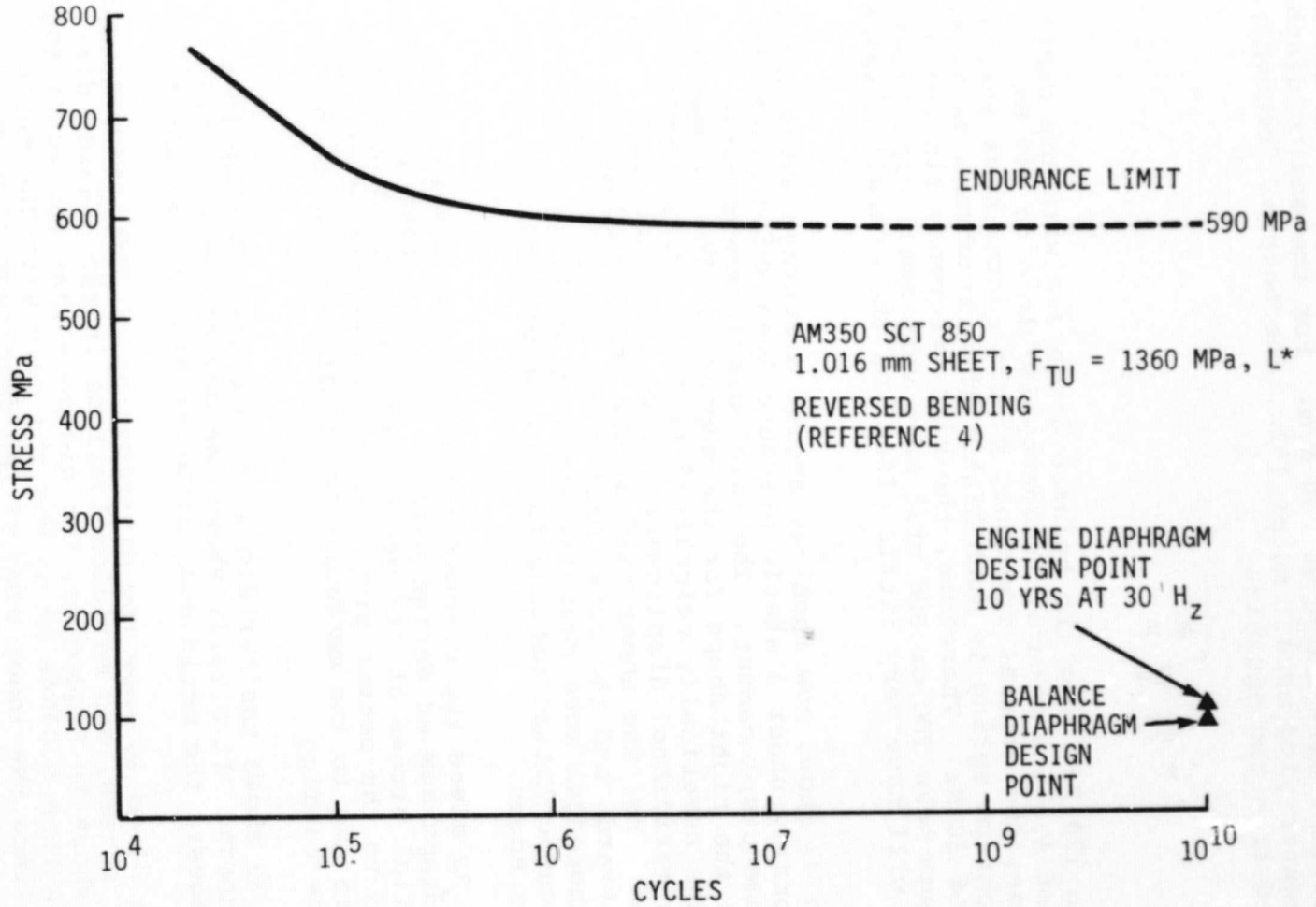

*ULTIMATE TENSILE STRENGTH IN LONGITUDINAL DIRECTION OF ROLLING.

Figure 37. - Stress versus cycles to failure for AM 350 SS sheet.

The spring constants, k, for both diaphragms near the TDC or BDC positions were about 96,000 N/m. For the engine diaphragm with the center plug mass, m, of 181g, the natural frequency, f, obtained from the equation

$$f = \frac{1}{2\pi}\sqrt{\frac{k}{m}} \qquad (1)$$

is close to 120 Hz. For the balance diaphragm with the center plug mass of 45g the natural frequency is close to 240 Hz. In each case, the natural frequency of the center mass sprung by the diaphragm spring is much higher than diaphragm oscillating frequency of 30 Hz. Therefore, the high frequency ringing of the diaphragm near TDC or BDC will have very small amplitudes so that it will have very little effect on the overall diaphragm dynamics.

Figure 31 shows how much the engine diaphragm moves axially and meridionally under a static pressure load which gives the design volume displacement. The axial displacement curve is used to get the right shape for the supports. The volume displacement was numerically calculated from the axial displacement curve. The meridional displacement curve indicates that qualitatively speaking, the inner half of the annular diaphragm moves radially outward, and the outer half moves radially inward. The distances the edges move radially are very small (< 0.03048 mm) which will cause little rolling fatigue problem for the O-ring seals at the edges.

Figure 32 gives the circumferential stress distribution in the engine diaphragm at design point. It shows that the maximum circumferential stress of 103 MPa occurs where the diaphragm is connected to the center plug. About two-thirds of the maximum stress is due to the membrane stretching and about one-third is due to the bending.

Figure 33 shows the meridional stress distribution in the engine diaphragm. It clearly shows the advantages of simply supported edges: the meridional stresses are zero at the edges.

Figures 34 to 36 show the distribution of displacement, circumferential stress, and meridional stress in the balance diaphragm. As shown in Figure 34, the distance that the outer edge moves is less than 0.03048 mm as was the case with the engine diaphragm. Since the inner edge of the diaphragm is clamped axially to the plug, the meridional stresses in Figure 35 show considerable level of stresses, up to 48 MPa at the inner edge. Still the maximum stress in the balance diaphragm is only about 90 MPa in the circumferential direction as shown in Figure 36.

Figure 37 shows the stress versus cycles to failure data for AM 350 SS sheet of 1.016 mm thickness. Although our diaphragm design has half the thickness of the fatigue test specimen, the endurance limit is not expected to depend significantly on thickness within practical design ranges. The maximum equivalent stresses of the two diaphragms are 100 to 110 MPa which is well below the endurance limit of 590 MPa for AM 350 SS.

3.2.2 Thermodynamic Performance Predictions

3.2.2.1 Methods of analysis. - For the detailed analysis of the hydraulic output Free Displacer Stirling engine, Sunpower used their third order Stirling engine analysis.

There are two modes in the above analysis: the constrained mode and the unconstrained mode. The constrained mode deals only with the thermodynamic aspect of the Stirling engine. The dynamics of the reciprocating components are predetermined by a separate dynamics analysis using a simplified thermodynamics. The unconstrained mode combines the dynamics of the piston, the displacer and the load, and thermodynamics. This mode takes into account the interaction between the dynamics of the moving parts and the engine thermodynamics by solving them simultaneously. The unconstrained mode requires many cycles of calculation in order to reach the steady state, and therefore is quite expensive to use.

In the present problem, the null center band hydraulic pump has a load function which resembles truncated square waves. The highly impulsive or step function like nature of the load necessitated the use of the unconstrained mode to closely simulate the actual processes of the engine. The less expensive, constrained mode analysis was used to obtain the performance trend and to perform a sensitivity analysis of important operating parameters.

3.2.2.2 Critical parameters. - Within the scope of the design program, there are two parameters significantly affecting the power output and the efficiency of the engine. They are displacer phase angle with respect to the piston motion and the cylinder heat transfer. Brief discussion of each follows.

3.2.2.2.1 Displacer phase angle. - The displacer phase angle is closely linked to the overall engine dynamics. Varying the displacer phase angle will change the frequency, the amplitudes of the piston and the displacer, the pressure wave phase angle and also the engine performance. It will also change the frequency slightly. For a displacer of a given mass, the phase angle depends on the following:

- The displacer gas spring constant which is inversely proportional to the mean volume of the gas spring.

- The displacer load which is determined by the pressure drop loss through the heat exchangers and the gas spring hysteresis loss.

The phase angle of the displacer can be easily changed by varying gas spring volume. The original RE-1000 FHSE had two displacer rod sets, the main difference of which was the gas spring volume. The rod set with the larger gas spring volume had the low displacer phase angle of 45 deg, which was determined by the optimization of the engine for the highest efficiency. The rod set with the smaller gas spring volume had the displacer phase angle of 80 deg. The high phase angle would result in the highest power.

For the hydraulic output Stirling engine, however, the unconstrained mode analysis indicated that the rod set should be redesigned as will be discussed later.

3.2.2.2.2 Cylinder heat transfer. - With the increased heat transfer area and the extremely narrow spaces in the compression space of the diaphragm engine, the magnitude of the heat transfer coefficient has a significant consequence in the predicted performance of the engine.

Two methods were used to estimate the heat transfer coefficient inside the cylinders: Taylor's Internal Combustion (I.C.) engine correlation (ref. 5) and FMA's cyclic heat transfer analysis (ref. 6, 7).

Taylor's I.C. engine correlation is based on data gathered from 19 different types of engines for automobiles, aircrafts, trucks, locomotives and other commercial use. It is expressed by

$$h = 10.4 \frac{k_g}{B} \left(\frac{GB}{\mu g_o} \right)^{0.75} \qquad (2)$$

where

h = Heat transfer coefficient, based on piston top area

k_g = Conductivity of the engine gas

B = Bore

G = Average mass flow rate per cycle divided by piston area

μ = Viscosity

g_o = Gravitational constant.

Sunpower previously observed that when the above correlation had been used in their third order analysis, it had resulted in a close agreement of the analysis with the test data. Also, for normal bore/stroke cases, the values of the heat transfer calculated from the above equation were not too different from the values calculated by FMA's cyclic heat transfer analysis which is described in the following paragraphs.

It is fair to say that the Taylor's formula is a very valuable empirical correlation for the heat transfer in cylinders. But the lack of combustion process and values in the Stirling engine makes it difficult to be accepted without actual testing of Stirling engines. Especially, this correlation is invalid for high bore/stroke case such as diaphragm piston engines.

The FMA's cyclic heat transfer analysis has been partially published (ref. 6, 7). The analysis is valid for

- The normal bore/stroke cylinder-piston cases.
- The high bore/stroke cylinder-piston or close gap diaphragm cases.

For the normal bore/stroke case, the FMA analysis utilizes empirical heat transfer enhancement factor correlation based on an unpublished gas spring data (ref. 6).

For the narrow gap case, the FMA analysis includes the effect of mixing or eddy conductivity. Although no test data exist, the effect of mixing modeled here represents a conservative estimate due to the fact that a steady-flow, not periodic flow, assumptions were used to obtain the heat transfer enhancement factor.

3.2.2.3 Results of the third order analysis. - The results include:

- The base-point, or reference simulations of the standard RE-1000 FPSE with the 80 deg phase displacer and the diaphragm piston engine.
- The sensitivity analysis of the diaphragm piston Stirling engine with respect to the cylinder heat

transfer h, the phase angle of the displacer, ϕ_d, and the pump load force, F_{load}.

- The predicted performance of the diaphragm piston Stirling engine.

3.2.2.3.1 Reference simulations. - Sunpower used the constrained mode third order analysis for the reference simulations. The purpose of the reference simulations was to establish the base-point performance of the standard RE-1000 FPSE to be compared with the predicted performance of the diaphragm piston engine. Also, the constrained mode simulation of the diaphragm piston engine serves as an initial condition for the unconstrained mode simulation.

In each simulation, FMA supplied the heat transfer coefficients for both expansion and compression spaces from the cyclic heat transfer analysis mentioned earlier.

Run 20a and run 28 of Table 7 show the results of the simulation of the standard RE-1000 FPSE with Taylor's heat transfer correlation and FMA heat transfer correlation, respectively. Run 29 gives the results for the diaphragm engine simulation. Note that the piston swept volume for the diaphragm engine is 36 percent higher than that of the standard RE-1000 FPSE. The increased stroke was to compensate for the decrease in mass flow amplitude for the near isothermal diaphragm engine, and to maintain the pressure amplitude level.

The displacer rod is of the high phase angle design (80 deg) for all three simulations.

The magnitudes of the heat transfer calculated by Taylor correlation are 14 to 118 percent higher than those predicted by FMA correlation. This can be explained by the fact that the I.C. engines have a violent combustion period and an intentionally augmented inlet turbulence level which is known to persist over the entire cycle whereas the Stirling engines do not experience either condition.

Although the increased piston swept volume maintains the pressure wave amplitude, the increased heat transfer in the compression space of the diaphragm engine changes the engine performance noticeably. It considerably lowers the pressure wave phase angle and more than doubles the available energy loss in the compression space. The end result is a drop in power and efficiency as shown in Table 7. In run 29, the compression space,

TABLE 7. - RE-1000 REFERENCE SIMULATIONS CONSTRAINED THIRD ORDER ANALYSIS

Run No.	20a	28	29
Displacer phase (deg)	80	-	-
Piston swept vol (m^3)	58.8E-6	-	80.1E-6
h_{cmp} (W/m^2-K)	1.36E5	9.9E3	3.07E4
S_{cmp} (m^2)	2.57E-3	3.1E-2	8.5E-2
hs_{cmp} (W/K)	350	307	2610
T_{cmp} (K)	320	-	313
h_{exp} (W/m^2-K)	5.68E4	4.8E3	4.8E3
S_{exp} (m^2)	2.57E-3	1.4E-2	1.4E-2
hs_{exp} (W/K)	146	67	67
T_{exp} (K)	839	835	827
PV power (W)	2094	2220	1930
Indicated η	0.353	0.373	0.311
P_{cmp} amplitude (N/m^2)	1.31E6	1.33E6	1.35E6
P_{cmp} phase (deg)	26.3	27.6	16.0
Reference enthalpy flux (W)	1080	1020	1020
Sum pumping loss (W)	390	370	340
Available energy loss due to heat transfer and mixing			
Cooler (W)	230	180	150
Regenerator (W)	730	700	690
Heater (W)	120	120	140
Compression space (W)	350	310	740
Expansion space (W)	110	70	70
Net heat transfer from compression space (W)	-	-	1370
Remarks	RE-1000 engine reference Taylor IC heat transfer used	RE-1000 engine reference FMA cylinder heat transfer analysis used	Diaphragm engine reference FMA cylinder heat transfer analysis used

especially the diaphragm area experienced a large amount of heat transfer. Under the assumption of the constant wall temperature at the sink temperature, the compression space had a net heat transfer of 1370W out of the space. About half of this heat had to be transferred through the hydraulic side, which necessitated the heat transfer augmentation measures in the hydraulic side of the diaphragm described in subsection 3.1.

3.2.2.3.2 Sensitivity analysis. -

Heat transfer in the compression space: From run 29 of Table 7 the large available energy loss in the compression space of the diaphragm engine reflects the fact that the processes are far from being isothermal. Here, the available energy loss refers to the decrease in available portion of the heat due to heat transfer across finite temperature differences and due to mixing of gases at different temperatures. It would be interesting to find out how much heat transfer increase or decrease would cause an appreciable improvement in performance.

Figure 38 illustrates the effect of varying the magnitude of the heat transfer in the compression space on the predicted performance of the diaphragm engine. Included in Figure 38 are PV work, indicated efficiency and available energy loss for the compression space as a function of the heat transfer (hA) in the compression space. The analysis was done using the Sunpower constrained mode third order analysis. The detailed operating conditions and performance parameters are listed in Table 7. From Figure 38 the following observations were made:

- The P-V power of the adiabatic end (small hA) is higher than the isothermal end (large hA). This is because the mass flow in and out of the compression space for the near adiabatic case is higher than that of the near isothermal case. The increased mass flow amplitude is translated into an increased pressure wave amplitude, and thus a higher power output as shown in Table 8.

- The efficiency for the near isothermal case is much higher than that of the near adiabatic case. It is explained by the difference in the available energy loss in the compression space for the two cases. In the perfectly isothermal case, the available energy loss would be zero. In the perfectly adiabatic case, the available energy loss would not be zero because there is still the mixing of gas at different temperatures in the compression space.

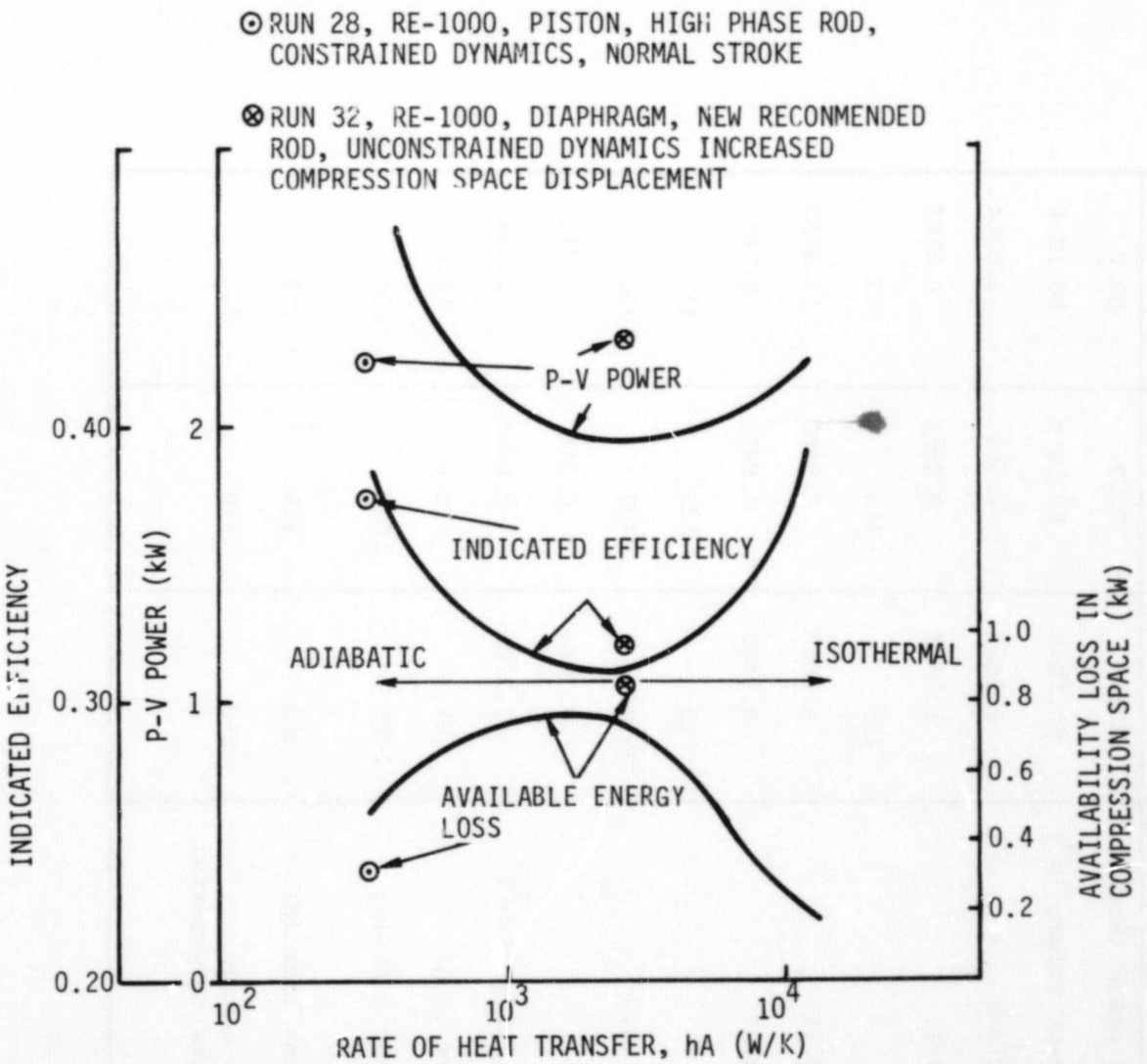

Figure 38. - Predicted performance of the diaphragm piston, free displacer Stirling engine as a function of heat transfer in the compression space.

TABLE 8. - THE PERFORMANCE OF HYDRAULIC OUTPUT, FREE DISPLACER, DIAPHRAGM PISTON STIRLING ENGINE VERSUS COMPRESSION SPACE HEAT TRANSFER

Run No. / Parameters*	26	27	29
Displacer phase (deg)	80.2	80.2	80.2
Piston swept volume (m^3)	80.1E-6	80.1E-6	80.1E-6
h_{cmp} (W/m^2-K)	1.36E5	4.5E3	3.07E4
$h\ S_{cmp}$ (W/K)	1.16E4	3.83E2	2.61E3
T_{cmp} (K)	313	313	313
h_{exp} (W/m^2-K)	4.88E3	4.88E3	4.88E3
$h\ S_{exp}$ (W/K)	6.84E1	6.84E1	6.84E1
T_{exp} (K)	835	822	827
PV power (W)	2210	2700	1930
η_i	0.384	0.366	0.311
P_{cmp} amplitude (N/m^2)	1.25E6	1.65E6	1.35E6
P_{cmp} phase (deg)	21.4	18.6	16.0
Regenerator enthalpy flux (W)	1080	1060	1020
Sum pumping loss (W)	364	409	338
Available energy loss in the compression space (W)	210	570	740

*For the nomenclature, refer to subsection 2.4.

- In the intermediate region between the adiabatic and the isothermal case, the efficiency and the power drop to their respective minimum values. This is because the available energy loss peaks in the intermediate region as shown in Figure 38. As it happens, the run 29 of Table 7 is in this fairly wide, low performance region. An interesting thing about this is that even if our estimate of the heat transfer was off by a factor of 2 in either direction, the performance of the diaphragm engine would not differ much.

- Toward the adiabatic end, the piston engine (run 28,) puts out much less P-V power than the diaphragm engine (solid curve), although the efficiencies seem to match approximately. This is only because the diaphragm engine had 36 percent higher piston swept volume than the piston engine, and being adiabatic, there is no decrease in effective stroke as with a near isothermal case.

Displacer phase angle: Using the constrained third order analysis, the performance of the diaphragm engine was simulated for a wide range of the displacer phase angle. Table 9 gives the detailed information on operating conditions and output variables. The Taylor's correlation (ref. 5) was used for the heat transfer calculation. The increased piston swept volume was used as before. The pressure wave amplitude increases as the displacer phase angle increased from 40 deg to 100 deg. The phase angle of the pressure wave has a maximum near 70 deg. The P-V power, which is directly related to the amplitude and the phase of the pressure wave peaks around 80 deg of displacer phase angle. Figure 39 shows the efficiency and power variation with respect to the displacer phase angle. The maximum efficiency occurs around 60 deg. Note the shift in maximum efficiency phase angle: the original RE-1000 FPSE had been designed to have 45 deg phase angle for maximum efficiency. The 15 deg phase shift is thought to be due to the increased heat transfer in the compression space of the diaphragm engine.

Hydraulic pump load force: The dynamically unconstrained, third order analysis was used to predict what would happen if the hydraulic load force was varied over a range of 900 to 1300 Newtons. The following is the brief description of how the null center band hydraulic pump is incorporated in the unconstrained third order analysis.

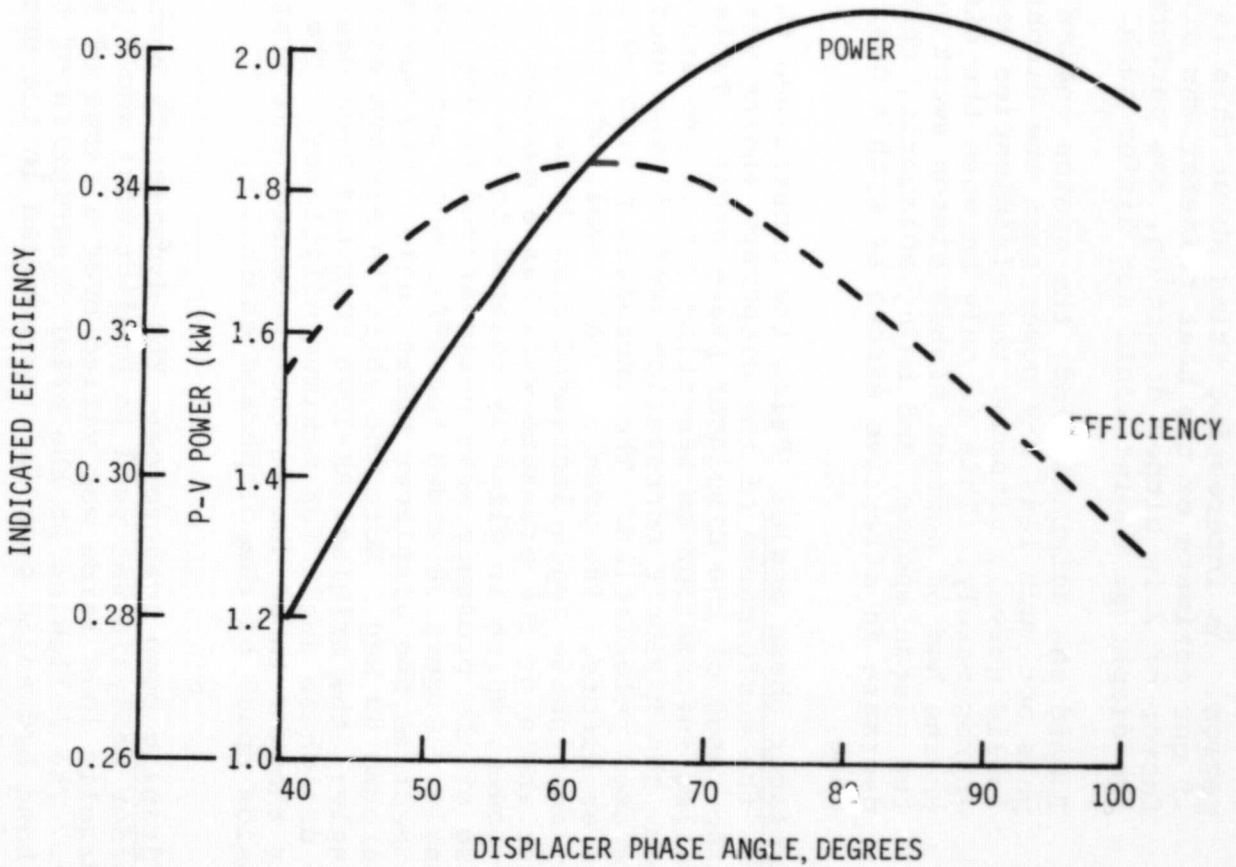

Figure 39. - Influence of displacer phase angle on the performance of the diaphragm piston, free displacer, hydraulic output Stirling engine.

TABLE 9. - THE PERFORMANCE OF DIAPHRAGM PISTON, FREE DISPLACER, HYDRAULIC OUTPUT STIRLING ENGINE VERSUS DISPLACER PHASE ANGLE

Run No.	25-1	25-2	25-3	25-4	25-5	25-6	25-7
Displacer phase (deg)	40	50	60	70	80	90	100
Piston swept volume (m^3)	80.1E-6						
h_{cmp} (W/m^2-K)	1.36E5 (Taylor's correlation)						
S_{cmp} (m^2)	2.48E-2						
T_{cmp} (K)	313						
h_{exp} (W/m^2 - K)	5.68E4						
S_{exp} (m^2)	2.57E-3						
T_{exp} (K)	823	822	822	825	830	835	843
PV power (W)	1185	1534	1810	1993	2056	2036	1947
Indicated efficiency	0.315	0.336	0.344	0.341	0.326	0.310	0.293
ΔP_{cmp} (N/m^2)	9.54E5	1.05E6	1.15E6	1.26E6	1.37E6	1.46E6	1.56E6
ΔP_{cmp} phase (deg)	14.2	16.7	17.9	18.0	17.1	16.0	14.5
Regenerator enthalpy flux (W)	673	745	850	945	1049	1130	1270
Sum pumping loss (W)	168	204	249	302	364	427	497

The hydraulic load is described mathematically by a subroutine which offers a square wave force, F to the engine piston defined as follows:

$$F = 0.0 \text{ if abs } (x_p) < 1.1 \text{ cm}$$
$$F = \pm F_{LOAD} \text{ if abs } (x_p) \geq 1.1 \text{ cm} \quad (3)$$

where the sign of F_{LOAD} depends on the piston velocity, and x_p refers to the displacement amplitude of the hydraulic transformer piston. In other words, there is no force for a null center band around the piston mid-position of 55 percent of the design stroke of 4.0 cm. Outside the null center band, the piston sees a force of $\pm F_{LOAD}$, where the positive force opposes the piston motion. F_{LOAD} is the product of hydraulic pressure and the pump piston area and is chosen to absorb the correct power from the engine at the design point.

The diaphragm engine simulated for this purpose has the high phase angle displacer rod set, the effective piston mass of 2.8 kg, and a fixed null center band of 2.2 cm. Figure 40 shows that as the load force increases, the load clearly shows the tendency of restricting the piston motion: the piston stroke, the frequency, and the power decrease by 30 percent and 43 percent, respectively as the load force is increased from 900 to 1300 newtons. The displacer phase angle remained almost constant despite all the other changes. In these simulations, there was no transient overstroking or collisions which again demonstrates the inherent dynamic stability of the present design.

3.2.2.3.3 Performance prediction for the diaphragm-piston, free-displacer, hydraulic output Stirling engine. - The diaphragm engine was to be designed to have the displacer phase angle of 80 deg for maximum power production. Therefore the reference simulation run 29 of Table 7 shows 80 deg displacer phase. However a dynamic analysis performed on the diaphragm engine of run 29 indicated that the gas spring stiffness in the existing displacer spring of the RE-1000 FPSE was too stiff to give desired displacer phasing in the unconstrained mode. The dynamic analysis suggested a spring stiffness of 2.95E4 N/m whereas the existing spring has a stiffness of 4.15E4 N/m. It was decided to simulate the existing gas spring. A series of simulations were made with various piston masses and hydraulic discharge pressures to obtain an acceptable run.

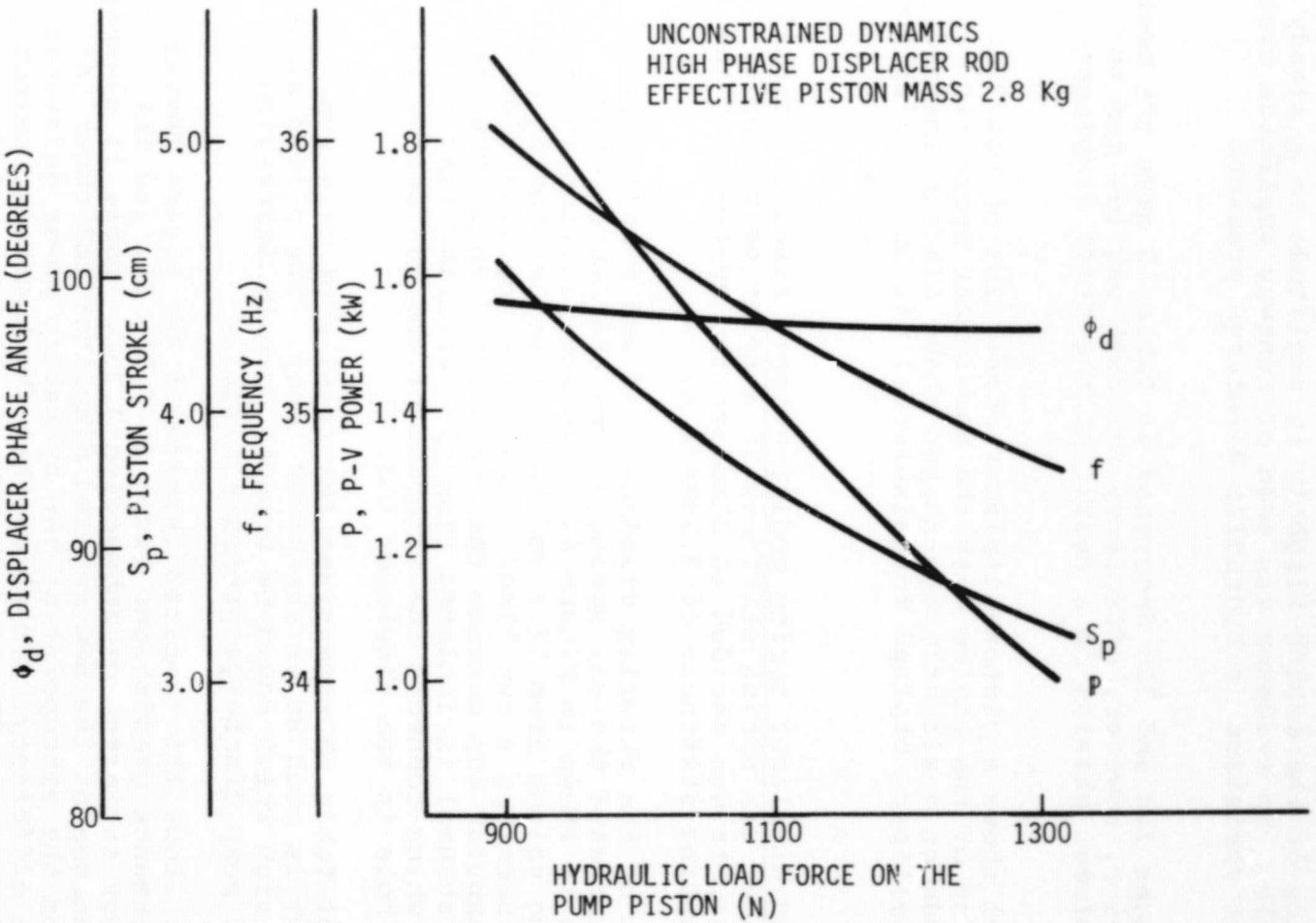

Figure 40. - Effect of null center band load force on hydraulic pump load force on the performance of the diaphragm piston, free displacer hydraulic output Stirling engine.

The simulations were started with initial conditions provided by the output of constrained run 29. In other words the piston and displacer were already moving with design point amplitude and phasing. All simulations were dynamically stable, either decaying or increasing slightly in amplitude to a steady operating cycle. No evidence was seen of runaway amplitude over the 40 percent variation in hydraulic discharge pressure investigated.

Simulations 32d and 32e described in Table 10 gave the best dynamic behavior, however, efficiency for both was low due to improper displacer phasing as a result of the stiff displacer spring.

Figure 41 shows a piston-displacer phase plot of run 32d. The interaction of the engine with the non-linear hydraulic pump load produces a slightly egg-shaped phase diagram instead of a perfect ellipse obtained for sinusoidal piston and displacer motion.

Suggested displacer spring modification: Since modification of the displacer gas spring stiffness is a relatively simple shop operation, it was decided to simulate the system with the correct gas spring stiffness of 2.95E4 N/m.

A sketch of the existing displacer rod and a modification which would increase the gas spring volume and hence reduce its stiffness is shown in Figure 42. The modification increases the gas spring volume from 17.9 cm^3 to 25.1 cm^3 by boring out the rod and inserting a cup liner. The centering leak flows through the annular gap between the cup and the rod. The pressure pick up channel is isolated from the centering leak by a tube segment which connects the interior of the gas spring to the existing hole in the displacer rod.

Run 33 of Table 10 summarizes the results of this run. The efficiency is good as is the power level. The piston stroke is a bit too high which could be brought down by increasing the hydraulic pump discharge pressure slightly.

Table 11 shows the combined results of the engine thermodynamic performance predictions given in Table 10, and the additional loss estimates of subsection 3.2.3. Table 11 clearly recommends the use of the new revised displacer rod shown in Figure 31 from the standpoint of the hydraulic power delivered and the brake efficiency. It shows that the hydraulic output Stirling engine is capable of delivering 1.87 kW at 29.7 percent overall efficiency without the dynamic balance mechanism.

TABLE 10. - UNCONSTRAINED SIMULATIONS OF THE HYDRAULIC OUTPUT, FREE DISPLACER, DIAPHRAGM PISTON STIRLING ENGINE

Run No.	32d	32e	33
Piston amplitude (m)	1.85E-2	2.10E-1	2.22E-2
Displacer amplitude (m)	1.24E-2	1.39E-2	1.61E-2
Displacer phase (deg)	98	117	77
PV power (W)	1410	1360	2300
Power to load (W)	1210	1170	2010
Power to displacer gas spring hysteresis (W)	200	190	290
Indicated efficiency (W)	0.242	0.221	0.320
Frequency (Hz)	35.6	31.4	32.7
Piston mass (kg)	2.8	4.0	2.8
Displacer mass (kg)	0.381	-	-
Hydraulic load force (N)	1100	900	1340
Displacer spring (N/m)	4.15E4	4.15E4	2.95E4
Displacer rod area (m^2)	2.57E-4	-	-
Remarks	Unconstrained run with low piston mass and high frequency	Unconstrained run with high piston mass and low frequency	Unconstrained run with reduced displacer spring predicted by dynamic analysis

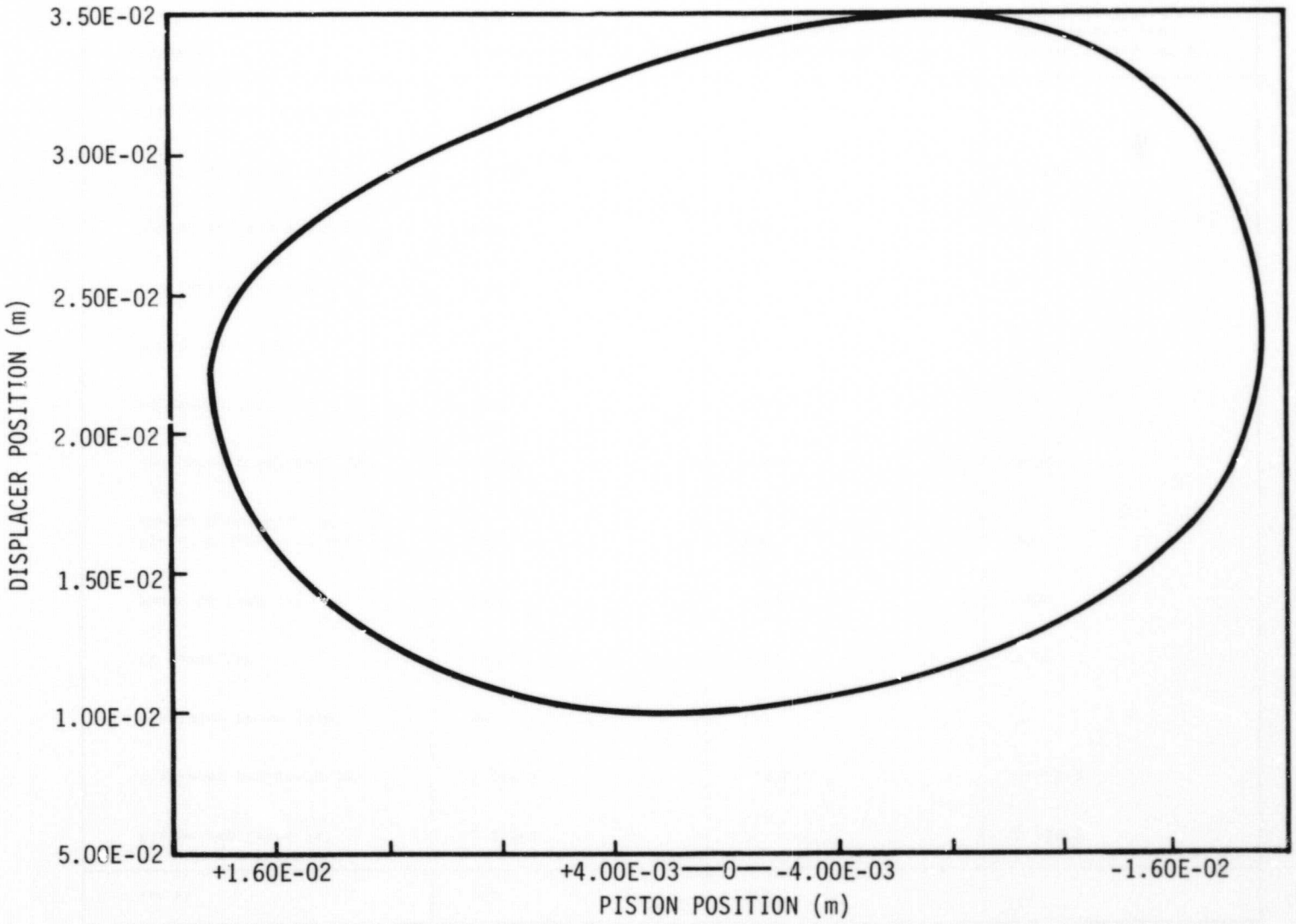

FIGURE 41. - Piston-displacer phase plot for the diaphragm piston plot displacer, hydraulic output Stirling engine

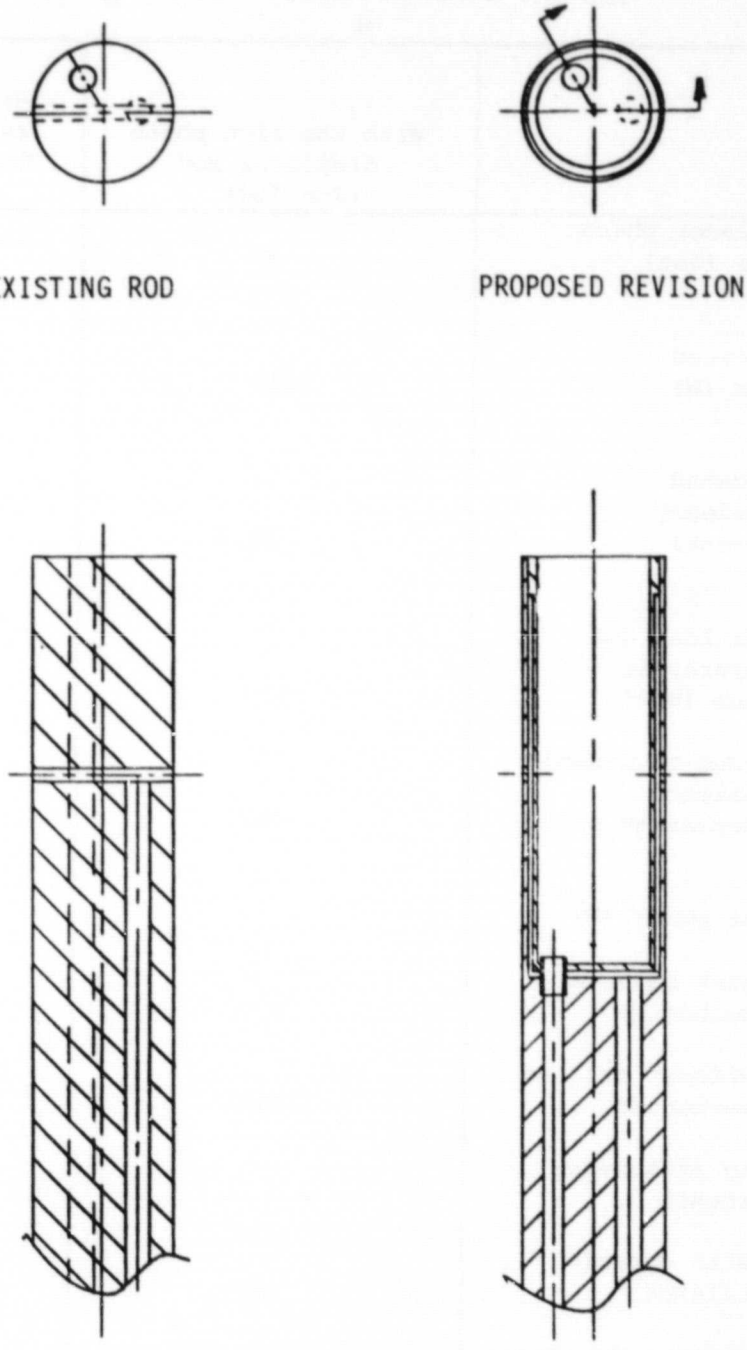

Figure 42. - Proposed displacer rod design to increase the gas spring volume.

TABLE 11. - PERFORMANCE PREDICTIONS* OF DIAPHRAGM PISTON, FREE DISPLACER, STIRLING ENGINE WITH NULL CENTER BAND HYDRAULIC PUMP OUTPUT

	With the high phase displacer rod (Run 32d)	With the new recommended displacer rod (Run 33)
Displacer phase angle (deg)	98	77
Indicated power (W)	1210	2010
Indicated efficiency (percent)	24.2	32.0
Power loss due to hydraulic system (W)**	212	212
(due to dynamic balance mechanism only)	(70)	(70)
Brake power (W)		
With balance mechanism	998	1798
Without balance mechanism	(1068)	(1868)
Brake efficiency (percent)		
With dynamic balance	20	28.6
Without dynamic balance	21.4	29.7

* Sunpower third order analysis, unconstrained mode, FMA heat transfer correlation and loss estimates.
**See subsection 3.2.3.

Considering the fact that this engine design is not fully optimized, the level of performance as predicted here looks promising.

3.2.3 Estimates of power losses due to the diaphragm assemblies and the hydraulic system. - The conversion of RE-1000 FPSE shown in Figure 1, into a hydraulic output Stirling engine as shown in Figure 18 introduced additional power losses for the engine. These losses are divided into three groups:

- Pressure drop loss in various gaps, passages and valves.
- Friction loss in the hydraulic side associated with the reciprocating components.
- Leakage loss in the hydraulic system.

These losses will decrease the hydraulic power output available for use and lower the engine brake efficiency. Each loss will be discussed in the following subsections.

3.2.3.1 Pressure drop loss. - Table 12 lists the locations where the pressure drop loss occurs. The methods of calculating the pressure drop losses are briefly described below. Basically the analysis utilizes steady flow pressure drop correlations at each instant and location.

For the gap between the diaphragm and its support, and for the inner cooler plug in the compression space, the instantaneous pressure drop, $\Delta P(t)$, between two points, x_1 and x_2, is obtained from

$$\Delta P(t) = \int_{x_1}^{x_2} 2f \frac{\rho v|v|}{d_h} dx \qquad (4)$$

where

f = friction factor

ρ = fluid density

v = instantaneous, local fluid velocity

$d_h(t)$ = instantaneous, local hydraulic diameter

TABLE 12. - ADDITIONAL PRESSURE DROP LOSS LOCATIONS

Gas Side
Inner cooler in the compression space
The gap between the diaphragm and the gas side support (engine diaphragm and balance diaphragm)
Hydraulic Side
The gap between the diaphragm and the oil side support (engine diaphragm and balance diaphragm)
Inlet valves of the pump
Discharge valve of the pump

For the valves, the instantaneous pressure drop is obtained from a standard orifice equation, such as

$$\Delta P(t) = \frac{\rho v|v|}{2\, C_d^{\,2}} \qquad (5)$$

where

C_d = flow coefficient of a value

ρ = fluid density.

The loss of power, $\dot{W}$, due to the pressure drops expressed by Equations (4) and (5) is obtained by

$$\dot{W} = \frac{1}{T} \int_{o}^{T} \Delta P(t)\ q(t)\ dt \qquad (6)$$

where

T = cycle period

$q(t)$ = instantaneous volume flow rate of fluid

The integrands in Equations 4 and 6 contain the instantaneous local values for the velocity, the hydraulic diameter, and the flow rate. For a fixed geometry flow passage, such as the inner cooler, with known, d_h, and known instantaneous mass flow rate, the velocity can be easily calculated from

$$v = \frac{\dot{m}}{\rho A} \qquad (7)$$

where

$\dot{m}$ = instantaneous mass flow rate

A = flow cross-sectional area

By assuming that the valves of the hydraulic pump open and close instantly, the valves can also be viewed as fixed geometry flow passages for the duration of the valve flow.

However, if the flow passage changes its shape constantly with time as is the case with the diaphragm gap, the expressions for v, d_n, and $q(t)$ become quite involved. For the diaphragm gap shown in Figure 43 the variables v, d_h, and q are expressed by

$$v = \frac{\xi\ \omega}{\sigma\ (1 + \xi \sin \omega t)\ x} \left[x_2^{\,2} + x_2\, x - 2x^2\right] \qquad (8)$$

$$d_h = \frac{2\ h_o\ (x_2 - x)}{x_2 - x_1}\ (1 + \xi \sin \omega t) \qquad (9)$$

$$q = \frac{\xi\ \omega\ \pi\ h_o}{3}\ (x_2^{\,2} + x_1 x_2 - 2\ x_1^{\,2}) \cos \omega t \qquad (10)$$

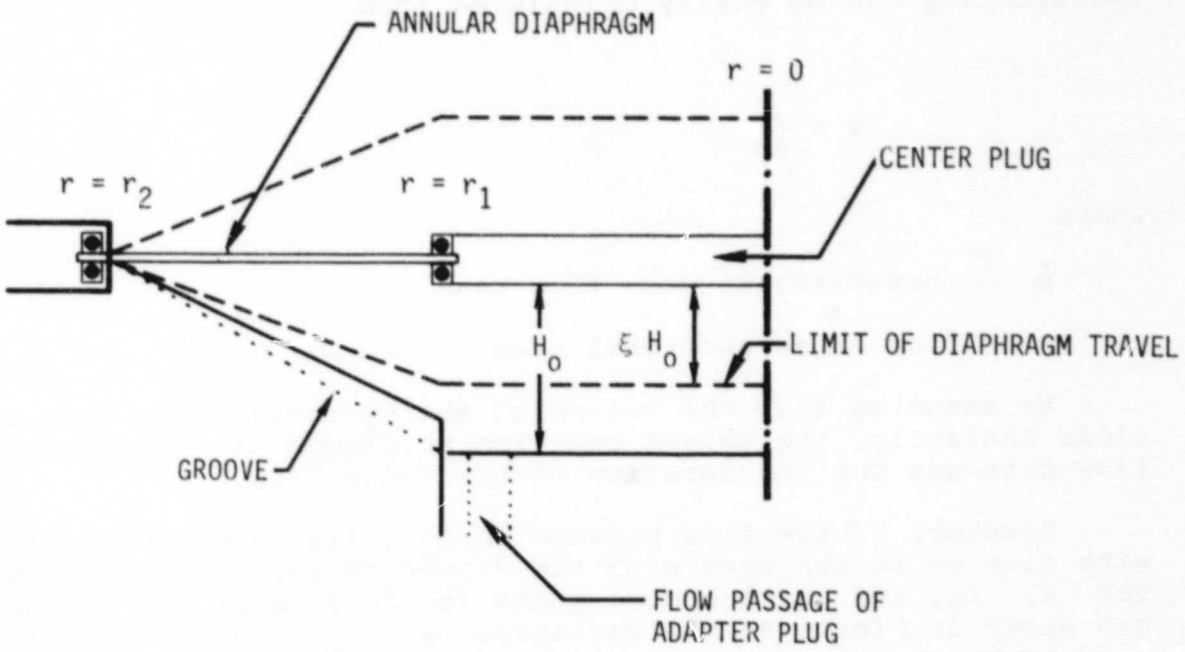

Figure 43. - Diaphragm support gap schematic.

where

ξ = $\frac{\text{diaphragm design volume amplitude}}{\text{maximum theoretical volume amplitude}}$

ω = rotational speed

h_o = maximum diaphragm center deflection

x = radial distance.

Now the instantaneous pressure drop through the diaphragm gap, P(t), and the resulting loss of power can be obtained from Equations 3 and 5 after substituting the expressions for V, d_h, and q of Equations 8, 9, and 10. The remainder of the analysis is a straightforward mathematical procedure, and therefore not given here. The results are instead given in Table 13, and will be briefly discussed.

The high pressure drop loss of the inner cooler is a result of designing the inner cooler passage dimension to be smaller than the thermal diffusion layer thickness. The thermal diffusion layer thickness was calculated from the FMA cyclic heat transfer analysis mentioned earlier.

The pressure drop losses in the diaphragm gaps of the gas side and the hydraulic side are negligible. The gaps were designed to have almost negligible pressure build up due to opening or closing of the gap. The pressure build up was calculated to be 690 Pa (0.1 psi) maximum for the two diaphragms. It was necessary to maintain a small pressure drop in order to prevent local deformations of the thin diaphragms.

3.2.3.2 Viscous friction and leakage loss. - The viscous friction loss means the hydrodynamic viscous friction occurring at the sliding surfaces of reciprocating components in the hydraulic system. The leakages occur past the same sliding surfaces. The locations for these losses are:

- Transformer piston and rod.
- Dynamic balance mechanism.
- Null center band hydraulic pump and pump rod.

Figure 44 is a schematic showing these locations which are indicated by thickened lines. The Roman numerals I to VI indicate the individual spaces that have different dynamic pressures.

TABLE 13. - PRESSURE DROP LOSS INTRODUCED BY THE CONVERSION OF RE-1000 FPSE INTO HYDRAULIC OUTPUT ENGINE

Locations	Pressure drop loss (W)
Gas side	
Inner cooler	22
Diaphragm gap	Negligible (<1.0)
Hydraulic side	
Diaphragm gap	Negligible (<1.0)
Slots in the support	1.5
Inlet valve	10
Discharge valve	23
Total	58

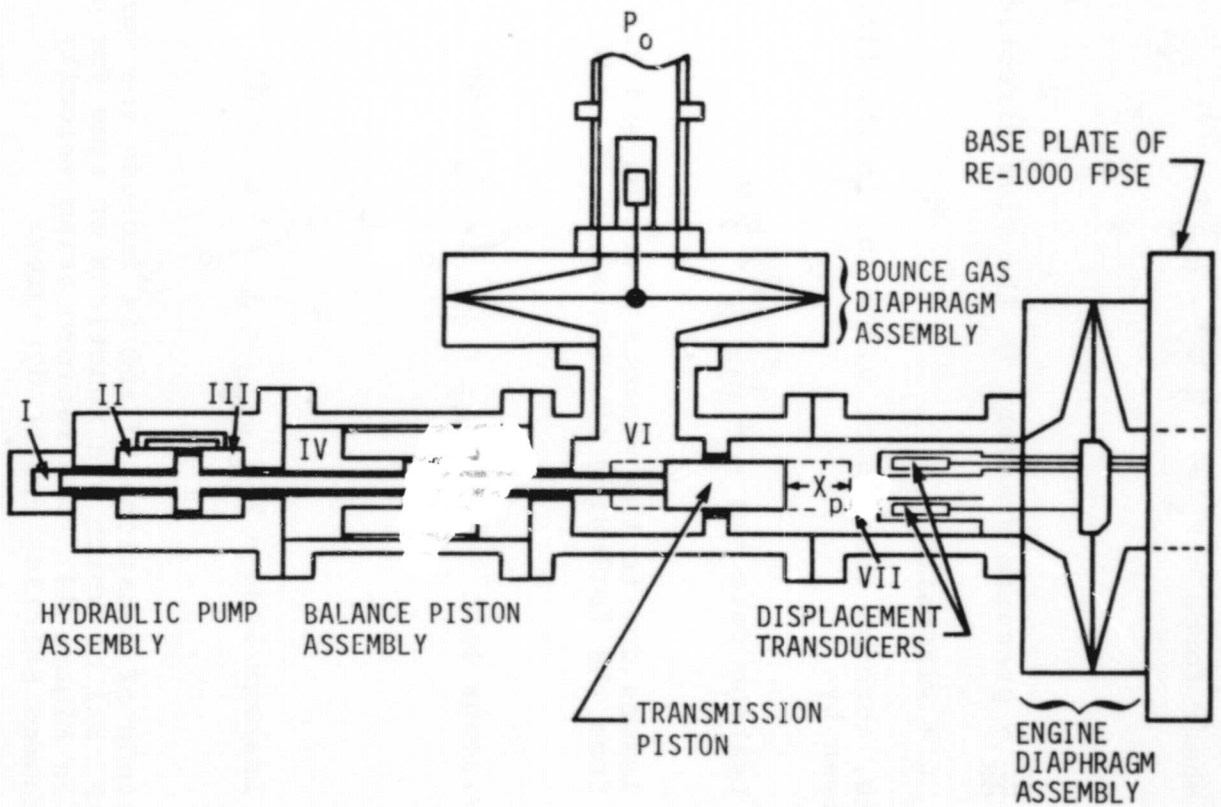

Figure 44. - Schematic of hydraulic system showing locations of viscous and leakage loss.

The calculation method of the losses at these locations is based on a steady laminar flow between stationary and moving flat, parallel plates. The shear force experienced by the plate moving at velocity V in x direction, at the distance b away from the parallel stationary plate, is given by

$$\text{Shear force} = F_s = -\frac{b}{2}\frac{dP}{dx} - \mu\frac{V}{b} \tag{11}$$

where

$\frac{dP}{dx}$ = pressure gradient in the flow direction

μ = viscosity

The leakage rate, through the gap of width b, in the flow direction is given by

$$\text{Leakage rate} = q = -\frac{b^3}{12\mu}\frac{dP}{dx} + \frac{b}{2}V \tag{12}$$

The power losses due to the viscous friction and the leakages are calculated from the following equations:

$$\text{Viscous loss} = \dot{W}_{\text{Viscous}} = \frac{1}{T}\int_0^T F_s V\, dt \tag{13}$$

$$\text{Leakage loss} = \dot{W}_{\text{Leakage}} = \frac{1}{T}\int_0^T q\,\Delta P\, dt \tag{14}$$

The integrands of Equations 13 and 14 include the variables F_s, V, q, and ΔP, all of which are functions of time for each location shown in Figure 44. The reciprocating velocity V is given by the assumed Stirling engine dynamics:

$$V = x_p\,\omega \sin \omega t \tag{15}$$

where x_p = the displacement amplitude of the output piston.

At each location, the pressure gradient dP/dx is required to calculate the two variables F_s and q from Equations 11 and 12. The dynamic pressures of spaces IV and V shown in Figure 44 were obtained by applying a dynamic force balance for each reciprocating components. The detail of the dynamic force balance will be omitted here. The resulting pressures are approximately given by the following equations.

$$P_I \simeq P_o$$

$$P_{II}, P_{III} \simeq P_H \text{ : when pumping}$$

$$0 \text{ : when not pumping}$$

$$P_{IV} \simeq P_o + \frac{m_B x_p}{2 A_B} \omega^2 \sin \omega t$$

$$P_V \simeq P_o - \frac{m_B x_p}{2 A_B} \omega^2 \sin \omega t \qquad (16)$$

$$P_{VI} \simeq P_o$$

$$P_{VII} \simeq P_o + P_c \sin (\omega t - \phi_p)$$

where

P_o = mean engine gas pressure

P_H = high pressure hydraulic accumulator pressure

m_B = mass of the balance piston

A_B = cross-sectional area of the balance piston

P_c = engine compression space pressure amplitude.

Now, the pressures of the spaces I through VII given by Equation 16 can be used to calculate the shear force, F_s, and the leakage rate, q, from Equations 11 and 12, respectively. Then, the shear force, F_s, and the leakage rate, q, are substituted into Equation 13 to calculate the viscous loss and the leakage loss. The remaining detail will be again omitted and the results are given in Table 14.

TABLE 14. - VISCOUS FRICTION LOSS AND LEAKAGE LOSS INTRODUCED BY THE CONVERSION OF RE-1000 FPSE INTO HYDRAULIC OUTPUT ENGINE

Location	Viscous friction loss (W)	Leakage loss (W)
Transformer piston and rod	17	5
Dynamic balance piston	58	12
Hydraulic pump piston	17	22
Hydraulic pump rod	3	20
Total	95	59

Adding all three losses as shown in Table 13 and 14 the total additional loss caused by the conversion of the RE-1000 FPSE into a hydraulic output engine is 212W. The *optional* dynamic balance mechanism accounts for approximately 70W of this total additional loss.

4. SUMMARY AND RECOMMENDATIONS

4.1 Summary

By modifying the Sunpower-built RE-1000 Free-Piston, Free-Displacer Stirling engine, the Foster-Miller/SUNPOWER team designed a hydraulic output version of the RE-1000 FPSE. The new engine has a diaphragm piston which is hydraulically coupled to a novel, null center band hydraulic pump as the output method. The pump provides the inherent dynamic stability to the new engine.

The engine is a test-bed engine rather than a prototype engine. Some of the notable features are listed below:

- It is relatively simple in its design and inexpensive to build.
- The modular design approach was used to facilitate the modification and replacement of the components.
- A complete inertial balance of the moving parts is achievable in a horizontal or a vertical set up.
- The start/stop operation is easily controllable.

As a test-bed engine, the engine will be quite suitable for obtaining the following:

- Cylinder heat transfer data in the narrow diaphragm space.
- High cyclic rate diaphragm data.

From the detailed analysis, the following observations were made:

- For the simulation of the Free Displacer/Diaphragm Piston Stirling engine with the null center band hydraulic pump output, the dynamically *unconstrained* third order Stirling engine analysis should be used.
- The two critical parameters influencing the overall engine performance are the heat transfer in the diaphragm space and the displacer phase angle. The heat transfer can be marginally controlled. However, the displacer angle can be changed fairly easily.

- In order to achieve a reasonable performance, the diaphragm space should be actively cooled utilizing coolant passages, fins and flow patterns.

- The proposed engine design is not optimized. To optimize properly, more knowledge in fluid flow and heat transfer phenomena near the diaphragm is required. Also, the optimization should include the entire engine: expansion space, regenerator, heater, cooler, diaphragm space, hydraulics, etc.

- The diaphragm will last an indefinite period of time due to a very conservative design. The diaphragm edge supporting method using an ordinary rubber O-ring not only provides an effective sealing method but also reduces the diaphragm stress for a given diaphragm volume displacement.

Without the dynamic mass balancing mechanism, the engine will put out 1.87 kW of hydraulic power at 29.7 percent brake efficiency with a new, recommended displacer rod, and 1.07 kW at 21.4 percent with an existing displacer rod. The hydraulic output Stirling engine design concept can be easily scaled up to, say, 50 kW. For more power, any number of cylinders, can be ganged up. The hydraulic output is suitable for typical hydraulic accumulator powered systems at 100 to 200 bar range.

4.2 Recommendations

As a result of the design study, the following is recommended:

- Build the hydraulic output Stirling engine with the new revised displacer rod design. This minor modification of the hot section will drastically increase the power and the efficiency of the engine.

- Refine centering control schemes.

- Test the hydraulic pump separately first. Modify and debug the pump before testing it in conjunction with the engine.

- In the test plan, pay particular attention to the following:

  1. Diaphragm dynamics and positioning.

  2. Thermodynamics in the diaphragm region.

3. Displacer dynamics and the phase angle.

4. Losses in hydraulic system.

By varying the diaphragm midstroke position, it will be possible to see the effect of the dead volume change on engine performance, especially since varying the rate and the temperature of the coolant flow in the diaphragm region will show the effect of heat transfer on the engine performance.

5. REFERENCES

1. Martini, W.R., Stirling Engine Newsletter, Martini Engineering, Richland, Washington, November, 1981.

2. Kalnins, A., and Lestingi, J.F., "On Nonlinear Analysis of Elastic Shells of Revolution," ASME Trans., Vol. 34, Series E, No. 1, pp. 59-64, March, 1967.

3. Wahl, A.M., Mechanical Springs, McGraw-Hill Book Co., Second Edition, pp. 170-172.

4. Allegheny Ludlum Data Sheet 115-92358-350, Allegheny Ludlum Steel Corporation, Research Laboratory, Brackenridge, Pennsylvania.

5. Taylor, C.F., The Internal Combustion Engine in Theory and Practice, Second Edition, MIT Press, Cambridge, Massachusetts pp. 266-311.

6. Lee, K., Smith, J.L. Jr., and Faulkner, H.B., "Performance Loss Due to Transient Heat Transfer in the Cylinders of Stirling Engines," Proceedings of the Fifteenth IECEC Conference, Seattle, Washington, August, 1980.

7. Foster-Miller Associates, Inc., "Design and Development of Stirling Engines for Stationary Power Generation Applications in the 500 to 3000 hp Range," Phase I Final Report to Argonne National Laboratory, Argonne, IL, No. DE-AC02-79ET15208, October, 1980.